STUDY ON FAMILIARITY EFFECT ON ATTENTION AND EMOTION: A DIRECTED FUNCTIONAL CONNECTIVITY ANALYSIS OF EMOTIONAL EEG DATASETS

ハドリアナ, イッダス

https://hdl.handle.net/2324/6787434

出版情報：Kyushu University, 2022, 博士（システム生命科学）, 課程博士
バージョン：

STUDY ON FAMILIARITY EFFECT ON ATTENTION AND EMOTION: A DIRECTED FUNCTIONAL CONNECTIVITY ANALYSIS OF EMOTIONAL EEG DATASETS

A Dissertation Written by

Hadriana Iddas

In Partial Fulfillment of the Requirements

For the Degree of

Doctor of Systems Life Sciences

Kyushu University

2023

Abstract

Several studies have mainly addressed the detection of attention to stimuli with various approaches, such as (1) subjective evaluation — experimenter assumption; and (2) objective evaluation — eye tracking and BCI. However, the detection of subjects' attention levels while watching a music video using directed functional connectivity features has never been investigated. In addition, none have explored the differences in directed functional connectivity patterns between attention levels. In the current study, we proposed a novel framework, including (1) the alpha/theta ratio of frontocentral (the frontal to central and the central to frontal) as an attention index; 2) the hierarchical clustering approach to group subjects based on the attention index, and 3) the Dunn index as cluster quality evaluation metrics to determine the number of groups (clusters). The experimental results show that our proposed framework performs well on the DEAP and AMIGOS datasets. In the DEAP dataset, subjects were clustered into three groups: low index (LI), medium index (MI), and high index (HI), and in the AMIGOS dataset, subjects were clustered into two groups: low index (LI), and high index (HI). Furthermore, connectivity strengths from the frontal area to other regions (central, parietal, and occipital) were enhanced with an increased attention index during familiar conditions in the DEAP dataset. In addition, information flows from central to parietal were consistent in competition between attention index groups during familiar and unfamiliar conditions in the AMIGOS dataset. Our results show the potential of the proposed approach for attention detection that may support an intelligent video management system.

Numerous studies describe that familiarity perception is associated with pleasant emotions, which are typically appraised using traditional methods such as subjective ratings and power spectrums. This study focused on the differentiation of quantitative evaluation between positive and negative emotional valence responses to familiar and unfamiliar music videos by utilizing the directed transfer function (DTF) and graph theory analysis (GTA). The results showed that familiar music videos evoked positive valence (PV), including (1) an enhanced node degree in all evaluated frequency bands (i.e., the theta, alpha, beta, and gamma bands), specifically a significant node degree of PV in the right frontal alpha band and the right central beta band; (2) significantly stronger information flow in the theta, alpha, and beta bands; and (3) a higher clustering coefficient and local efficiency in all examined bands, reflecting that familiarity enhances the speed of information processing in the brain. In contrast, unfamiliar music videos evoked negative valence (NV), including (1) an enhanced node degree in the theta, alpha, and gamma bands and (2) significantly higher information flow in the alpha, beta, and gamma bands. Our study confirmed prior findings that, the more familiar the stimuli, the more positive the emotional valence and, thus, the better the cognitive performance. In conclusion, our study demonstrated that brain networks and graph theory could help to improve insight into the relationship between familiarity, emotional valence, and cognitive processing.

Contents

List of Figures

List of Tables

Chapter 1 Introduction

1.1 Overview and problem statement

Auditory and visual stimuli such as watching music videos can impact the human brain, specifically attention and emotion. Familiarity is an additional crucial component that influences audiovisual perception. Findings from previous studies have shown that familiarity significantly enhances attraction in live interaction[1]. In the learning process, familiar contexts improve the level of interest and engagement [2]. Furthermore, in the human-computer interaction (HCI) field, familiarity was considered a primary design concept when developing the digital feedback for a safety alarm robot for the elderly [3].

The neuronal networks of the brain are more intricately organized, with stronger connections between different brain regions. Functional connectivity analysis can reveal important details about the brain's complex interactions and functional organization. Functional connections can be made between parts of the brain that are physically close together or far apart, allowing them to separate and combine information effectively.

Interactions between regions of the brain that are functionally specialized in different ways are essential for maintaining healthy brain function. Magnetoencephalography (MEG) and electroencephalography (EEG) are appropriate methods for capturing these interactions because they offer millisecond-level measures of brain activity across the head.

However, reliable and objective evaluation of how watching music videos can elicit different attention levels with directed functional connectivity features remains unclear. Furthermore, although the positive impacts of familiar stimuli are confirmed, none have evaluated their effects on emotional valence and cognitive performance using neuroimaging techniques, specifically the directed functional connectivity approach.

To our knowledge, this is the first study that applied directed functional connectivity and graph-theoretic indexes to study the influence of familiarity on directed functional connectivity in attention and emotion while watching emotional music videos.

1.2 The Dissertation objective and research plan

The primary goal of this research is to identify the impact of watching music videos on eliciting different attention levels across subjects and how familiar and unfamiliar stimuli affect human emotion via directed functional connectivity. Two studies were performed to achieve this aim. The first study investigated the information flow between the frontal and central areas that may be associated with attentional processing. These were the goals of this study:

- To investigate whether watching music videos can elicit different attention indexes across subjects.
- To investigate whether the information flow between the frontal and central can be used to categorize different attention indexes.
- To identify the differences in directed functional connectivity patterns between attention index groups under familiar and unfamiliar conditions.

In the second part of our study, we investigated the effects of familiar and unfamiliar stimuli on emotional valence (positive and negative) in the four-frequency bands. To this effect, we calculated the directed functional connectivity of EEG channels, followed by graph analysis (i.e., node degree, node strength, clustering coefficient, and local efficiency). The goals of this study were:

- To determine the node degree of functional connectivity in positive valence (PV) and negative valence (NV) under familiar and unfamiliar states.
- To evaluate the node strength of functional connectivity in positive valence (PV) and negative valence (NV) under familiar and unfamiliar states.
- To investigate the clustering coefficient in the brain regions of interest (ROIs) in positive valence (PV) and negative valence (NV) under familiar and unfamiliar states.
- To evaluate the local efficiency in positive valence (PV) and negative valence (NV) under familiar and unfamiliar states.
- To evaluate inter-hemisphere and intra-hemisphere information flows in positive valence (PV) and negative valence (NV) under familiar and unfamiliar states.

1.3 Structure of the dissertation

This dissertation contains five chapters:

Chapter 1: General Introduction

This chapter reports the introduction and formulation of the problem. This chapter also describes the overall purpose of the study and a concise research strategy.

Chapter 2: Fundamentals

This chapter provides an overview of brain anatomy, electrophysiological signal generation, and how these signals can be recorded using neuroimaging techniques. A brief summary of the many types of brain connection analysis, including structural, functional, and effective connectivity. Focus on the analysis of functional connectivity and graph theoretical metrics.

Chapter 3: EEG features of directed EEG functional connectivity to categorize attention indexes using hierarchical clustering

In this section, a paper was published in IEEE ACCESS (DOI: 10.1109/ACCESS.2021.3072224; Hadriana Iddas, Keiji Iramina) on April 23, 2021, was discussed. This chapter describes the pattern of effective connectivity between different attention indexes during familiar and unfamiliar conditions.

Chapter 4: Investigation of familiarity effects on emotional valence using directed functional connectivity and graph theory analysis

In this chapter, a study published in IEEE (DOI: 10.1109/ICIIBMS52876.2021.9651562; Hadriana Iddas, Keiji Iramina) on December 29, 2021, was discussed. This chapter shows how familiar and unfamiliar stimuli affect emotional valence (positive valence (PV) and negative valence (NV)) under familiar and unfamiliar states, using a directed functional connectivity approach and graph analysis (node degree, node strength, clustering coefficient, and local efficiency).

Chapter 5: General conclusion and future work

This chapter abstracts the results of chapters 3-4, with suggestions for future studies.

Chapter 2 Fundamentals

2.1 Human brain

The brain is the most essential and maybe the most sophisticated part of the human body. The brain is composed of ~86 billion neurons that are connected by ~150 trillion synapses [4], [5]. It weighs around 3 pounds and is protected by a strong bone shell called a skull. The brain is the center part of our body which has the function of managing several things such as perception, emotion, attention, cognition, and action [6]. Certain actions, like thinking, reading, writing, etc., will generate different areas in the brain, while others will produce electrical signals that let parts of our body communicate with each other.

2.1.1 Brain structure

Three basic components of the brain are the cerebrum, cerebellum, and brainstem that make up the anatomy of the brain [7], as described in Figure 2.1.

- **Cerebrum:** is located at the front of the brain and is the most extensive part of the brain, is composed of white matter and gray matter. This part initiates and directs movement and controls body temperature. Other parts of the cerebrum are responsible for speaking, logical thinking, problem-solving, empathy, and knowledge. Additional roles include the senses of sight, vision, smell, and sound. The cerebrum is divided into two sections called hemispheres, right and left, with the frontal lobe, the temporal lobe, the parietal lobe, and the occipital lobe [8], as indicated in Figure 2.1.

- **Cerebellum:** This structure is located in the bottom back of the head and consists of two hemispheres.

- **Brainstem:** The brainstem links the brain's cerebrum to the spinal cord and cerebellum. It is comprised of the diencephalon, midbrain, pons, and medulla oblongata in decreasing order. Numerous critical activities, such as respiration, awareness, blood pressure, heart rate, and sleep, are controlled by the brain.

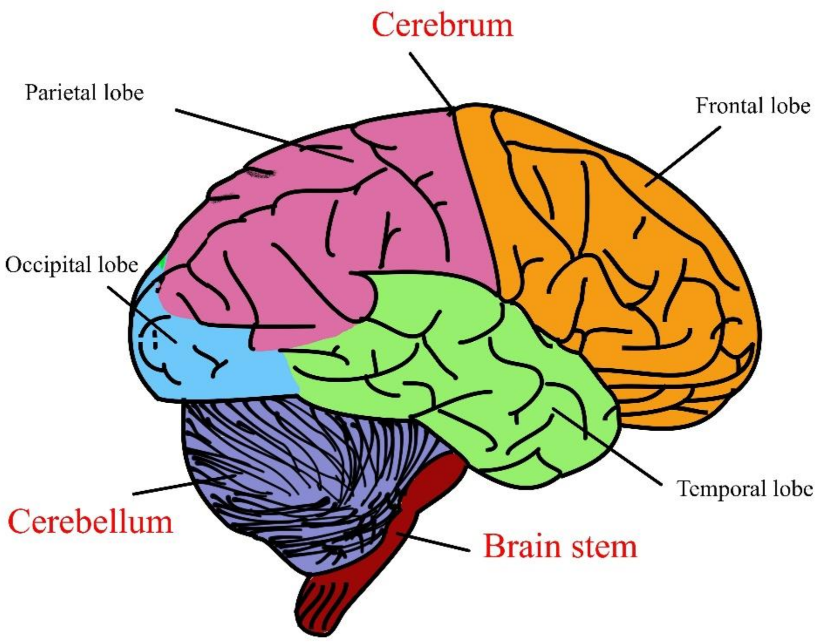

Figure 2.1: Brain anatomical regions.

Body position, handwriting, and sensation are accomplished in the parietal lobes. The occipital lobes are essential for the brain's visual management system. The frontal lobes process motor function, judgment, and problem-solving. Memory and hearing are held in the temporal lobes.

2.1.2 Neurophysiology

Neurons in the brain send and receive signals from other neurons through electrical or chemical impulses. While neurons share many characteristics with other cell types, they are physically and functionally distinct [8]. Neurons are structurally and functionally identical to other cells, but their electrochemical function allows them to send electrical impulses and information across long distances [9]. Neurons consist of three essential parts: the cell 13 core, the axons, and the synapses. [6], [7].

The core of the cell serves as the cell's centre, transmitting orders to the rest of the cell. Every neuron in the brain has a single long cable, namely an axon, that spreads from the cell's main body. Inside this axon, the neuron's electrical impulses are delivered to neighbouring neurons in order to be processed. It is considerably smaller than a human thread. Dendrites link neurons 19 to other cells to enable interaction (tree branch). The action potential enables this communication [8]. Figure 2.2 shows the interneuron communication mechanism.

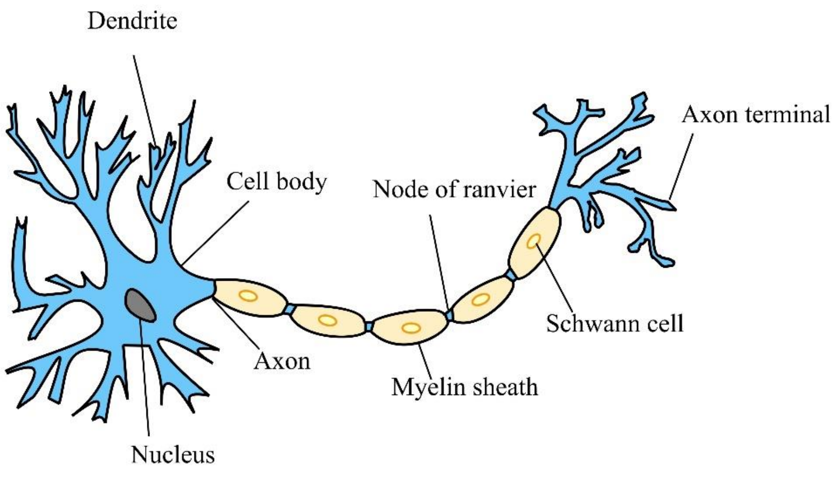

Figure 2.2: The fundamental anatomy of neurons.

An action potential happens when an ion pumps along the axon's exterior, changing its ionic composition and enabling an electronic current to travel rapidly to the subsequent dendrite [10]. This quick reversal of polarity generates a voltage on both sides of the neuron's cell membrane [11], [12]. These neurons are responsible for the release of a chemical classed as neurotransmitters [11], [12]. The present transmission that makes a significant contribution to the ambient EEG via net external input is depicted in Figure 2.3. Small electron flow are generated if nerves are triggered by an electrical concentration difference [9]. There are two forms of synaptic electric signals: action potentials (AP) and postsynaptic potentials (PSP). If the PSP is larger than the cutoff conductance value of the postsynaptic cell, the neuron engages and an AP is emitted [9], [10].

Interneurons PSPs from pyramidal neuronal networks contribute to the formation of the electrical potentials that may be sensed on the human scalp. These potentials take the form of electrical dipoles that are formed between the nucleus and the terminal dendrites [9] (see Figure 2.3). Some PSPs merge into the cortex and extend to the scalp's layer, which is recorded by the electroencephalogram (EEG).

Nerve cell APs have a significantly narrower dispersion of potential fields and a much shorter duration than PSPs. As a result, APs make no meaningful contribution to head or therapeutic electroencephalography recordings. Only large groups of active neurons can generate electrical activity that can be recorded on the scalp [6], [7], [10]. When a single cell emits voltage, it is often too low to be effectively measured with today's equipment [8].

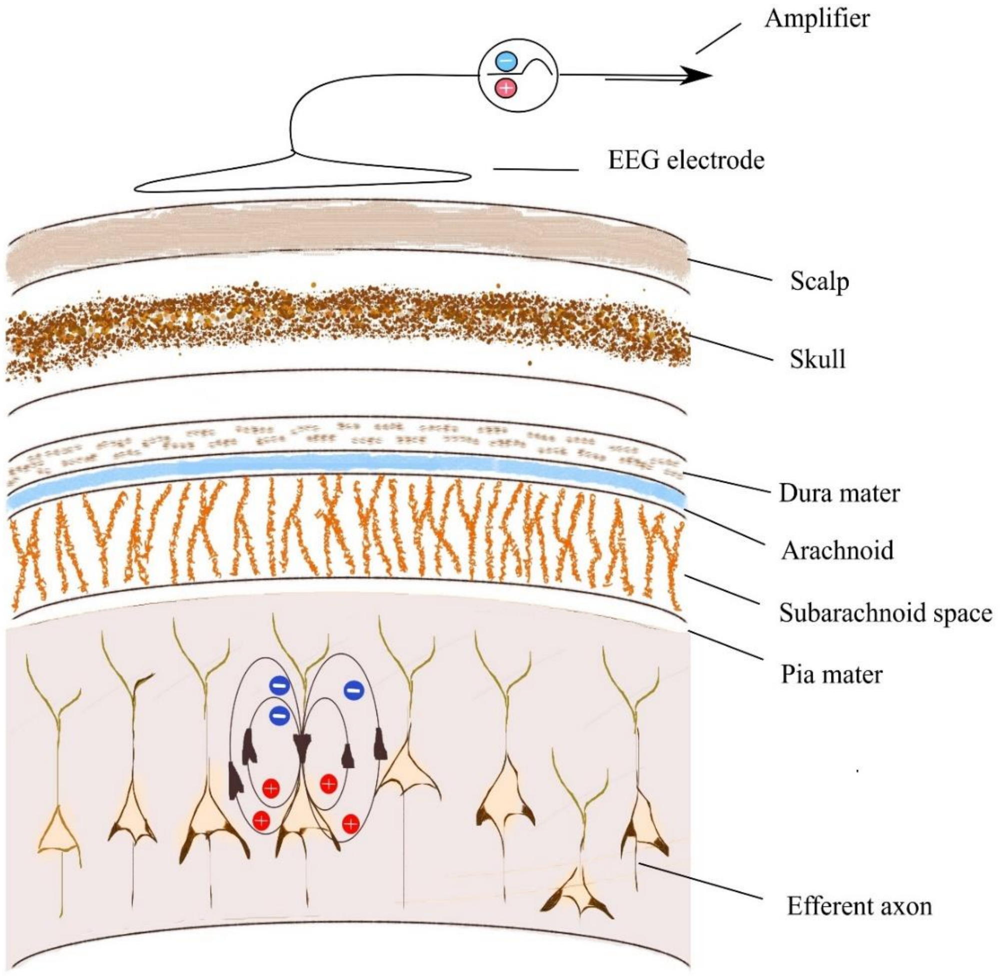

Figure 2.3: Illustration of synaptic currents in pyramidal cells that generate extremely small electrical fields Electroencephalography.

2.1.3 The characteristic of EEG signals

An electroencephalogram, often known as an EEG, is a diagnostic procedure that detects the brain's electrical activity by strapping a series of small iron plates, known as electrodes, to the scalp. Even while we sleep, brain cells are still communicating with one another via electrical impulses. An EEG recording will reveal these fluctuations as wavy lines when they occur [13], [14]. Frequency is a simple approach for characterizing EEG waves. Many waveforms have been examined, such as delta (0.5–3 Hz), theta (4–7), alpha (8–12 Hz), beta (13–30 Hz), and gamma (> 35 Hz) [15]. The delta wave has the largest amplitude and is the slowest wave. It is connected to very deep sleep as well as significant problems in the brain. The theta wave typically has an amplitude of more than 20 volts and an oscillation frequency that ranges from 4 to 8 hertz. Theta can be observed in older children and adults during sleep or arousal; it can also be observed during meditation [16]. The alpha has a frequency range of 8–13 Hz and an amplitude of 30–50 mVIt mostly shows up in the occipital lobe when the brain is at rest. Typically, stress and tension are related to it. Beta is the frequency band between 12 and about 30 Hz. It is often visible on both sides in a symmetrical pattern and is most noticeable frontally. Beta activity is strongly associated with motor behavior, and it is typically reduced during active movements [16]. Gamma is the frequency range between 30 and 100 hertz. It is associated with a number of different cognitive and physical functions [15]. Figure 2.4 provides an example of the numerous types of normal EEG rhythms in their most basic form.

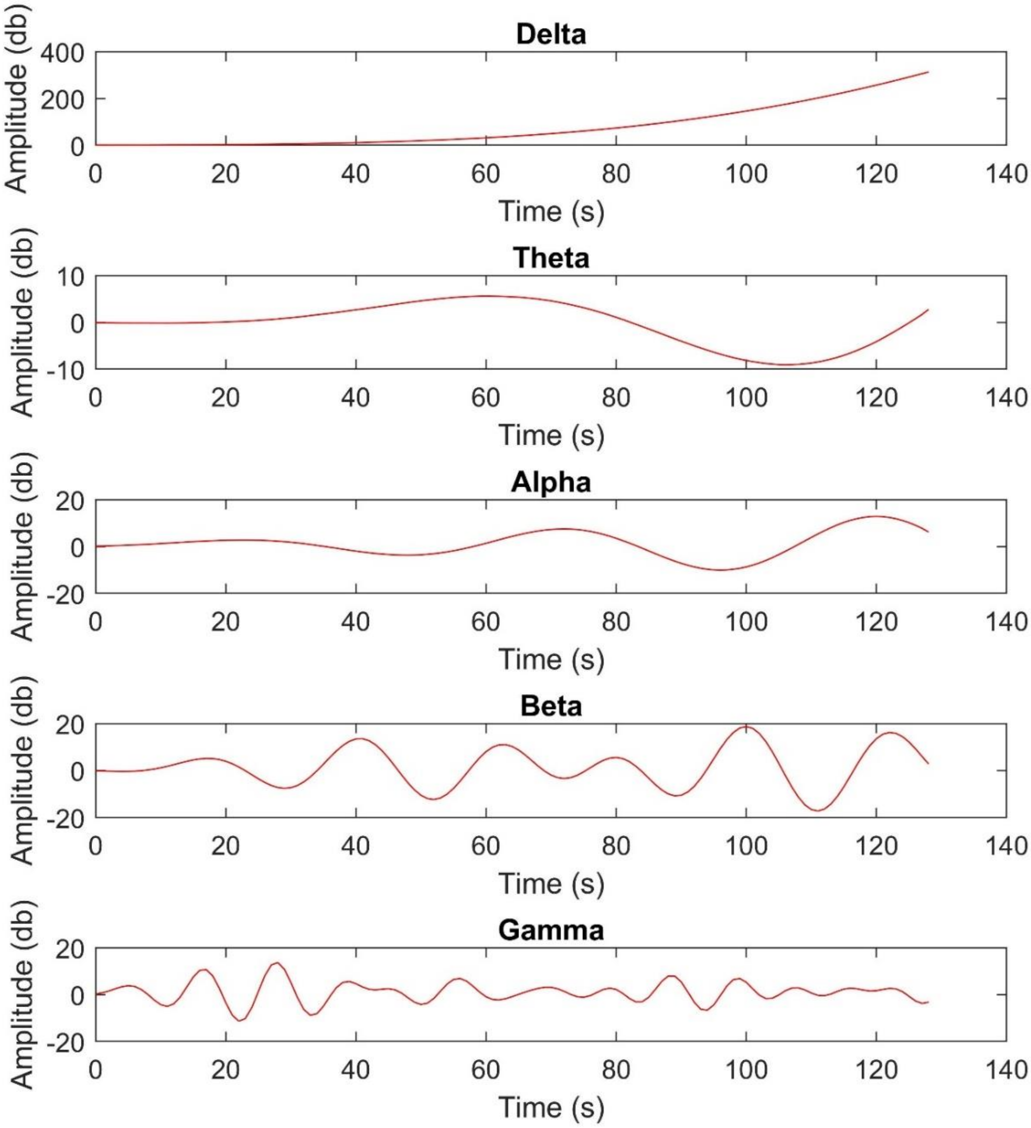

Figure 2.4: An illustration of the various forms of normal EEG rhythms.

2.1.4 EEG signal acquisition

The international 10-20 electrode system is the standard for scalp electrode localization [17], as shown in Figure 2.5. The term 10-20 is the percentage of the distance between neighboring electrodes to the distance between the beginning and end of a row, including the midline between nasion and inion, the diameter above the forehead and ears, or the frontal electrodes linking the left and right earlobes

[18]. Electrical conductivity between electrodes and shielded wires is necessary for the recognition of EEG signals with extremely low amplitude. Electrode gel, alcohol, or other liquids are often used to improve the transmissibility between the skin and the electrodes [18], [19], [20]. A montage is the arrangement of electrodes. Display montages are categorised as either bipolar or monopolar/referential [15]. Each electrode is connected to one or two adjacent electrodes in bipolar montages. Every channel in monopolar montages represents the difference between a selected electrode and a reference electrode.

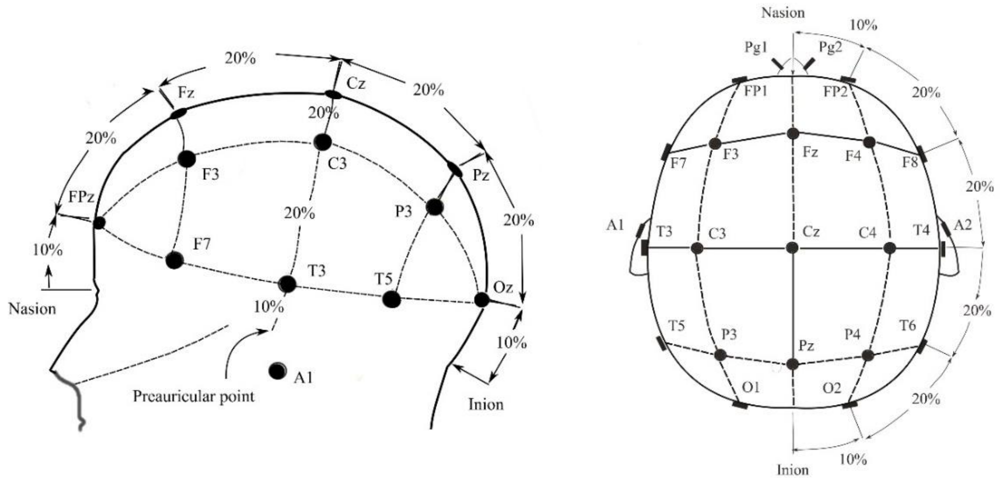

Figure 2.5: International 10-20 Standard EEG electrode configuration. Nz and Iz represent nasion and inion, respectively.

2.2 Brain Connectivity

Brain networks connect with other parts in order to perform a certain function or task. Brain connectivity is the term used to define the phenomenon of interconnection that occurs in the brain. Brain connection exposes the routes or the manner in which information is transferred across different parts of the brain [21]. Most measurements of brain connectivity are bivariate, which involves interactions between two brain areas or electrodes. Brain connectivity exists in three different methods: structural, functional, and effective [22], [23].

2.2.1 Structural connectivity

Anatomical connectedness or structural connectivity is described as: a structure of synaptic transmission that connects clusters of neurons or neuronal components., as well as the related structural biophysical properties encoded by measurables including the synaptic strength or efficacy. Diffusion-weighted imaging (DWI) is among the most common imaging techniques, and it may be applied in a variety of ways to examine the transit of hydrogen atoms in the brain [24]. Anatomical connectivity is constant for short periods (seconds to minutes). It is impacted by neurological disorders, including Alzheimer, schizophrenia, and epilepsy.

2.2.2 Functional connectivity

The term "functional connectivity" refers to "temporal correlations between spatially distant neurophysiological events" [22], [25]. Functional connectivity is based on time series data from brain recordings and is symmetrical, therefore, the connection between i and j is the same as the connectivity between j and i. Neuroimaging techniques like EEG, MEG, and fMRI can capture this data. Several approaches have been utilized to estimate functional connectivity between time series, such as correlation, phase synchronization, and coherence [26], [27].

2.2.3 Effective connectivity

Effective connectivity or directed functional connectivity estimates causal relationships and shows the flow of information between various parts of the brain [22]. This supports researchers in better understanding the processes that underlie neural dynamics [28], [29].

2.2.3.1 Granger causality

Granger causality states that if a signal X_1 "Granger-causes" another signal X_2, then previous values of X_1 should include information that helps predict X_2 [30]. Let $x_1(t)$ and $x_2(t)$ be zero-mean signals with t = 1, 2, 3,..., M in the context of linear Granger causality (GC) and the bivariate case. Consequently, the Q-order univariate autoregressive (AR) model for $x_1(t)$ and $x_2(t)$ is as follows:

$$x_1(t)=\sum_{k=1}^{q} a_{1_k} x_1(t\text{-}k)+E_1(t) \tag{2.1}$$

$$x_2(t)=\sum_{k=1}^{q} a_{2_k} x_2(t\text{-}k)+E_2(t) \tag{2.2}$$

where $e_1(t)$ and $e_2(t)$ are the estimation error of $x_1(t)$ and $x_2(t)$ respectively. They depend only on each signal's past a_{1_τ} and a_{2_τ} are the autoregressive coefficient [31]. The Q-order bivariate ARX (autoregressive with external input) model is considered by [32].

$$x_1(t)=\sum_{k=1}^{q} a_k x_1(t\text{-}k)+\sum_{k=1}^{q} b_k x_2(t\text{-}k)+E_1(t), \tag{2.3}$$

$$x_2(t) = \sum_{k=1}^{q} c_k x_1(t\text{-}k) + \sum_{k=1}^{q} d_\tau x_2(t\text{-}k) + E_2(t), \qquad 2.4$$

where a_j, b_j, c_j and d_j are the ARX coefficients and $e_1(t)$ and $e_2(t)$ are the prediction errors.

2.2.3.2 Multivariate data

A multivariate data set is defined as a set of two or more than two signals (channels), since these signals were recorded simultaneously. This extra information can be found in the relationships between signals. Cross-quantities, such as correlation and covariance, are examples of metrics that describe such relationships.

2.2.3.3 Autoregressive (AR) model

The definition of the multivariate AR model (MVAR) for p-channels set (a set of p concurrently discovered signals) is:

$$X(t) = \sum_{k=1}^{q} A(j) X(t\text{-}k) + E(t), \qquad 2.5$$

where: $X(t) = [X_1(t), X_2(t), \ldots X_k(t)]^T$ is a vector containing the values of p signals at time t, $E(t) = [E_1(t), E_2(t), \ldots E_p(t)]^T$ is a vector of p values of noise at time t, q is the sample rank, and $A(k)$ is a m x m matrix of parameters with latency k.

2.2.3.4 Model selection

The most standard method for selecting model order (p) is to create a series of sample rank and then pick one that eliminates one or more informational requirements when compared all through the model order range. The following are two frequently applied information criteria: Akaike's Information Criterion (AIC) and Bayesian’s Information Criterion (BIC).

$$AIC\ (q) = e^{[det(V)]} + 2pk^2/N \qquad 2.6$$

$$BIC\ (q) = e^{[det(V)]} + e^{[(N)pk2/N]} \qquad 2.7$$

where V is the noise $E(t)$ autocorrelation, N represents the total of observations, q is the model order, and k is the number of channels.

2.2.3.5 Effective connectivity measures

Direct transfer function

The frequency domain may be used to translate the AR model equation 2.5. obtaining:

$$E(f) = A(f) * X(f),$$

$$(f) = A^{-1}(f)E(f) = H(f)E(f),$$

$$(f) = \left(\sum_{m=0}^{q} A(m) exp(-2\pi imf\Delta t) \right)^{-1} \qquad 2.8$$

That relationship is represented by a strainght filter that operates on noise input Ei and outputs signals Xi. The power spectrum may be simply estimated using the formula.:

$$S(f) = \boldsymbol{X}(f)\boldsymbol{X}^*(f) = \boldsymbol{H}(f)\boldsymbol{E}(f)\boldsymbol{E}^*(f)\boldsymbol{H}^*(f) = \boldsymbol{H}(f)\boldsymbol{V}\boldsymbol{H}^*(f) \qquad 2.9$$

The preceding equation yields the whole spectral power matrices with auto-spectra on the lateral and merge off the diagonal. In a single step, the (standard) coherence can be determined from the cross-spectra:

$$K_{ij}(f)=\frac{S_{ij}(f)}{\sqrt{S_{ii}(f)S_{jj}(f)}} \tag{2.10}$$

In addition to spectrum information, the essential parts of the matrix *H* also carry phase component; consequently, they can be used to establish the causal value — the directed transfer function. It was initially given in its the standardized form [33]:

$$\gamma_{xy}{}^{2}(f)=\frac{\left|\boldsymbol{H}_{xy}(f)\right|^{2}}{\sum_{m=1}^{k}\left|\boldsymbol{H}_{im}(f)\right|^{2}} \tag{2.11}$$

This value represents the proportion of the input from channel *y* to channel *x* versus the total flows at channel *x*. The normalised DTF has a value from 0 and 1, where 0 represents no influence and 1 represents the maximum influence.

For detection of a transmission, the DTF without normalization was proposed, in the form of:

$$\theta_{ij}{}^{2}(f)=\left|\boldsymbol{H}_{ij}(f)\right|^{2} \tag{2.12}$$

The nonnormalized DTF is not constrained to the interval 0 to 1. As seen in [34], its quantity is equivalent to the channel connection intensity.

In multivariate systems, several transmission patterns between channels are available. For example, a signal can be transferred directly or indirectly from one channel to another via one or more channels. Common effective connectivity measures are:

PDC (partial directed coherence)

Kaminski et al. [35] introduced PDC as a frequency domain indicator of direct causal relationships, This is determined by the modified frequency response theory parameters *A(f)* as opposed to the components of $H(f) = 1/(A\,(f))$.

$$PDC_{ij}(f) = \frac{A_{ij}(f)}{\sqrt{\boldsymbol{a}^{*}_{j}(f)\boldsymbol{a}_{j}(f)}} \qquad 2.13$$

2.3 Networks and graphs

The human brain's connectivity patterns have been a growing subject of interest in the area of human neuroscience and can be explored using graph theory [36]–[38]. Graph theory is a mathematical model that was created with the objective of studying physiological, medical, and computational modeling [26]. Recently, graph theory-based techniques have made important contributions to our understanding of the brain's connectivity architecture, especially in functional and anatomical brain networks [39], [40]. Additionally, it assists to our study of brain disorders, higher cognitive functions, and the elderly [41]–[44].

2.3.1 Nodes and edges

Networks in graph theory have two basic components: nodes and their pairwise connections as edges/links. A graph can be divided into four categories: 1) weighted and directed, 2) binary and directed, 3) weighted and undirected, and 4) binary and undirected [45], as shown in Figure 2.6A. Each of them has its own characteristics. An other method for displaying a graph is using an adjacency matrix, where nodes are represented by rows or columns and edges by matrix components (Figure 2.6B).

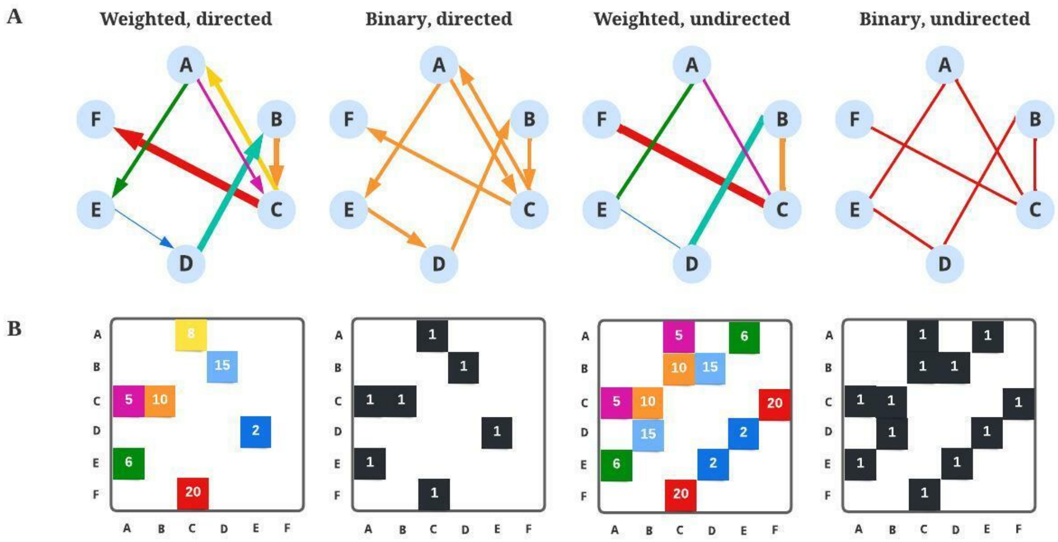

Figure 2.6: The different kinds of graph and their associated adjacency matrix (modified from [45])

In functional brain networks, nodes represent brain regions or scalp EEG electrode locations (Figure 2.7—nodes) [46]. Edges (links) quantify functional connectivity between nodes (Figure 2.7—links), in which they can be characterized based on their weight and directionality [47]. Binary links indicate the existence or lack of connections (Figure 2.6A), whereas weighted links provide information about the strength of the connections (Figure 2.6A,B) [47]. The size, density, or coherence of anatomical pathways can be described by their weights in anatomical networks, whereas weights in functional and effective networks can be used to reflect the magnitudes of correlational or causative relationships [47].

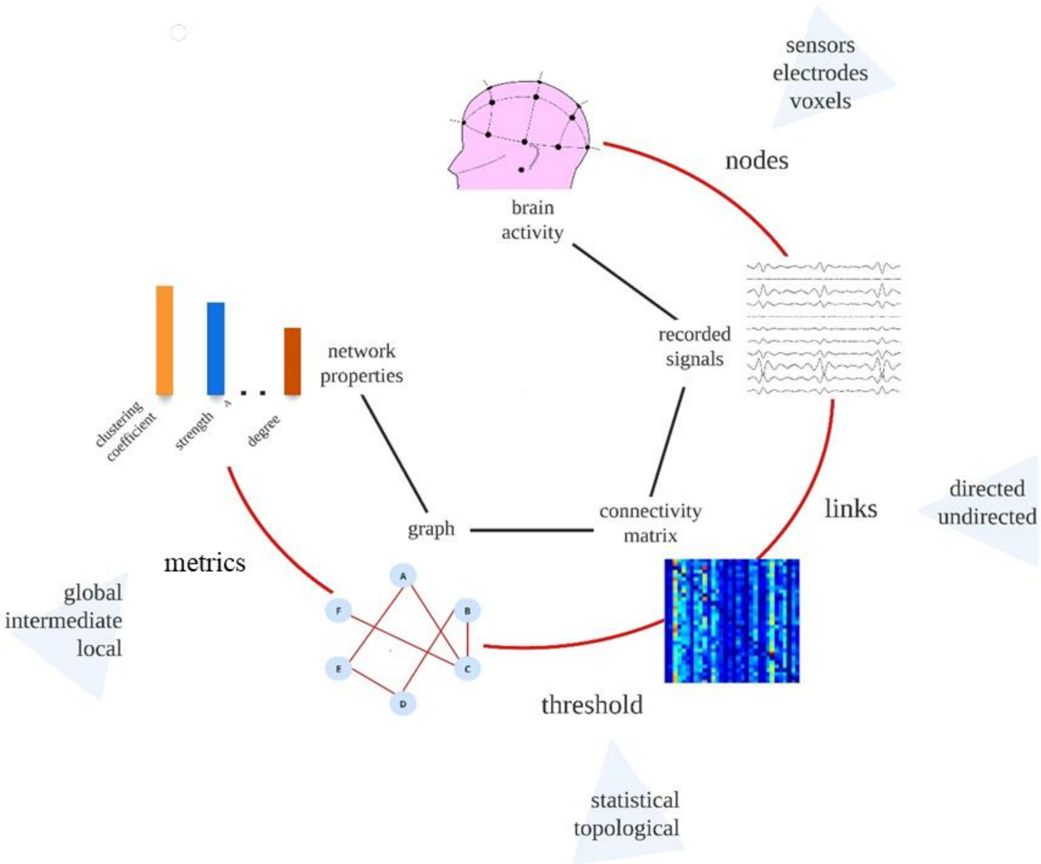

Figure 2.7: Flowchart for analysis of functional connectivity and graph theory (modified from [47])

2.3.2 Threshold

The graph is first thresholded before the network metrics are computed (Figure 2.7—threshold). The threshold is essential for improving the ratio of signal/noise by eliminating low and insignificant connections that correspond to spurious connections. There have been a variety of techniques utilized, such as absolute-thresholding, in which a uniform threshold is used to preserve only connections with a certain weight [48], [49]; density-thresholding, in which a relative threshold is applied to keep quantity of edges consistent among subjects [47], for example, 10000 edges [50]. Recently, more advanced thresholding algorithms are being considered that utilize group-level statistics to eliminate network connections [51]. Proportional-thresholding was used to keep just the connections that were observed in a certain proportion of participants [52].

2.4 Graph network measure

Graph theory can characterize global and local network features quantitatively (Figure 2.7—metrics). In this part, our attention is drawn to the network measurements that are employed throughout this thesis (chapter 4), i.e., node degree and node strength.

2.4.1 Node degree

In a network, node degree is described as the number of connections that connect it to the other nodes in the network. The degree of the nodes is used as a foundation for all other network measurements, and most other metrics are eventually related to node degree [53]. For example, nodal degree is the simplest method of identifying hubs in a network. A high degree node in a network may often influence its neighbors. In the directed graphs, the in-degree and out-degree represent the number of entering and exiting links, respectively [40].

2.4.2 Node strength

Linked nodes in a binary system are either zero or one, whereas in weighted networks, edges can provide a range of values that indicate variations in the intensity of connectivity between brain regions [53]. These values should be integers and can vary from null to a huge number. In other circumstances, like correlation-based networks, edge weights range from -1 to 1. The strength of a node corresponds to the total of the strengths of its neighboring links [47], denoted by *s*.

$$s_i = \sum_{j \neq i} w_{ij} \tag{2.14}$$

where *wij* denotes the strength or weight of the edge linking the nodes *i* and *j*. Equation (2.1) describes the in-strength of node i in directed networks. Instead of summing the rows of the weighted adjacency matrix, the out-strength can be calculated [53].

2.4.3 Clustering Coefficient

Clustering Coefficient (CC) is a calculation of network clustering or segregation [54], a description of the ratio being used of a node's neighbors that are also linked among themselves (nodes with high CC thus form locally interconnected clusters) [9]. The clustering coefficient quantifies the propensity of nodes to build local clusters and is thus an indicator of the graph's local segregation. The CC of the entire network is the mean of all nodes' CCs. In this study, we calculate the strength and CC of each ROI that previously averaged several channels into each ROI [55].

The graph's clustering coefficient may be expressed mathematically as

$$CC=\frac{1}{N}\sum_{i\in N}C_i=$$

$$\frac{1}{N}\sum_{i\in N}\frac{t_i}{\left(k_i^{out}+k_i^{in}\right)\left(k_i^{out}+k_i^{in}-1\right)-2\sum_{i\in N}A_{ij}A_{ij}} \quad 2.15$$

where C_i is the local clustering coefficient; t_i quantity of triangles surrounding each node; k_i^{in} and k_i^{out} is the a node's in-degree and out-degree; and A_{ij}, A_{ji} is the entry of the adjacency matrix.

2.4.4 Local Efficiency

The opposite of the average length of the shortest path to each neighbor of a given node. It is a measure of the average efficiency of information transport within local subgraphs or neighborhoods, as expressed by equation 2.14:

$$E_{loc}=\frac{1}{N_{G_i}\left(N_{G_i}-1\right)}\sum_{j,k\epsilon G_i}\frac{1}{L_{j,k}} \quad 2.16$$

where N_{G_i} stands for the total number of vertices in subgraph G_i. Network nodes' local efficiency is measured on a scale from 0 to 1, with 1 being the highest possible local efficiency.

Chapter 3 Directed EEG Functional Connectivity Features to Reveal Different Attention Indexes Using Hierarchical Clustering

3.1 Introduction

Previous studies suggest that watching movies has an impact on the human senses [56], [57]. For instance, using functional magnetic resonance imaging (fMRI), Anderson et al. [57] investigated the connectivity of the subjects' brain networks while they watched regular movie fight scenes. Furthermore, an EEG study discovered that viewing various music video clips elicited human emotion [58]. In addition, brain activity in responses to the video could be used in BCI (Brain–Computer Interface) applications and recovery. For example, Moon *et al.* [59] proposed using interval electroencephalography (EEG) features with various band combinations to regulate a viewer's attention span for video segments. Mercado *et al.* [60] created a game based on a BCI video for autism neurofeedback training.

Familiarity is another critical factor that affects audiovisual perception. Familiarity is described as the condition of being extremely knowledgeable about something, and it is believed to play an essential role in our daily lives because it directly impacts decision-making [61], business [62], and social interaction [63]. It also makes a significant contribution to the field of human–computer interaction [64]. Recently, researchers have used neuroimaging techniques to investigate familiarity effects [65], [66]. For example, Thammasan *et al.* [66] examine the relation between brain response and song familiarity in terms of EEG power spectrum and connectivity. They discovered that musical familiarity influences a person's strength and functional connectivity. Interestingly, numerous recent studies have established that familiarity has the ability to alter attention. Barenholtz et al. determined that a person's attention to a video is affected by familiarity [67]. In face recognition study, unknown faces attract less attention than familiar ones [68]. Kumagai *et al.* [65] explored the concept that familiarity and attention level have an effect on the level of entrainment.

Attention is a challenging state to quantify across self-report. EEG is a powerful tool for assessing changes in attentional states. Several studies have evaluated attention using a brain–computer interface (BCI). For instance, Patsis *et al.* [69] used BCI to assess the attention states of Tetris players. Lim *et al.* [70] created a novel technique for regulating ADHD children during a stroop exercise utilizing EEG sensors. They recommend that a training game in accordance with BCI could be employed to treat ADHD effectively. According to Rosenberg *et al.* [71], the strength of functional connectivity during a vigilance task predicted subject-to-subject achievement variance. In addition, several studies have been conducted to investigate the EEG features associated with ADHD [72], [73]. They showed that amplitudes of ADHD patients decreased in the ratio of $\beta 1$/theta compared with healthy children over the frontal regions.

The goal of this study was to evaluate whether attention indexes differed among subjects while viewing a music video. To accomplish this, we estimated functional connectivity using the Directed Transfer Function (DTF), and subjects were then grouped with hierarchical clustering techniques based on their attention index (alpha/theta ratio). DTF has been utilized effectively in prior studies [74]–[76] and has been shown to be virtually resistant to volume conduction. DTF is an effective connectivity approach that employs the Multivariate Autoregressive Model and is based on the phase difference between channels (MVAR).

Individual variability based on an EEG characteristic has been explored using clustering analysis. For instance, Buckelmüller *et al.* [77], used an EEG sleep study to investigate intra-individual and inter-individual variability using a similarity measure and cluster analysis. Maksimenko *et al.* [78] performed a cluster analysis based on the subject's EEG features using a hierarchical clustering approach. They discovered that the EEG activity associated with mental tasks varied significantly between subjects.

In this study, we examined the association between between directed connectivity characteristics and attention indexes. Based on [65], [29], [30], we propose the following hypotheses:

1) Subjects' attention indexes can differ significantly when watching familiar or unfamiliar videos.
2) Fronto-central information flow may be associated with attentional processing.

This is the first study that shows attention index clustering through directed functional connectivity.

3.2 Method

3.2.1 Dataset

In this study, we have evaluated the performance of our proposed framework on two publicly available emotional EEG datasets, the DEAP dataset [81], and the AMIGOS dataset [82], presented in the following detail these two datasets.

3.2.1.1 DEAP Dataset

DEAP is a comprehensive dataset consisting of electroencephalograms, physiological, and visual inputs, collected from 32 participants (16 female) in age from 19 to 37 using the Biosemi ActiveTwo system from 32 silver chloride (AgCl) electrodes with frequency sampling of 512 Hz. Participants viewed 40 video stimuli presented on the 17-inch screen. Across the entire experiment, a total of 40 videos were presented across 40 trials, with each trial including a progress display lasting two seconds, a baseline recording lasting five seconds, and a music video lasting sixty seconds, as displayed in Figure 3.1. Participants were instructed to report their valence, arousal, dominance, and liking at continuous rating at the end of each video session for scale of 1 (low) to 9 (high), as well as their familiarity on a discrete scale of 1 ("never saw the video before the experiment") to 5 ("knew it very well ").

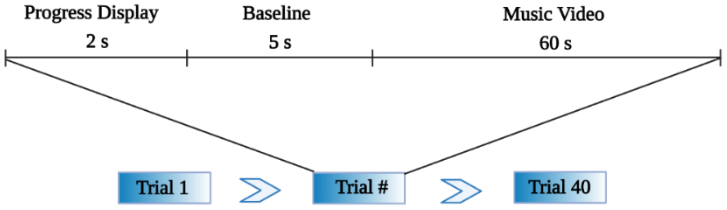

Figure 3.1: Experiment protocol of the DEAP dataset.

Table 3.1: A review of the literature utilizing the DEAP dataset.

Author (year)	**Method**	**Main Findings**
Naser et al. (2021) [83]	Power spectral density (PSD), wavelet, Spearman's correlation, graph analysis	The importance of high-frequency bands and hemisphere features in emotions
Preira et al. (2021) [84]	Higher Order Crossings extraction (HOC) and Support Vector Machines (SVM)	Signals longer than 60 seconds provide more accurate classification results
Khateeb et al. (2021) [85]	Hjorth parameters and entropy, short-time Fourier transform, and wavelet. Support vector machine (SVM)	Average accuracy was 65.92 percent for nine categories of emotions, comprising pleased, satisfied, relaxed, aroused, neutral, quiet, stressed, and unpleasant
Sharma et al. (2020) [86]	Higher order statistics (HOS) and deep learning	Eighty-one point one percent classification accuracy with four-labeled emotion classes
Lan et al. (2019) [87]	Machine learning with Domain adaptation approach	The applied approach improves accuracy by 7.25 to 13.40 percent
Zheng et al. (2019) [88]	Power spectral density (PSD), differential entropy (DE) for feature extraction methods. SVM, KNN, and discriminative Graph regularized Extreme Learning Machine (GELM)	A classification accuracy of 69.67 percent throughout all quadrants of VA space.
Alazrai et al. (2018) [89]	Quadratic time-frequency distribution (QTFD) and SVM	The classification accuracies ranged from 73.8 percent to 86.2 percent on average across the four different labeling methods for emotions.
Thammasan et al. (2016) [66]	PSD, Fractal Dimension, Phase synchronization index (PSI), Correlation, and Coherence for feature extraction. SVM, Multilayer perceptron	Unfamiliar songs are great for the development of an emotion recognition system.

3.2.1.2 AMIGOS Dataset

In the AMIGOS dataset, EEG signals were obtained in two experiments, however, in this study, we only used recorded EEG signals presented 16 short movies (length 250 s) to 40 participants in an individual setting (the first experiments) [82].

Each trial consist of a 5 - second baseline signal is shown at the beginning of the recording session and video (< 250s), as displayed in Figure 3.2. Following each trial, participants were asked to report their emotional states in terms of arousal, valence, dominance, liking, and familiarity on a nine-point scale.

In this dataset, the EEG was recorded with the use of the Emotiv EPOC Neuroheadset, which included 14 channels, 128 hertz, and 14 bit resolution. The following EEG channels are: AF3, F7, F3, FC5, T7, P7, O1, O2, P8, T8, FC6, F4, F8, and AF4, according to the 10-20 [90] system. Table 3.1 demonstrates several studies that have already used the AMIGOS dataset.

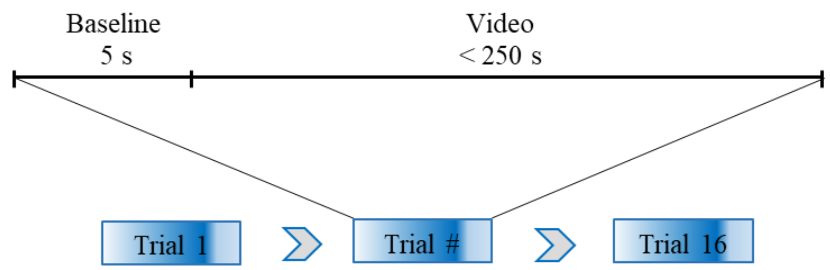

Figure 3.2: Experiment protocol of the AMIGOS dataset.

Table 3.2: A review of the literatugre utilizing the AMIGOS dataset

Author (year)	Method	Main Findings
Tejada et al. (2020) [91]	Machine learning using Fractal dimension (FD), the differential entropy (DE), the rational asymmetry (RASM) and differential asymmetry (DASM) as features	The average classification performance of valence and arousal labels were greater than chance, but did not pass 70 percent accuracy in the various situations studied
Bhattacharyya et al. (2022) [92]	Machine learning using Multivariate variational mode decomposition (MVMD) and multivariate time–frequency (TF)	Applied method reached 99.03, 97.59, and 97.75 percent accuracy for categorizing arousal, dominance, and valence emotions, respectively
Yin et al. (2022) [93]	Deep learning model and multimodal Fusion (electrodermal activity (EDA) and music feature) for Emotion Recognition	The combination of EDA with music provides a solution that is both reliable and efficient for emotion identification on a broad scale
Topic et al. (2021) [94]	Deep learning with Feature maps based on the topographic (TOPO-FM) and holographic (HOLO-FM)	The proposed approaches have the potential to enhance the rate of emotion identification on datasets of varying sizes
Zhao et al. (2015) [95]	Multiscale Convolutional Neural Networks (Multiscale CNNs) and a biologically inspired decision fusion model for multimodal affective states recognition	The fusion model greatly enhances the accuracy of the identification of emotional states compared to the results obtained using single-modality signals

3.2.2 EEG signal preprocessing

For both the DEAP and AMIGOS datasets, the EEG signals were preprocessed as described below [81][96]: 1) EEG data were resampled at 128 Hz; 2) electrooculography (EOG) artifacts have been eliminated through the application of the blind source separation (BSS) approach.; 3) high-frequency electromyography (EMG) artifacts were eliminated using a bandpass filter (4–45 Hz); and 4) EEG data were averaged to the common reference. The present study examined the correlation of directed functional connectigggvity features and attention indexes during familiar and unfamiliar conditions. Furthermore, we used the experiment's familiarity rating. The following procedure was used to define familiarity ratings: 3–5 are considered to be familiar, while 1–2 are considered to be unfamiliar.

In the DEAP dataset, three subjects lacked familiarity ratings: subjects 2, 15, and 23. Subjects 4, 5, 25, and 27 were also eliminated due to an unbalanced familiar-to-unfamiliar stimulus ratio of 0.30. Finally, subjects 9, 11, 22, and 24 were ignored due to bad channels (> 25% of total channels). We then conducted an analysis using only the data from the remaining 21 subjects. In the AMIGOS dataset, S39 did not provide an unfamiliar rating, therefore S39 was removed for further analysis. Furthermore, we analyzed 39 subjects' EEG data from the AMIGOS dataset. An illustration of the EEG data analysis is presented in Figure 3.3.

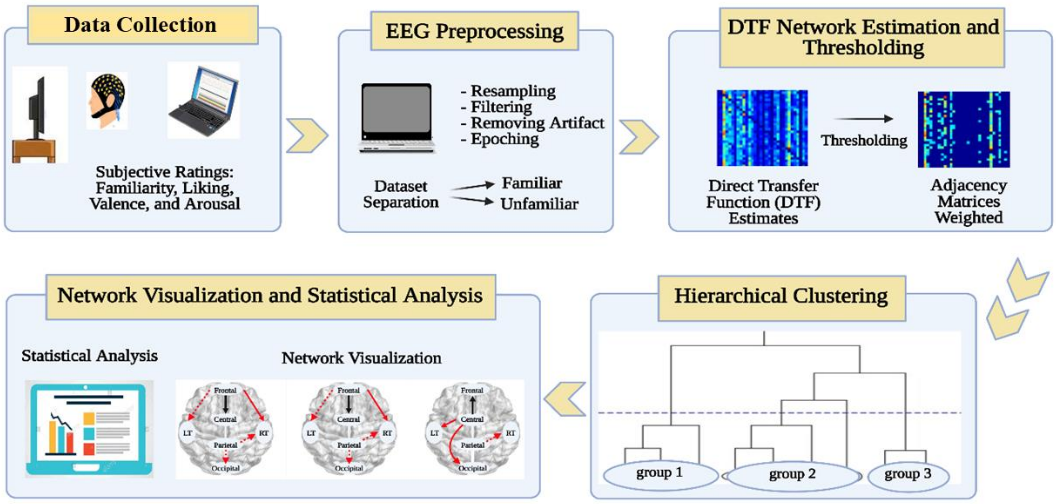

Figure 3.3: Flowchart of EEG data analysis.

3.2.3 Directed Transfer Function

As we explained in Chapter 2, the Directed Transfer Function (DTF) was used to assess the functional connectivity between cortical areas of the human brain.

In the estimation of DTF, the following expression describes the attribute of the fit of the model given in the equation below:

$$k * d < 0.1 * N, \qquad 3.1$$

where N represents the window size, d represents the model order, and k represents the number of EEG channels. The model order d was estimated using the Akaike information criterion (AIC).

For both evaluated datasets, we employed the eConnectome toolbox [77] to calculate the DTF from each subject with model order O = 5 for the window length N = 1920 (128 Hz *15 s). The m x m adjacency matrix of *DTFij (f)*, derived from *m*-channel EEG data at frequency *f*, reflects "information flow" through electrode *j* towards electrode *i*. Furthermore, we obtained a 32 x 32 matrix of DTF values for the DEAP dataset and a 14 x 14 matrix of DTF values for the AMIGOS dataset by using the median over the frequency bands of interest, as calculated using equation:

$$mDTFj{\rightarrow}i(f) = median(DTFj{\rightarrow}i\ (\Delta f)), \qquad 3.2$$

This value was decomposed into the theta (4-7 Hz) and alpha (8-13 Hz) bands. Second, we applied a threshold for each subject's DTF matrix. The threshold was defined as one standard deviation after the median [98]. Then, the ratio between alpha and theta was calculated with the following formula:

$$mDTF^{k} = mDTF_{j\rightarrow i\ alpha}/mDTF_{j\rightarrow i\ theta}, \qquad 3.3$$

The ratio between the alpha and theta bands is often employed as a measure of attentional processing in the brain [79], [99].

In the DEAP dataset, the DTF adjacency matrix (32x32) was segmented into six regions of interest (ROIs) as follows: frontal (FP1, FP2, Fz, F3, F4, AF3, AF4, F7, F8), central (FC1, FC2, FC5, FC6, Cz, C3, C4), left temporal (T7, CP5), right temporal (T8, CP6), parietal (CP1, CP2, Pz, P3, P4, P7, P8), and occipital (PO3, PO4, Oz, O1, O2). Besides, in the AMIGOS dataset, the DTF adjacency matrix (14 x 14) was segmented as follows: frontal (AF3, AF4, F3, F4, F7, F8), central (FC5, FC6), left temporal (T7), right temporal (T8), parietal (P7, P8), and occipital (O1, O2).

Finally, $mDTF^k$ values (equation 3.6) were calculated for both familiar and unfamiliar conditions. Then, we averaged the $mDTF^k$ between two ROIs—for example, between frontal and central areas—which was computed according to equation:

$$mDTF^k{}_{central \rightarrow frontal} = \frac{1}{xy} \sum_x \sum_y mDTF_{j(x) \rightarrow i(y)}, \qquad 3.4$$

where x denotes electrodes in the central region and y represents electrodes in the frontal region. As a result, for each participant, we achieved a 6 x 6 DTF adjacency matrix.

3.2.4 Analysis of clustering

When evaluating individual variability, the clustering approach attempts to group the subjects' EEG features according to their similarity. Hierarchical clustering is a type of clustering algorithm that is widely used. In comparison to other methods, hierarchical clustering has several advantages: 1) It provides meaningful presentation and investigation since the output is displayed in the form of a dendrogram, and the number of groups can be estimated by analyzing the dendrogram [100]; and 2) When applied to datasets of a manageable size, its implementation is simple. A dendrogram is a specific kind of tree diagram that illustrates hierarchical clustering, or the links between objects that are very similar to one another. A dendrogram shows how far apart the objects or clusters are, starting with the individual objects at the bottom and going all the way up to the one huge number at the top, as illustrated in Figure 3.4b.

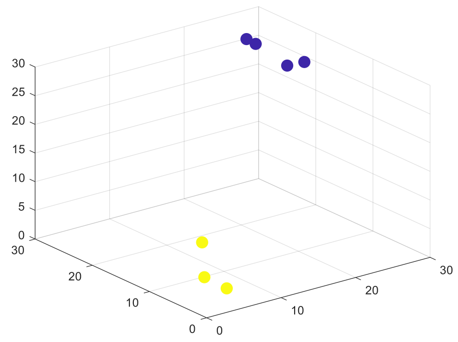

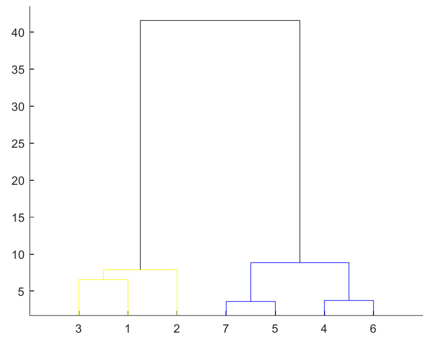

Figure 3.4: (a) Scatter plot and (b) dendogram.

3.2.4.1 The Euclidean distance

In unsupervised learning, we define objects as similar to each other if they are closer in distance, as described in Figure 3.5. Euclidean distance is the foundation of numerous similarity and dissimilarity measurements.

Figure 3.5: Distance and similarity

The Euclidean distance is the distance that is calculated to be the shortest between any two points. The formula below presents the Euclidean distance for data points *p* and *q*:

$$d(s,t)=\sqrt{(s_1-t_1)^2+(s_2-t_2)^2} \qquad 3.5$$

This formula is derived from the Pythagorean theorema. Observe the diagram in Figure 3.6 below:

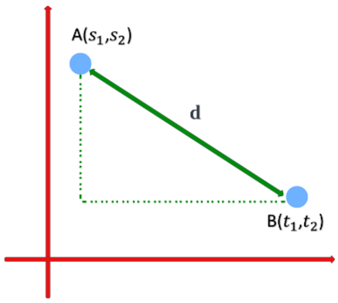

Figure 3.6: Euclidean distance

The formula of the Euclidean distance for n dimensional space:

$$D_e=\sqrt{\sum_{i=1}^{n}(s_i-t_i)^2} \qquad 3.6$$

where:

n = number of dimensions

s_i, t_i = data points

3.2.4.2 Hierarchical clustering

Hierarchical clustering is often associated with heatmap. A heatmap is a visual illustration of data that uses a color-coding method to indicate distinct values, in which the columns represent different samples and the rows represent measurements from different observations, as described in Figure 3.7a. Hierarchical clustering arranges rows and columns based on similarity (using the previously explained Euclidian distance formula).This makes it easy to see the correlations in the data, as described in Figure 3.7b. often comes with a dendogram (a visualization form of hierarchical clustering), which indicates the similarity and the order in which the clusters were formed, as described in Figure 3.7c.

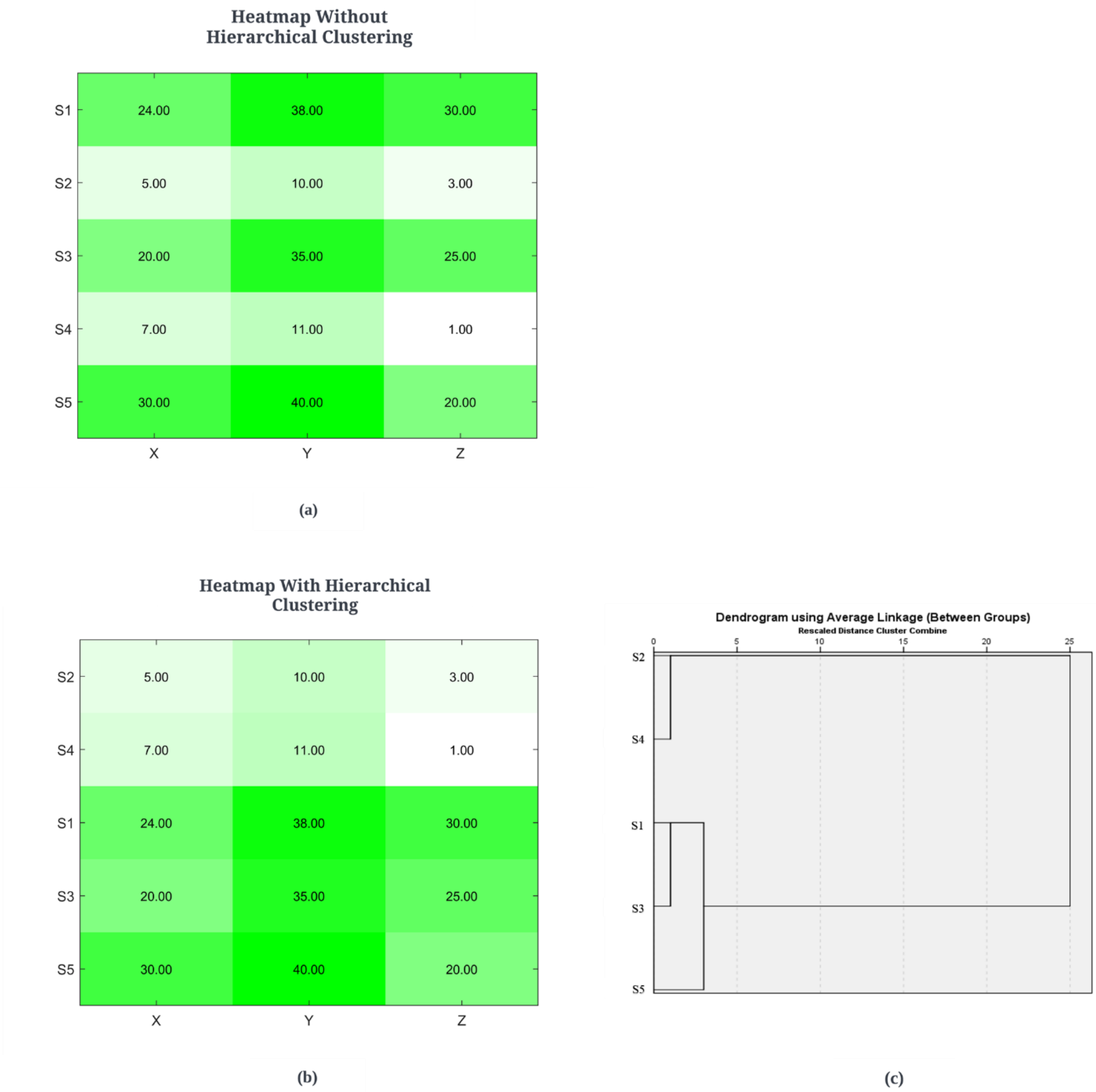

Figure 3.7: Data visualization using (a) a heatmap without hierarchical clustering, (b) a heatmap with hierarchical clustering, and (c) a dendogram corresponding with heatmap.

For example, in Figure 3.7, we explain in detail calculating the Euclidean distance between S2 and S4 and between S1 and S3 below:

$d_{S1,S2} = \sqrt{(5\text{-}24)^2+(10\text{-}38)^2+(3\text{-}30)^2}$

$d_{S1,S2} = \sqrt{(5\text{-}24)^2+(10\text{-}38)^2+(3\text{-}30)^2}$

$d_{S1,S2} = \sqrt{(19)^2+(28)^2+(27)^2}$

$d_{S1,S2} = \sqrt{361+784+729} = 43{,}29$

The distance between S1 and S2 = 43,29.

$$d_{S2,S4} = \sqrt{(difference\ in\ sample\ X)^2 + (difference\ in\ sample\ Y)^2 + (difference\ in\ sample\ Z)^2} \quad 3.7$$

$$d_{S2,S4} = \sqrt{(7-5)^2 + (11-10)^2 + (1-3)^2}$$

$$d_{S2,S4} = \sqrt{(2)^2 + (1)^2 + (-2)^2}$$

$$d_{S2,S4} = \sqrt{9} = 3$$

The distance between S2 and S4 = 3.

Based on this calculation, we can see the reason why S2 and S4 are in the same cluster (close to each other in the dendogram, visualized in Figure 3.7c).

3.2.4.3 The proposed framework

We used hierarchical clustering in this section [101], [102] to categorize participants according to the characteristics of their features, particularly the ratio of information flow between alpha and theta in the fronto-central areas. The clustering procedure for our proposed method is described below:

1) We used the Directed Transfer Function (DTF) to figure out connectivity features for both familiar and unfamiliar situations.
2) We performed hierarchical clustering using the Euclidean distance matrix.
3) We considered the number of groups using the Dunn Index, a cluster validity index proposed in [103] that aims to identify "compact and well-separated clusters". Dunn's Index, DI_m, for m clusters is defined by equation:

$$DI_m = \min_{1 \le j \le m} \left\{ \min_{1 \le i \le m, j \ne i} \left\{ \frac{\delta(C_i, C_j)}{\max_{1 \le k \le m} \Delta_k} \right\} \right\}, \quad 3.8$$

where $\delta(C_{i,} C_j)$ is the inter-cluster Euclidian distance between clusters Ci and Cj, Δ_k = max $d(s,t)$, and $d(s,t)$ represents the Euclidian distance of the observations s and t in cluster Ci.

3.2.5 Statistical analysis

We performed a one-way analysis of variance (ANOVA), then the Bonferroni post hoc test was applied for multiple comparisons (0.05) to assess whether there were significant differences between groups and between conditions.

3.3 Result

3.3.1 Clustering result

3.3.1.1 DEAP dataset

Table 3.3 presents the feature used in this study for hierarchical clustering, consist of the information flow in the fronto-central areas under familiar and unfamiliar conditions across 21 participants.

Table 3.3: Functional connectivity features of DEAP dataset from the frontal to central and from the central to frontal areas for both familiar and unfamiliar conditions for each of the 21 subjects.

Subject	Information flow from frontal to central		Information flow from central to frontal	
	Familiar (F2C_F)	Unfamiliar (F2C_Uf)	Familiar (C2F_F)	Unfamiliar (C2F_Uf)
1	0.022	0.038	0.039	0.000
2	0.163	0.190	0.096	0.176
3	0.028	0.013	0.000	0.014
4	0.000	0.000	0.022	0.110
5	0.016	0.063	0.093	0.006
6	0.086	0.045	0.116	0.307
7	0.123	0.127	0.021	0.198
8	0.104	0.084	0.167	0.290
9	0.107	0.103	0.082	0.024
10	0.000	0.056	0.109	0.165
11	0.157	0.080	0.071	0.000
12	0.116	0.230	0.051	0.105
13	0.084	0.209	0.009	0.068
14	0.031	0.088	0.035	0.075
15	0.125	0.261	0.161	0.108
16	0.014	0.037	0.049	0.009
17	0.096	0.212	0.000	0.180
18	0.000	0.000	0.011	0.066
19	0.037	0.000	0.140	0.143
20	0.096	0.008	0.083	0.119
21	0.109	0.082	0.041	0.100

Figure 3.8 presents the DEAP feature used for input in the clustering from 21 subjects, i.e., information flow from the frontal to central and from the central to frontal under familiar and unfamiliar conditions. The color in the heatmap indicates the values of feature.

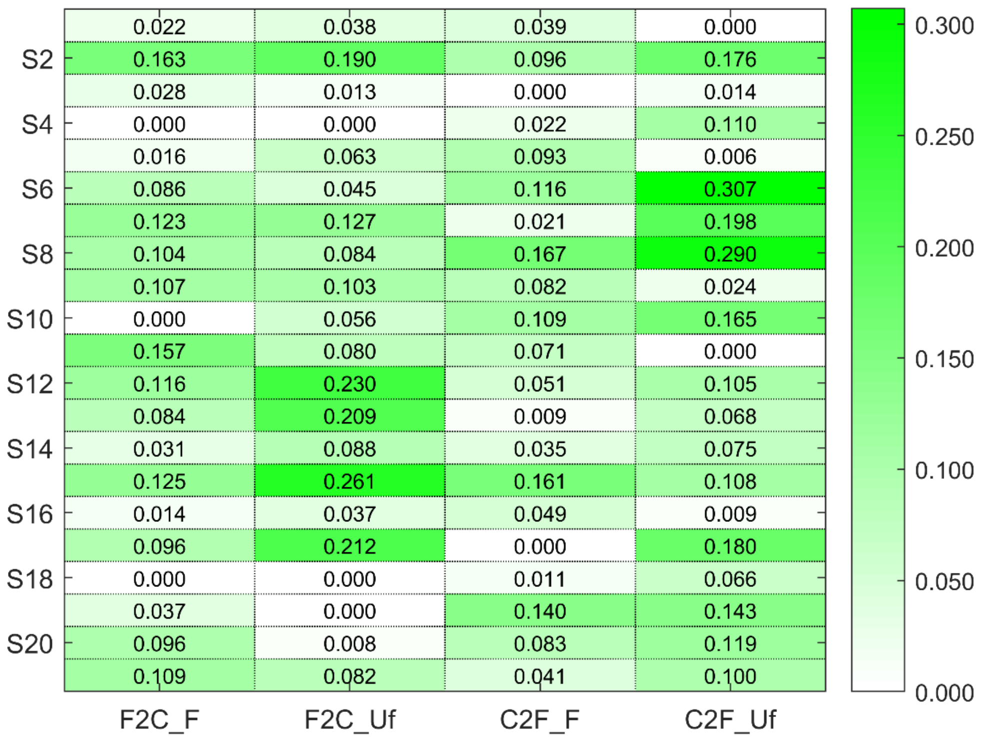

Figure 3.8: A heatmap represents feature of DEAP dataset applied for clustering, consisting information flow from frontal to central and information flow from central to frontal under familiar and unfamiliar conditions for each of the 21 subjects.

The dendrogram in Figure 3.9 displays the result of clustering. Furthermore, the Dunn Index was calculated to evaluate the performance of the hierarchical clustering technique, which ranged from 0 to 1, where a higher value indicated a more appropriate cluster framework [104]. It can be seen from Table 3.4 that the Dunn index obtained the highest value for three and four clusters.

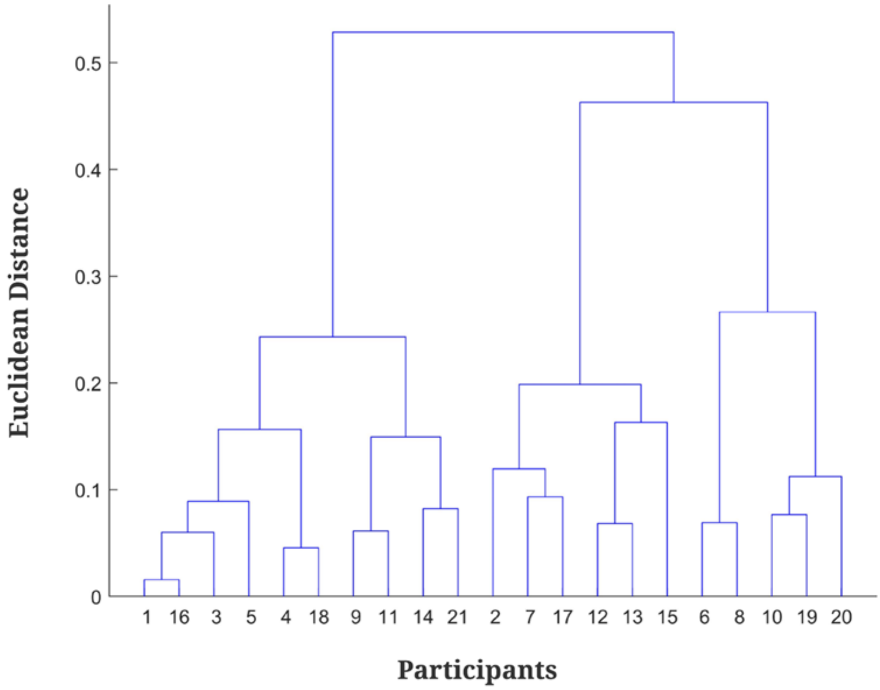

Figure 3.9: The clustering result of the DEAP dataset.

Table 3.4: Performance evaluation of the DEAP dataset

Number of Cluster	Dunn Index
2	0.286
3	0.416
4	0.416
5	0.405

From this table, we then observed the dendogram again to determine the best number of clusters based on the Dunn Index value. The group will then be easier to divide into three clusters rather than four. Based on this consideration, all participants were then divided into three clusters (groups), as demonstrated in Figure 3.10, particularly in the form of a heatmap (Figure 3.10a) and dendogram (Figure 3.10b).

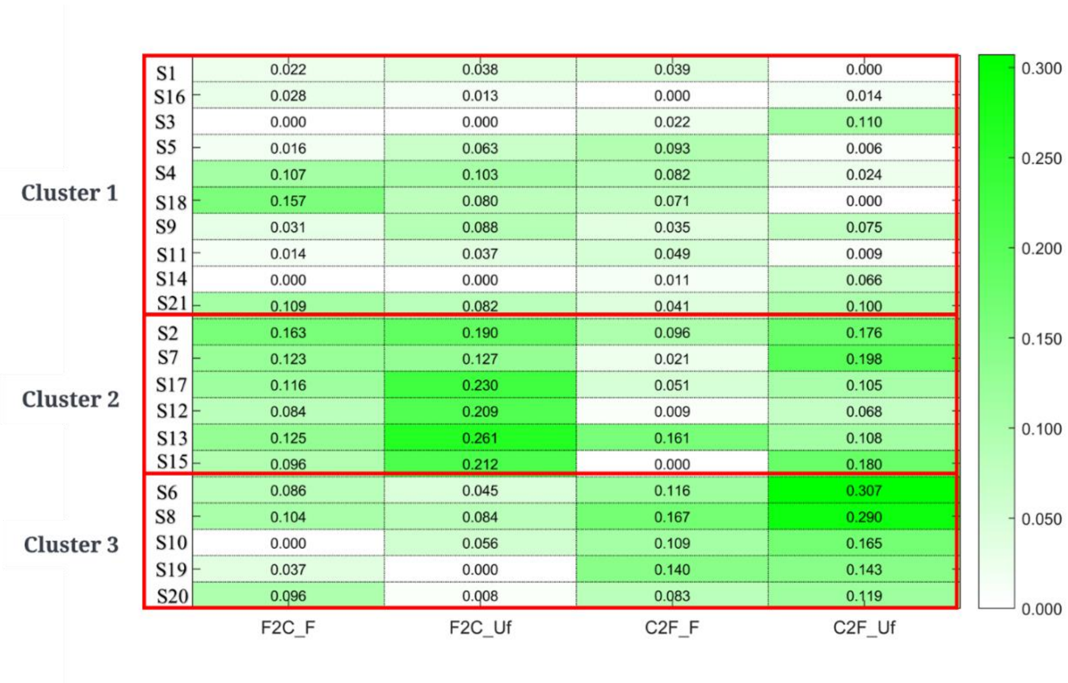

(a)

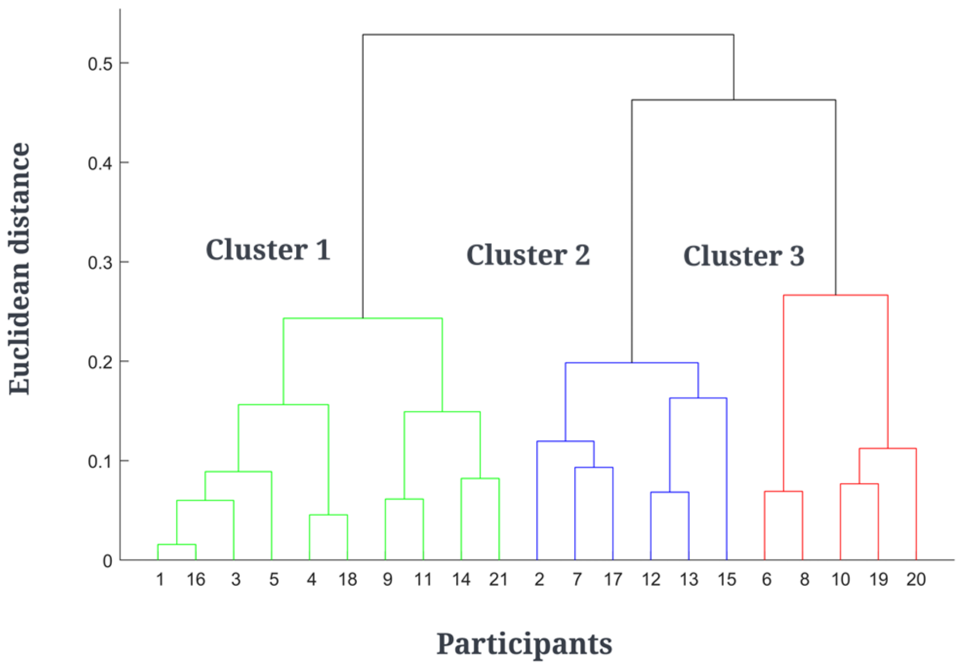

(b)

Figure 3.10: Hierarchical clustering on the DEAP dataset resulting in optimum performance in three clusters, then visualized in (a) the heatmap and (b) the dendogram .

The ratio of spectral energy in the high-to-low-frequency bands can be used to describe both attention and its stability [78]. Liutsyuk et al. [105] reported that the ratio of the spectral powers (SPs) of the beta 1 and theta rhythms was significantly higher in children with a good working performance (as determined by the scores of the go/no-go test and the corrective test). Palva *et al.* [106] discovered that attention-demanding tasks increase alpha-band amplitude. The power of the alpha band was increased during a training period with a video game in a paired-task presentation that required subjects to expand their attentional switching [107]. Based on previous findings, we believe that the alpha/theta ratio is positively related to attention level. Hence, we label index categories based on the value of the total feature calculated from all input features. For the DEAP dataset, we have three clusters (cluster 1, cluster 2, and cluster 3), which correspond to three index categories (low index (LI), high index (HI), and middle index (MI), respectively), as displayed in Table 3.5.

Table 3.5: A table showing the results of the average feature in each cluster in the DEAP dataset and then determining the index category based on the calculation of the total of all features.

Cluster	**Subject**	**Average Feature**				**Total**	**Index Category**
		F2C_F	**F2C_Uf**	**C2F_F**	**C2F_Uf**		
Cluster 1	S1, S16, S3, S5, S4, S18, S9 ,S11, S14, S21	0.048	0.050	0.044	0.040	0.183	Low Index (LI)
Cluster 2	S2, S7, S17, S12, S13, S15	0.118	0.205	0.056	0.139	0.518	High Index (HI)
Cluster 3	S6, S8, S10, S19, S20	0.064	0.038	0.123	0.205	0.431	Middle Index (MI)

3.3.1.2 AMIGOS dataset

Table 3.6 presents the feature of AMIGOS dataset used in this part for hierarchical clustering, consist of the information flow in the fronto-central areas under familiar and unfamiliar conditions across 39 participants.

Table 3.6: Functional connectivity features of the AMIGOS dataset used in this part for hierarchical clustering, consisting of the information flow in the fronto-central areas under familiar and unfamiliar conditions across 39 participants.

Subject	Information flow from frontal to central		Information flow from central to frontal	
	Familiar (F2C_F)	Unfamiliar (F2C_Uf)	Familiar (C2F_F)	Unfamiliar (C2F_Uf)
1	0.000	0.075	0.000	0.000
2	0.000	0.000	0.259	0.211
3	0.000	0.097	0.000	0.000
4	0.000	0.000	0.000	0.000
5	0.000	0.000	0.253	0.080
6	0.000	0.031	0.072	0.081
7	0.000	0.000	0.158	0.148
8	0.000	0.059	0.000	0.000
9	0.058	0.000	0.197	0.105
10	0.072	0.136	0.064	0.036
11	0.127	0.000	0.000	0.000
12	0.000	0.000	0.000	0.085
13	0.125	0.000	0.095	0.000
14	0.075	0.000	0.303	0.000
15	0.048	0.059	0.207	0.000
16	0.000	0.000	0.228	0.101
17	0.064	0.087	0.000	0.000
18	0.000	0.000	0.000	0.000
19	0.077	0.000	0.000	0.000
20	0.060	0.000	0.000	0.000
21	0.000	0.000	0.049	0.080
22	0.000	0.000	0.000	0.000
23	0.037	0.063	0.000	0.000
24	0.000	0.000	0.046	0.000
25	0.000	0.000	0.074	0.000
26	0.067	0.094	0.088	0.000
27	0.000	0.107	0.030	0.054
28	0.061	0.055	0.000	0.145
29	0.098	0.000	0.069	0.085
30	0.000	0.000	0.169	0.155
31	0.070	0.000	0.000	0.000
32	0.160	0.000	0.270	0.063
33	0.059	0.136	0.118	0.062
34	0.065	0.051	0.189	0.000
35	0.108	0.219	0.000	0.000
36	0.074	0.066	0.381	0.131
37	0.000	0.049	0.138	0.000
38	0.000	0.094	0.061	0.000
39	0.000	0.000	0.000	0.000

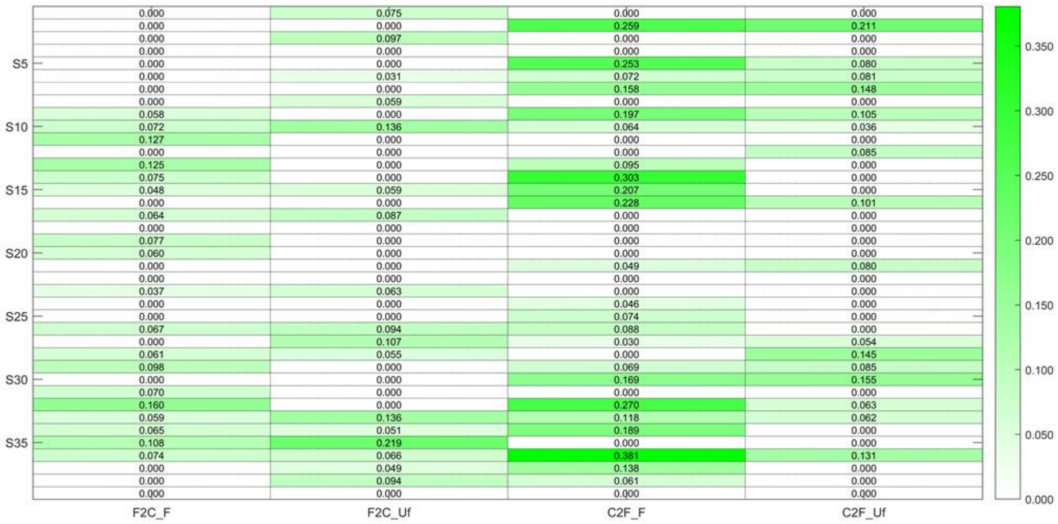

Figure 3.11: A heatmap represents features of the AMIGOS dataset applied for clustering, consisting of information flows in the fronto-central areas under familiar and unfamiliar conditions for each of the 39 subjects.

Figure 3.11 presents the DEAP feature used for input in the clustering of 39 subjects, i.e., information flow from the frontal to the central and from the central to the frontal under familiar and unfamiliar conditions. The color in the heatmap indicates the values of each feature.

The dendrogram in Figure 3.12 displays the result of clustering. Furthermore, the Dunn index was calculated to evaluate the performance of the hierarchical clustering technique, which ranged from 0 to 1. It can be seen from Table 3.7 that the Dunn Index obtained the highest value for two clusters. Based on this consideration, all participants were then divided into two clusters (groups), as demonstrated in the form of a heatmap (Figure 3.13a) and dendogram (Figure 3.13b).

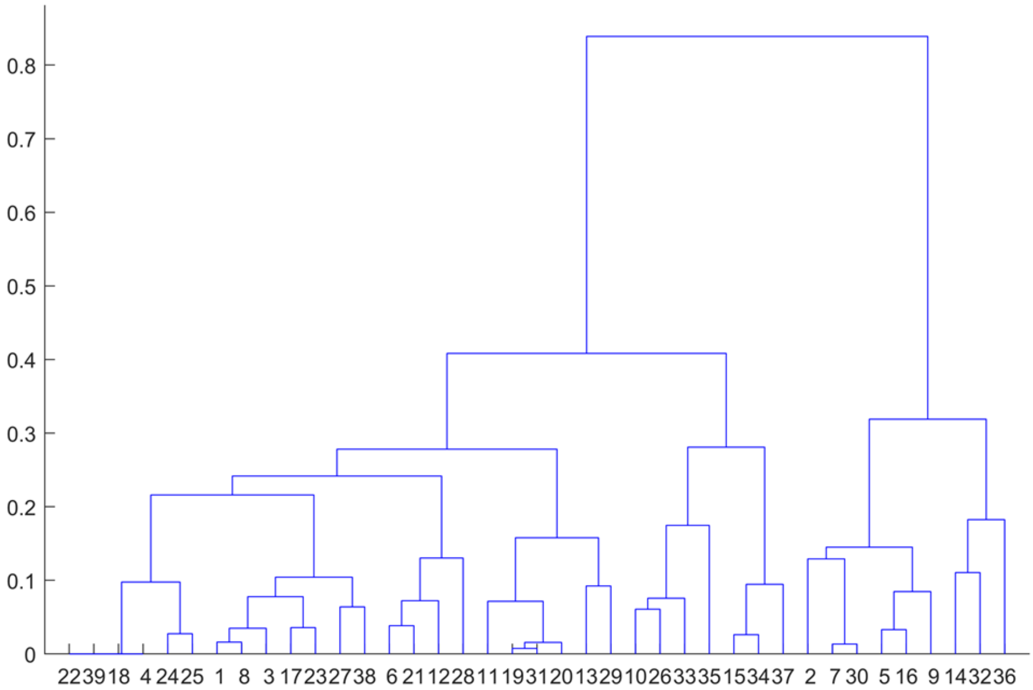

Figure 3.12: The clustering result of the AMIGOS dataset.

Table 3.7: Performance Evaluation of clustering for AMIGOS clustering.

Number of Cluster	Dunn Index
2	0.422
3	0.285
4	0.296
5	0.373

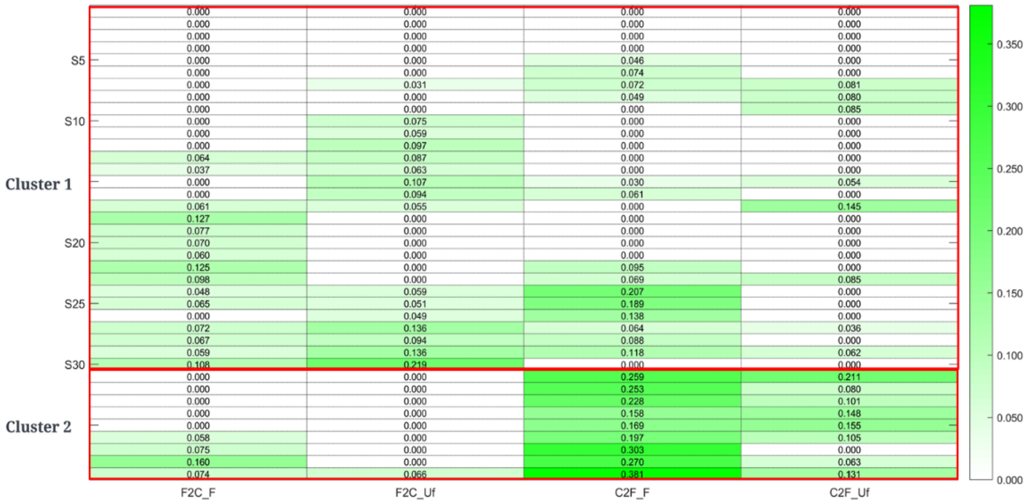

(a)

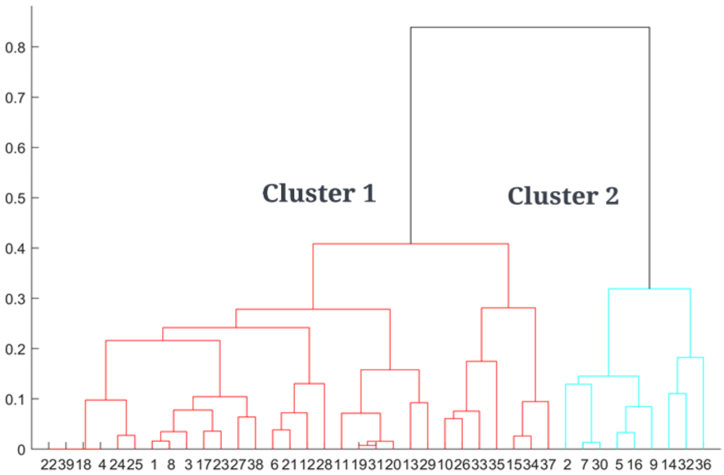

(b)

Figure 3.13: Hierarchical clustering on the AMIGOS dataset results in optimum performance in two clusters, which are then visualized in (a) the heatmap and (b) the dendogram.

As explained on page 55, the same consideration is used to determine the index category. We assume that the alpha/theta ratio is strongly related to the level of attention. This allows us to categorize cluster 1 and cluster 2 as having a low index (LI) and a high index (HI), respectively, as demonstrated in in Table 3.8.

Table 3.8: A table showing the results of the average feature in each cluster of the AMIGOS dataset and then determining the index category based on the calculation of the average, median, and total of all features.

Cluster	Subject	Average Feature				Total	Index Category
		F2C_F	F2C_Uf	C2F_F	C2F_Uf		
Cluster 1	S22, S39, S18, S4, S24, S25, S1, S8, S3, S17, S23, S27, S38, S6, S21, S12, S28, S11, S19, S31, S20, S13, S29, S10, S26, S33, S35, S15, S34, S37	0.038	0.047	0.043	0.021	0.149	Low Index (LI)
Cluster 2	S2, S7, S30, S5, S16, S9, S14, S32, S36	0.041	0.007	0.246	0.110	0.405	High Index (HI)

3.3.2 Group comparison

3.3.2.1 DEAP dataset

Based on the result of hierarchical clustering, three attention index groups were achieved, i.e., low index (LI), medium index (MI), and high index (HI) groups. We divide the average flow of information across subjects into three attention index groups as shown in the Table 3.9. Comparison between attention index groups under familiar and unfamiliar conditions were shown in Figure 3.14 and Figure 3.15, respectively. However, an increase in information flow that was positively related to an increase in the attention index was only seen from frontal to central, frontal to parietal, and frontal to occipital under familiar state.

Table 3.9: Group of subject and corresponding attention index level

No	Subject	Group of Attention Index
1	S1, S3, S4, S5, S9, S11, S14, S16, S18, S21	Low Index (LI)
2	S6, S8, S10, S19, S20	Middle Index (MI)
3	S2, S7, S12, S13, S15, S17	High Index (HI)

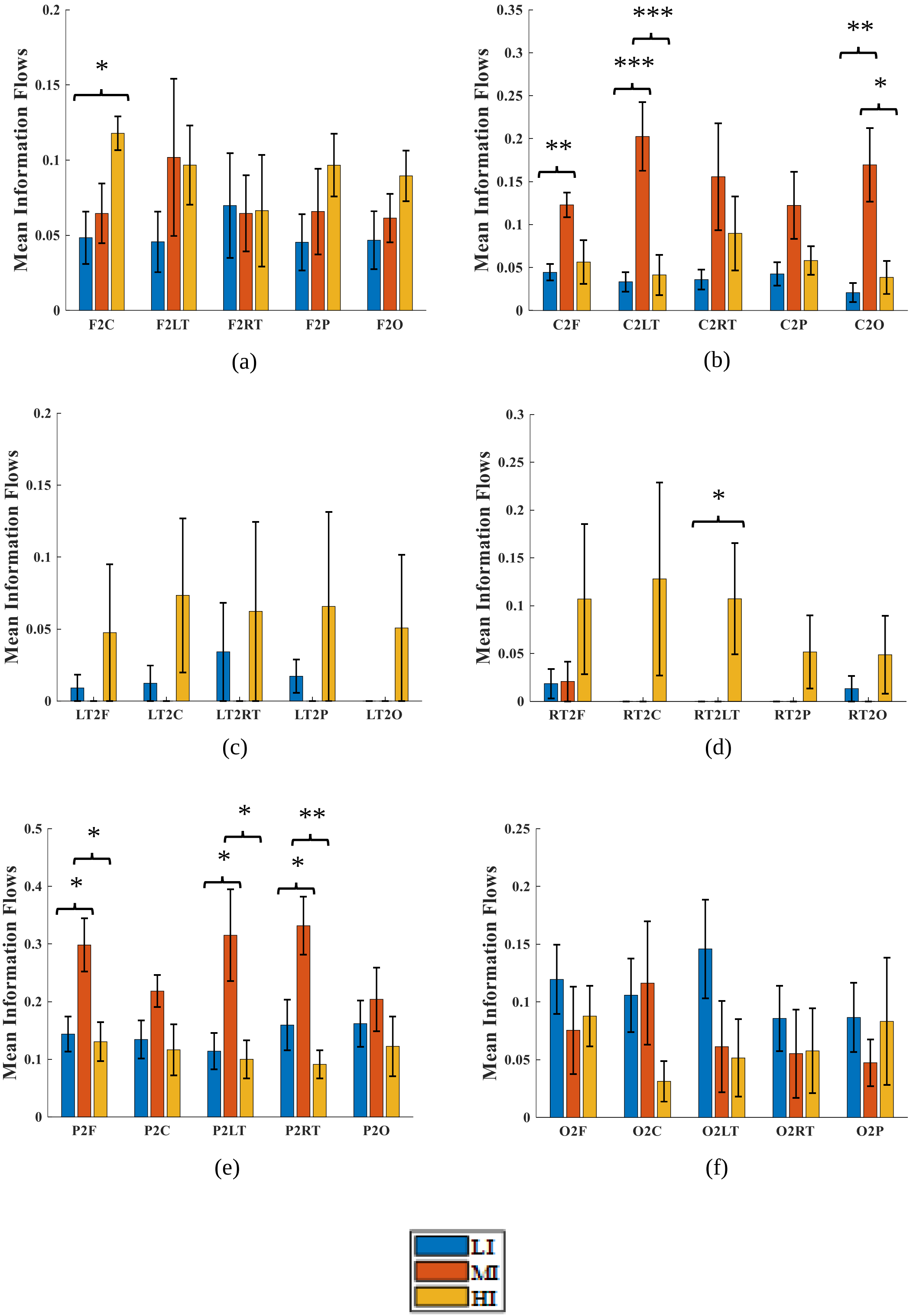

Figure 3.14: Averaged information flow strength for low index (LI), middle index (MI), and high index (HI) groups under familiar conditions from: (a) frontal (F), (b) central (C), (c) left temporal (LT), (d) right temporal (RT), (e) parietal (P), and (f) occipital (O) to other brain regions. * represents $\rho < 0.05$, ** represents $p < 0.01$, and *** represents $p < 0.001$. Error bars indicate standard deviation.

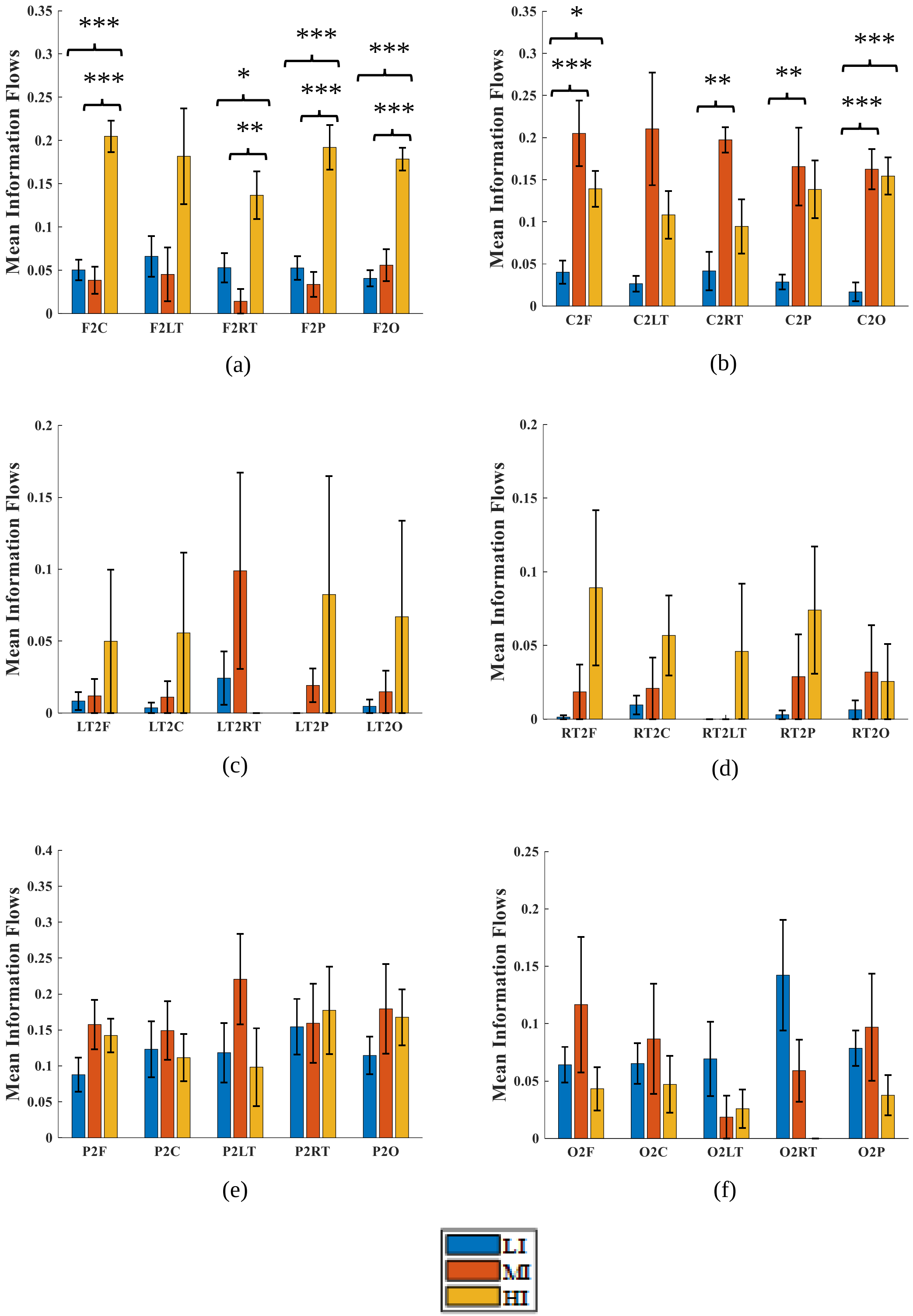

Figure 3.15: Averaged information flow strength for low index (LI), middle index (MI), and high index (HI) groups under unfamiliar conditions from: (a) frontal (F), (b) central (C), (c) left temporal (LT), (d) right temporal (RT), (e) parietal (P), and (f) occipital (O) to other brain regions. * represents $\rho < 0.05$, ** represents $p < 0.01$, and *** represents $p < 0.001$. Error bars indicate standard deviation.

In this study, the DTF adjacency matrix (32 x 32) was defined into six regions of interest (ROIs). From this, there are sixty features that represent information flows between six ROIs. Based on the result of hierarchical clustering, three attention index groups were achieved, i.e., low index (LI), medium index (MI), and high index (HI) groups. We divide the average flow of information across subjects into three attention index groups.

To evaluate the changes in information flows between ROIs, we performed a one-way ANOVA between attention index group (LI vs HI, LI vs MI, and LI vs HI), and between conditions (familiar vs unfamiliar) for each attention index groups (LI, MI, and HI). The Bonferroni correction was applied for multiple comparisons. Figure 3.16a-c demonstrate the statistical comparison of the directed connectivity of the three groups in the familiar condition. In Figure 3.16a, compared with the MI group, the LI group showed significant connections from central to frontal ($\rho < 0.01$), central to left temporal ($\rho < 0.001$), and central to occipital ($\rho < 0.001$). There were also flows from parietal to left temporal ($\rho < 0.05$), parietal to right temporal ($\rho < 0.05$), and parietal to frontal ($\rho < 0.05$). In the comparison of the LI group and the HI in Figure 3.16b, we found that the significant directed connectivity between ROIs was almost the same as LI vs MI with some differences; i.e., a significantly enhanced level of difference from parietal to the right temporal ($\rho < 0.01$), decreased level of difference from central to occipital ($\rho < 0.01$), and flows from central to frontal not exist. As shown in Figure 3.16c, the LI vs HI groups show a significant information flow from frontal to central (($\rho < 0.05$) and right temporal to left temporal ($\rho < 0.05$).

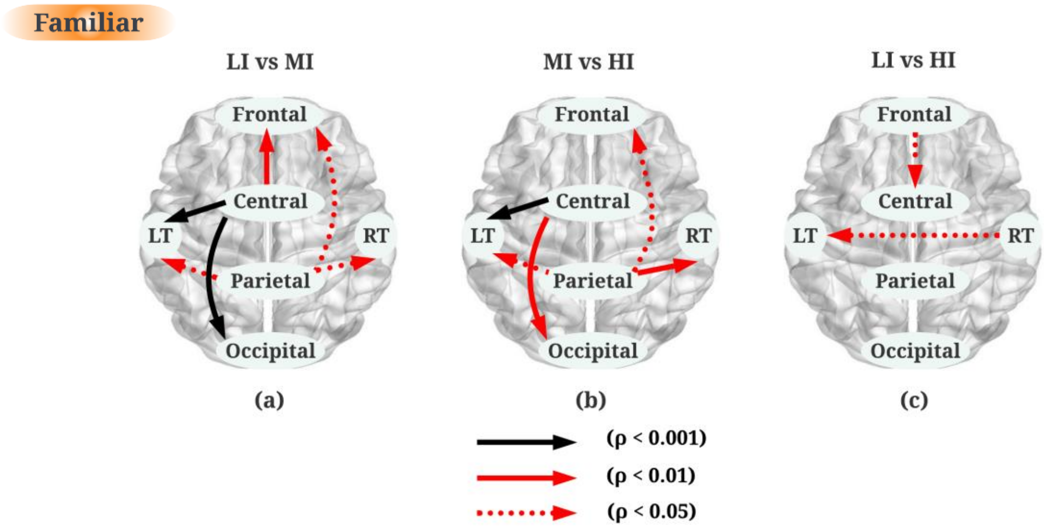

Figure 3.16: Comparison of connectivity strength between groups from all regions of interest (ROIs) during familiar conditions. LT and RT represent left temporal and right temporal areas, respectively. A one-way ANOVA was used to calculate significant differences with ρ values of $\rho < 0.001$, $\rho < 0.01$, and $\rho < 0.05$ (Bonferroni corrected), indicated by color.

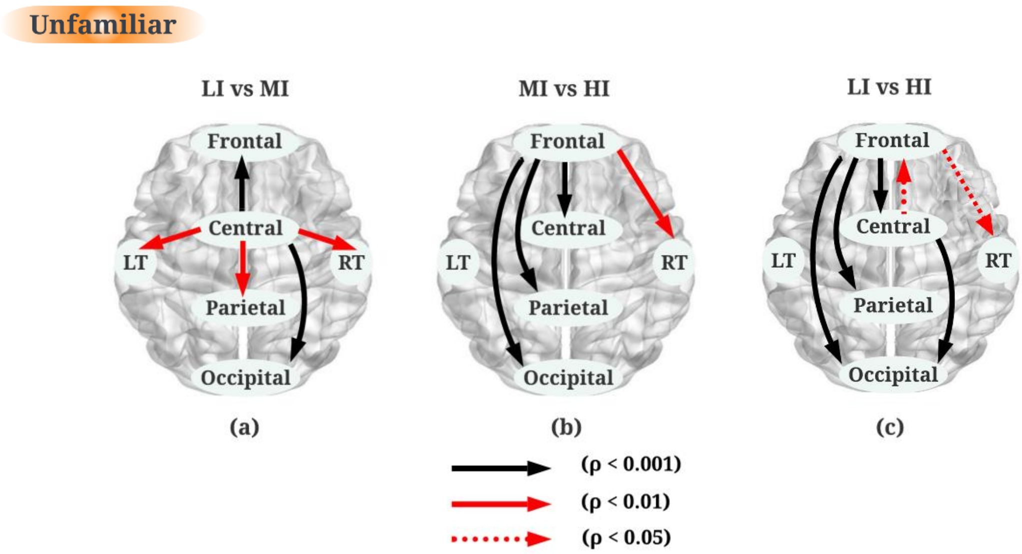

Figure 3.17: Comparison of connectivity strength between groups from all regions of interest (ROIs) during unfamiliar conditions. LT and RT represent left temporal and right temporal areas, respectively. A one-way ANOVA was used to calculate significant differences with ρ values of $\rho < 0.001$, $\rho < 0.01$, and $\rho < 0.05$ (Bonferroni corrected), indicated by color.

Figure 3.17a-c show information flows between groups in an unfamiliar state. For the LI vs MI groups in Figure 3.17a, we found significant connections from central to left temporal, central to right temporal ($\rho < 0.01$), central to parietal ($\rho < 0.01$), and central to occipital ($\rho < 0.001$). Comparison between MI and HI in Figure 3.17b demonstrates significant flows from frontal to central ($\rho < 0.001$), frontal to parietal ($\rho < 0.001$), frontal to occipital ($\rho < 0.001$), and frontal to right temporal ($\rho < 0.01$). Furthermore, competition of LI and HI in Figure 3.17c shows a pattern similar to MI vs HI with some differences; i.e., a significantly increased difference level from frontal to right temporal ($\rho < 0.001$) and additional significant flows from central to frontal ($\rho < 0.05$) and from central to occipital ($\rho < 0.001$).

3.3.2.2 AMIGOS dataset

Figure 3.18a-b show the statistical comparison of the directed connectivity of the two groups (LI and HI) under familiar and unfamiliar conditions, respectively.

As shown in Figure 3.18a, we found significant connections from central to frontal ($\rho < 0.001$), central to parietal ($\rho < 0.01$), and central to occipital ($\rho < 0.01$). There were also significant information flow from right temporal to frontal ($\rho < 0.05$) and from right temporal to left temporal ($\rho < 0.01$). Comparison between LI and HI in Figure 3.18b demonstrates significant flows from frontal to central ($\rho < 0.05$) and frontal frontal to occipital ($\rho < 0.05$). We also found significant connections from central to frontal ($\rho < 0.001$), and from central to parietal ($\rho < 0.05$). Significant information flow from left temporal to right temporal ($\rho < 0.05$) and from left temporal to occipital ($\rho < 0.05$).

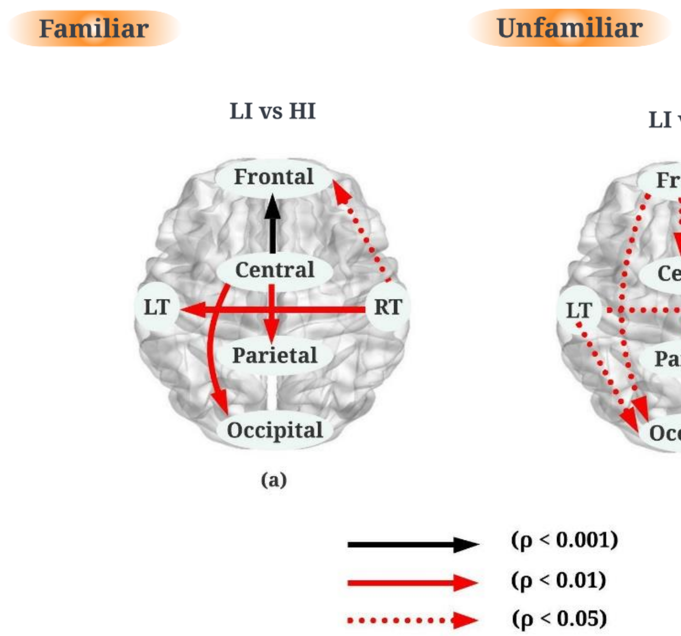

Figure 3.18: Comparison of connectivity strength between low-index (LI) and high-index (HI) groups of the AMIGOS dataset during (a) familiar conditions and (b) unfamiliar conditions from all regions of interest (ROIs). LT and RT represent left and right temporal areas, respectively. A one-way ANOVA was used to calculate significant differences, with ρ values of $\rho < 0.001$, $\rho < 0.01$, and $\rho < 0.05$ indicated by color.

3.3.3 State comparison

3.3.3.1 DEAP dataset

Comparisons between familiar and unfamiliar conditions for each of the three groups are shown in Figure 3.19, in which the unfamiliar state was higher than the familiar state. Significant information flows between two conditions only occurred in the HI group, as can be seen in Figure 3.19c. We discovered significant information flow from frontal central ($\rho < 0.01$), frontal to parietal ($\rho < 0.05$), and from frontal to occipital ($\rho < 0.01$). We also found significant connections from central to frontal ($\rho < 0.05$) and from central to occipital ($\rho < 0.01$).

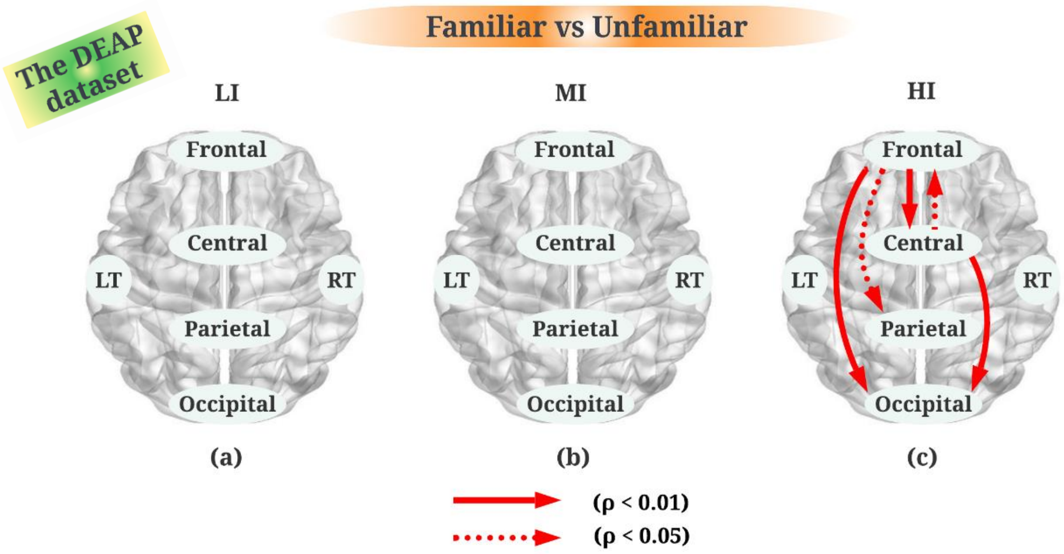

Figure 3.19: Evaluation of the strength of connectivity between familiar and unfamiliar conditions of the DEAP dataset across all ROIs: (a) low index (LI) group, (b)) high index (HI) group. The significant connection is reflected by line color with $\rho < 0.05$, where the unfamiliar conditions are higher than the familiar conditions.

3.3.3.2 AMIGOS dataset

The comparison between states (familiar vs unfamiliar) is shown in Figure 3.20.

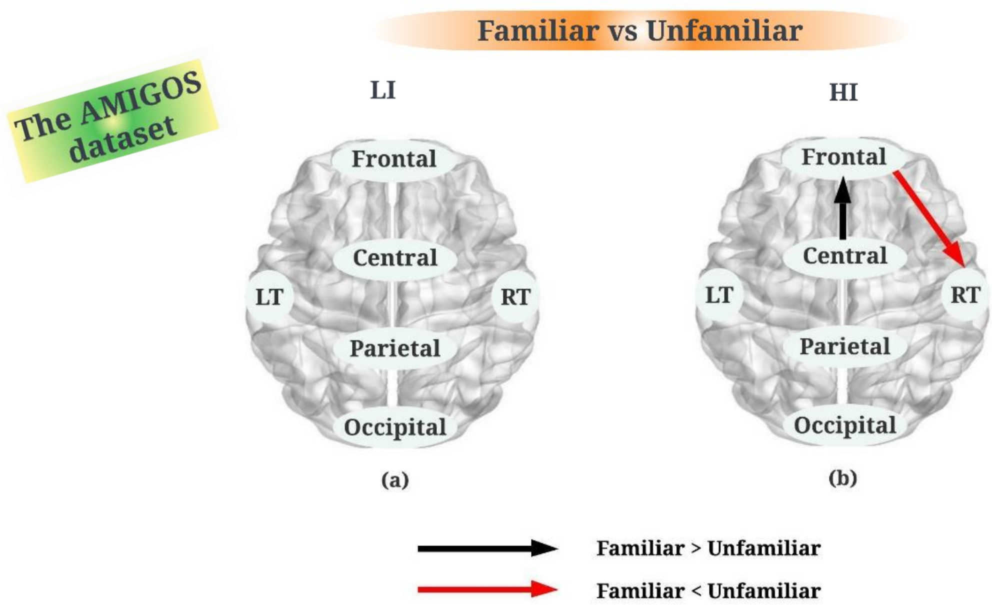

Figure 3.20: Evaluation of the strength of connectivity between familiar and unfamiliar conditions of the AMIGOS dataset across all ROIs: (a) low index (LI) group and (b) high index (HI) group. The significant connection is reflected by line color with $\rho < 0.05$.

In the AMIGOS dataset, we found significant information flow in the HI group, as shown in Figure 3.20b, from the central to the frontal regions, with familiar information being more important than unfamiliar information. Another significant link was discovered from the frontal to the right temporal ($\rho < 0.05$) with an unfamiliar state being greater than a familiar state.

3.4 Discussion

Previous studies have revealed that visual stimuli are an efficient way of engaging attention [33], [41], and [42]. Furthermore, Kumagai *et al.* reported that familiarity has the potential to generate attention [65]. For example, Barenholtz *et al.* found that familiarity can influence selective attention to audiovisual speech cues [67]. In this study, we examined subjects' attention indexes when they were watching familiar/unfamiliar movies. Hierarchical clustering was employed to cluster the attention index based on directed connectivity features. As we previously explained (see Methods), the attention index was obtained by the alpha/theta ratio from frontal to central and from central to frontal areas. Sadaghiani *et al.* confirmed this finding, observing a positive association between the alpha band and the blood oxygen level-dependent (BOLD) signal [110]. Additional research has revealed the presence of a fronto-central theta band in both healthy and ADHD subjects [111]–[113]. As an example, Mann *et al.* discovered that ADHD children's frontal and central theta activity increased when they were asked to draw [112]. An increase in activity has been reported in the dorsal anterior cingulate cortex (dACC) in attention to neutral stimuli [114]. Furthermore, an increase in activity was also observed in the ventrolateral prefrontal cortex (vlPFC) during the visual attention trial [115]. According to Dosenbach *et al.* [116], the cingulate, insular, and inferior frontal lobes are essential for mental ability. Similar to this, Banich *et al.* reported that the anterior cingulate cortex (ACC), dorsolateral prefrontal cortex (dlPFC), inferior frontal gyrus, and amygdala are the brain areas that are related to attention [117]. Taken together, our findings confirm and magnify previous results indicating that the increase in alpha/theta ratio over fronto-central regions was positively associated with attention performance.

In comparison between attention index groups, we observed significant information flows from the central to parietal. Interestingly, this phenomenon occurred for both the DEAP and AMIGOS datasets (Figure 3.16 and Figure 3.17). There is also evidence that the centro-parietal areas perform attention tasks [118]–[123]. For example, Horovits et al. reported that in an auditory oddball test, all participants had a P300 activation, mainly found in the centro-parietal regions [119]. In a ERP study conducted by Ferrary et al. [120], reported that late positive potential (LPP) over centro-parietal sensors was influenced by a classification task. Consistent with this, a greater late positive potential (LPP) is found at centro-parietal sensors for a target than for a nontarget [122]. These results are also in line with previous studies that found that the central and parietal regions play a critical role in attentional processing.

In addition, in comparison among groups in familiar states in the DEAP dataset, we observed significant information flows from the parietal to the left temporal and to the right temporal (Figure 3.16). Interestingly, flows from parietal to right temporal were enhanced with an increased attention index. According to a study by Wilterson *et al.*, the right temporoparietal junction (rTPJ) is engaged in an association that provides for the control of attention through awareness [124]. In a study integrating ERP and fMRI, Bledowski *et al.* reported the influential role of rTPJ in attentional tasks, e.g., identification of unusual stimuli in oddball tasks [125]. In addition, a summary meta-analysis confirmed the evidence about rTPJ's involvement in attention and social interaction [126]. These findings support the hypothesis that the TPJ, particularly the right TPJ, may be critical in the development of an attention schema.

Furthermore, we identified significant inflow in the occipital area in the DEAP and AMIGOS datasets. Our findings were corroborated by an earlier study of event-related potentials (ERPs), which revealed that during a visual stimulus in which respondents were required to determine the location of a target (vertical or reversed) in random flashes shown to each field, the first reaction increased by attention occurred at 75 milliseconds in the dorso-occipital regions. [127]. In a regular and complicated search assignment, Pantazatos *et al.* observed a distinct interplay between the ventromedial prefrontal cortex (vmPFC) and lateral occipital cortex (LOC) [128]. These findings strengthen the notion that the occipital lobe plays a critical role in visual information processing and attentional modulation.

In competition between familiar and unfamiliar conditions, we identified that the flow from central to frontal was higher in familiar than unfamiliar conditions in the AMIGOS dataset. This result is in agreement with the result reported by Pierce et al. [129] in which the medial frontal lobe identified that in normal subjects, neurons were more active in reaction to personally familiar members (such as mother or coworker) than to unfamiliar faces. In contrast, we observed that unfamiliar state was dominant over familiar ones in AMIGOS dataset, i.e., significant flow from frontal to right temporal. In line with our results, Calmels *et al.* showed that information processing was stronger over the frontal and right temporal areas during the unfamiliar presentation than during the familiar show in the 13–20Hz frequency band [130]. Leveroni *et al.* found that unfamiliar faces elicited extensive frontal lobe activation in comparison to recently learned faces [131]. Another fMRI study found that the middle temporal gyrus was one of the active areas that responds to unfamiliar grayscale faces and unrecognizable face scrambles [132]. Researchers found that the left ventral occipito-temporal cortex (vOT) was more active when recognizing unfamiliar letter strings than when recognizing regular words [133].

Chapter 4 Investigation of the Familiarity Effect on Emotional Valence Using Directed Functional Connectivity and Graph Theory Analysis

4.1 Introduction

Emotions are complex reaction patterns, including sensory, behavioral, and physiological components, that a person uses to cope with issues or significant events that they personally experience. Emotion regulation is directly related to executive function (EF). EF is the deliberate management of somebody's actions and thoughts. Emotional control can be broken down into its component pieces, which are personality, clinical, health, biological, cognitive, development, and social [134]. In the human body, emotions have a function in delivering information about the surrounding environment. These emotions are activated by external stimuli, such as pictures [135], music [136], [137], and videos [138] [58], and are processed by the body in order to elicit a variety of responses.

Previous studies have reported that familiarity perception is associated with pleasant emotions. For example, Garcia *et al.* [139] reported that the interpretation of familiar stimuli results in positive emotions for the individual. Using psychophysiological methods, Harmon *et al.* [140] presented additional evidence of the link between familiarity and subjectively pleasant emotion. They discovered that the link between participants' face muscles and positive emotions (zygomatic muscle area) was more active following exposure to photos that were already known, rather than those that were unknown. Guerra *et al.* [141] used Lang's picture-viewing paradigm to explore the affective processing of loved familiar faces, finding that the viewing of photos of loved familiar faces elicited an intensely positive emotional response. Nevertheless, it remains unclear how different levels of familiarity and emotional valence interact under neuroimaging.

Meanwhile, several functional magnetic resonance imaging (fMRI) studies have reported the effect of familiarity on the human brain; for instance, higher activation of the amygdala during familiar face imagery [142]. Pereira *et al.* [143] showed that there was a greater response in the limbic and paralimbic systems for familiar than for unfamiliar music. Blood oxygenation level-dependent (BOLD) signal reactions in the right amygdala have been shown to be greater for unfamiliar than for familiar faces [144]. Kosaka *et al.* reported that the posterior cingulate cortex might be essential in the development of facial familiarity [145].

Among the available non-invasive methods, electroencephalography (EEG) provides more detailed and complete data on brain activity, specifically in terms of temporal resolution. By using EEG, assessment of the individual perceptions and both internal and external emotions of an individual can shed light on his or her emotional condition [146]. Self-assessment evaluations, such as the self-evaluation manikin (SAM) [147], are frequently used to determine an individual's emotional state by quantifying three separate aspects [148], which are visualized as images of pleasure–disappointment, arousal level, and dominance–submissiveness. In another published EEG study [149], the SAM with nine valence, arousal, and dominance scales was utilized to evaluate the emotional resonance of individuals' responses to a movie clip. Mizuno *et al.* used EEG to investigate the response of the parasympathetic nervous system to unpleasant valence stimuli [150].

To date, few neuroimaging studies have reported how familiarity affects emotional states. For example, an EEG and ECG study discovered that painful stimuli that were familiar to the person rapidly aroused the brain [151]. Peer *et al.* found a substantial link between novelty and high pleasantness in the late stages of processing (650–800 ms), indicating that the processing of high pleasantness is contingent on an initial evaluation of novelty [152]. By employing a conventional EEG analysis approach, i.e., a power spectrum, Mishra *et al.* reported that a low level of familiarity of naturalistic stimuli was mainly related to negative emotion [153].

At present, the directed transfer function (DTF) is one of the preferred methods for understanding the brain network. It is robust from the perspective of volume conduction and presents information transfer between brain areas [154]. Studies have applied DTF to study Alzheimer’s [155], anesthesia [156], auditory hallucinations [157], emotion [158], epilepsy [159], mental tasks [160], motor imagery [161], transcranial magnetic stimulation (TMS) [162], and mood [163].

Graph theoretical analysis (GTA) is a mathematical approach that has been applied to quantify brain networks. In this technique, the brain is illustrated as a graph, which is composed of a set of nodes connected by edges. An EEG study by Stam *et al.*[164] was reported as the first study that applied GTA that characterized the brain networks of healthy subjects and Alzheimer's patients. Thee *et al.* [165] estimated brain functional connectivity (FC) based on EEG signals, followed by

GTA on a visual oddball paradigm, by employing four graph parameters, i.e., the node degree, network density, and betweenness centrality. Graph theory has also been widely used to better understand emotions. For instance, Prakash *et al.* [166] transformed EEG signals into graph features to differentiate different emotional states (anxiety, depression, and stress) via a machine learning approach. Another published work [167] assessed functional connectivity in healthy people generated by emotional visual stimuli for mental states of positive valence and negative valence. Additionally, this work evaluated graph metrics, including density and global and local efficiency, for each connection. This study found that enjoyment can modify the local efficiency of networks, with negative stimuli generating clustering networks more rapidly than pleasant ones.

To the best of our knowledge, the different levels of familiarity with music videos and their influence on emotional valence revealed via brain network and graph theory have never been reported. Hence, this study aimed to quantitatively evaluate the impact of familiar and unfamiliar stimuli on emotional valence using DTF and graph theory analysis. Several graph metrics were employed in this study, such as node degree, node strength, clustering coefficient, and local efficiency. Average flows in the inter- and intra-hemispheres were also computed.

4.2 Methods

4.2.1 Dataset

The DEAP dataset [81], which includes 32 subjects, was employed in this study. Each subject signed a consent form prior to the experiment. With 40 channels in total, the dataset comprises 32 EEG channels and eight peripheral physiological signals captured with the universally accepted 10–20 electrode placement technique. The electrode placement used in the experiment is described in Figure 4.1. In this study, 32 participants rated 40 one-minute music video clips on a scale from 1 to 9 for arousal, valence, like/dislike, and dominance, and from 1 to 5 for familiarity. The flow of the experiment is described in Error! Reference source not found..

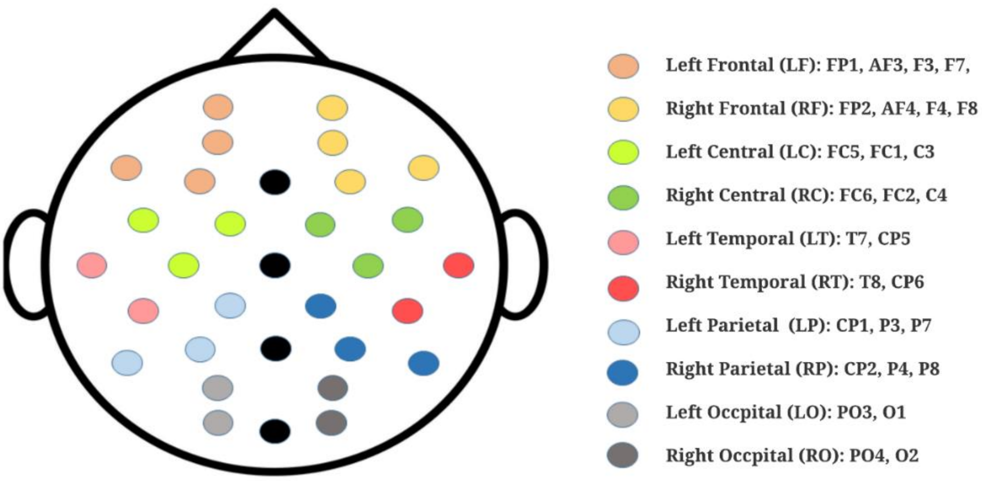

Figure 4.1: Arrangement of electrodes according to the international 10-20 systems.

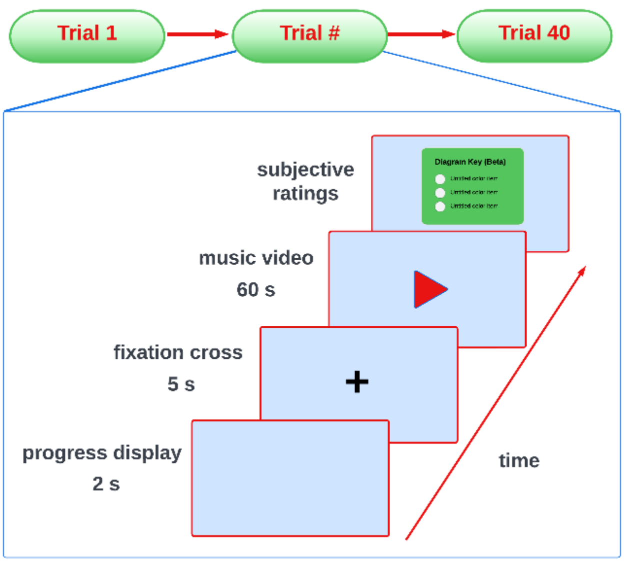

Figure 4.2: Design of the experiment.

4.2.2 EEG Signals Preprocessing

The collected EEG signals were preprocessed with the following procedures: down-sampling to 128 Hz, removing electro-oculograms (EOGs) using the blind source separation technique, re-referencing the EEG data to a common average reference, and filtering between 0.5 and 45 Hz. The flow of EEG analysis is described in Figure 4.3.

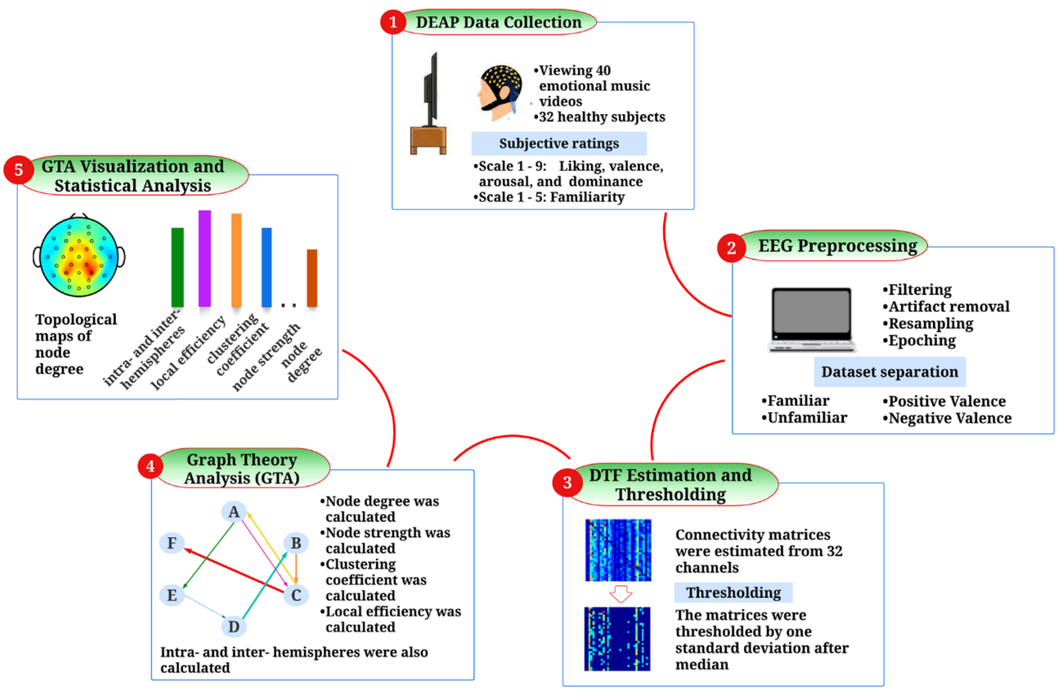

Figure 4.3: Flow of EEG analysis

We adapted the ratings of familiarity and valence that were collected during the experiment to match the objectives of this study. The primary purpose of this study was to use DTF and graph theory analysis to examine how familiarity affects emotional valence. We performed this by classifying subjects' levels of familiarity into two categories: 3–5 for familiar and 1–2 for unfamiliar (see Figure

4.4a). The valence ratings were also divided into two groups, the positive and negative groups, under familiar and unfamiliar classes. We classified them as positive valence states when the valence rating was greater than 4.5 and as negative valence states for the other data points, as illustrated in Figure 4.4b. Subjects 2, 15, and 23 did not report familiarity ratings. Furthermore, it was determined that the data from subjects 4, 5, 25, and 27 should be eliminated because the familiar/unfamiliar ratio criterion was lower than 0.30 [168][66]. We also discarded data from four subjects (subjects 9, 11, 22, and 24) because all of them had more than 25% of the total channel where the power spectral density (PSD) value was greater than 100 v2/Hz [168][66]. Finally, we analyzed the remaining 21 subjects.

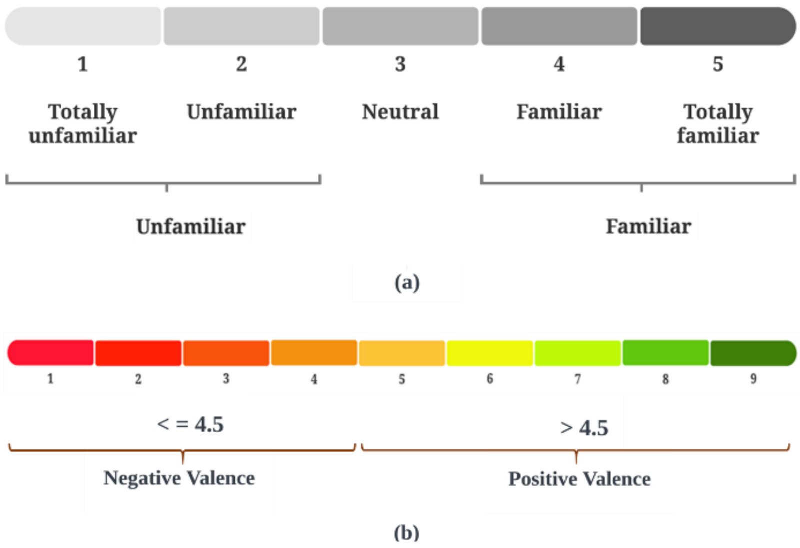

Figure 4.4: Collected ratings used in this study: (a) familiarity rating and (b) valence rating.

4.2.3 Directed Transfer Function

In this study, the directed transfer function (DTF) [33], a multivariate frequency dependent approach based on the multivariate autoregressive model (MVAR) and the concept of Granger causality, was applied to estimate brain connectivity patterns. For the interpretation of the MVAR model, we utilized equation 4.1:

$$X(t) = \sum_{j=1}^{p} A(j)X(t-j) + E(t), \tag{4.1}$$

where $X(t) = [X_1(t), X_2(t), \ldots X_k(t)]^T$ is a vector containing the values of k signals at time t., $E(t) = [E_1(t), E_2(t), \ldots E_k(t)]^T$ is a vector of k values of white noise at time t., p is the model order, and A(j) is an n x n coefficient matrix for delay j. The function that illustrated how channel j affects channel i is given in equation 4.2:

$$DTF^2{}_{j \to i}(f) = \frac{\left|H_{ij}(f)\right|^2}{\sum_{j=1}^{k}\left|H_{ij}(f)\right|^2} \tag{4.2}$$

The value of the normalized DTF was between 0 and 1, where 0 represented no influence and 1 represented the maximum influence.

The DTF was computed from preprocessed EEG data in the theta (4–7 Hz), alpha (8–12 Hz), beta (13–30 Hz), and gamma (30–45 Hz) bands using the eConnectome toolbox [97]. Then, a threshold was set up, with one standard deviation over the median [98] serving as the benchmark for determining the importance of the DTF values.

The DTF algorithm constructs a specific form of network with a weighted and directed topology, which can be represented as graphs (Figure 4.5a) and an adjacency matrix (Figure 4.5b). Nodes represent brain regions or scalp EEG electrode locations [46] and links (edges) measure functional connectivity between nodes (see Figure 4.5a), in which they can be characterized based on their weight and directionality [47]. Weighted links provide information about the strength of the connections [47].

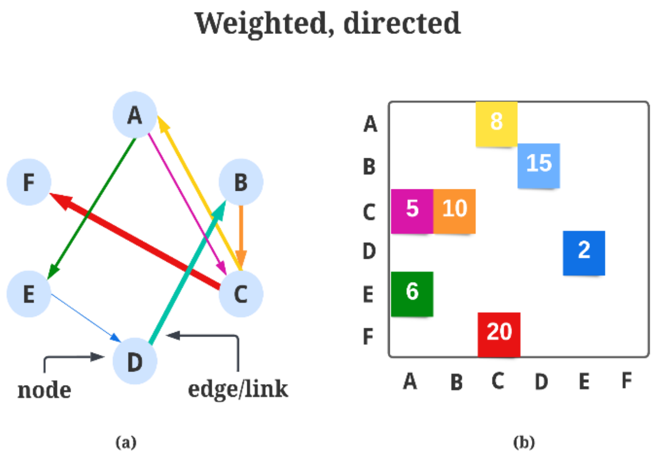

Figure 4.5: The weighted and directed DTF in the form of (a) graphs and an adjacency matrix (modified from [53]).

4.2.4 Theoretical Graph Analysis

Using graph theory, we constructed a map of the topological structure. Electrodes were considered as nodes in a network/graph, with the edges between them representing connections between different parts of the brain. From the directed and weighted adjacency matrices, BCT [47] was used to calculated key graph metrics characterizing the network architecture. In this study, we measured the degree, information flow strength, clustering coefficient, and hemispheric information flow. The measures are defined as follows:

4.2.4.1 Node Degree

As a basis for all other network measurements, can be described as the number of connected links to a node. In the directed graphs, the in-degree $\left(K_j^{in}\right)$ and out-degree $\left(K_j^{out}\right)$ represent the total number of received and sent links for node j, respectively [40]. Therefore, the total degree $\left(K_j^{out}\right)$ can be expressed in equation (4.3):

$$K_j^{total} = \sum K_j^{in} + \sum K_j^{out} \tag{4.3}$$

A high degree node in a network may often influence its neighbors.

4.2.4.2 Node Strength

The opposite of a node's degree in weighted networks. Node strength is the sum of the weights of edges to/from a node [47], as expressed by equation (4.4):

$$s_j = \sum_{j \neq i} w_{ij} \tag{4.4}$$

where w_{ij} denotes the strength or weight of the edge linking the nodes *i* and *j*.

4.2.4.3 Clustering Coefficient (CC)

A quantify of network clustering or segregation [54], describing the number of triangles in a graph. The local clustering coefficient (CC) for node j $\left(C_j\right)$ is determined as the ratio between the geometric mean of all weighted triangles and the total number of triangles. The clustering coefficient for the whole graph is the mean of the local values C_j, as expressed by equation (4.5):

$$C = \frac{1}{N} \sum_{j \in N} C_j \tag{4.5}$$

where *N* is the number of nodes in the network.

4.2.4.4 Local Efficiency(E_{loc})

The opposite of the average length of the shortest path to each neighbor of a given node. It is a measure of the average efficiency of information transport within local subgraphs or neighborhoods, as expressed by equation (6):

$$E_{loc}=\frac{1}{N_{G_i}\left(N_{G_i}-1\right)}\sum_{j,k\epsilon G_i}\frac{1}{L_{j,k}} \qquad 4.6$$

where N_{G_i} stands for the total number of vertices in subgraph G_i. Network nodes' local efficiency is measured on a scale from 0 to 1, with 1 being the highest possible local efficiency.

4.2.4.5 Hemispheric Analysis

Performed to identify information flow in the inter- and intra-hemispheres, in which information flows were averaged in four cases: (1) From the right hemisphere to the right hemisphere (RH2RH); (2) from the right hemisphere to the left hemisphere (RH2LH); (3) from the left hemisphere to the left hemisphere (LH2LH); (4) from the left hemisphere to the right hemisphere (LH2RH).

Furthermore, we averaged the node degree, node strength, clustering coefficient, and local efficiency into 10 regions of interest (ROIs), as follows: (1) Left frontal (LF: FP1, AF3, F3, F7); (2) right frontal (RF: FP2, AF4, F4, F8); (3) left central (LC: FC5, FC1, C3); (4) right central (RC: FC6, FC2, C4); (5) left temporal (LT: T7, CP5); (6) right temporal (RT: T8, CP6); (7) left parietal (LP: CP1, P3, P7); (8) right parietal (RP: CP2, P4, P8); (9) left occipital (LO: PO3, O); (10) right occipital (RO: PO4, O2).

4.2.5 Statistical Analysis

A one-way analysis of variance (ANOVA) at the 0.05 confidence level was used to identify statistically significant differences in degree, information outflow strength, clustering coefficient, and hemispheric analysis for each emotional state in valence (positive/negative) during familiar and unfamiliar conditions in four frequency bands. SPSS version 22 was employed for all statistical analysis.

4.3 Results

In this study, we used DTF and graph theory to investigate the effects of familiar and unfamiliar music videos on positive and negative valence. In this section, we present the results of graph theory analysis in five parts: node degree, node strength, clustering coefficient, local efficiency, and hemispheric analysis.

4.3.1 Node Degree

Figure 4.6 shows the average node degree over all subjects for positive valence (PV) and negative valence (NV) under familiar and unfamiliar conditions. As can be seen in Figure 4.6a–c, the topological plot demonstrates that the node degree of functional connectivity was stronger for PV compared to NV under familiar conditions for the four evaluated frequency bands. In contrast, the node degree of functional connectivity was higher during NV than during PV under unfamiliar conditions in the theta, alpha, and gamma bands. Statistical analysis of the mean node degree revealed no significant differences between PV and NV for both familiar and unfamiliar states across the four frequency bands, as shown in Figure 4.6a-c.

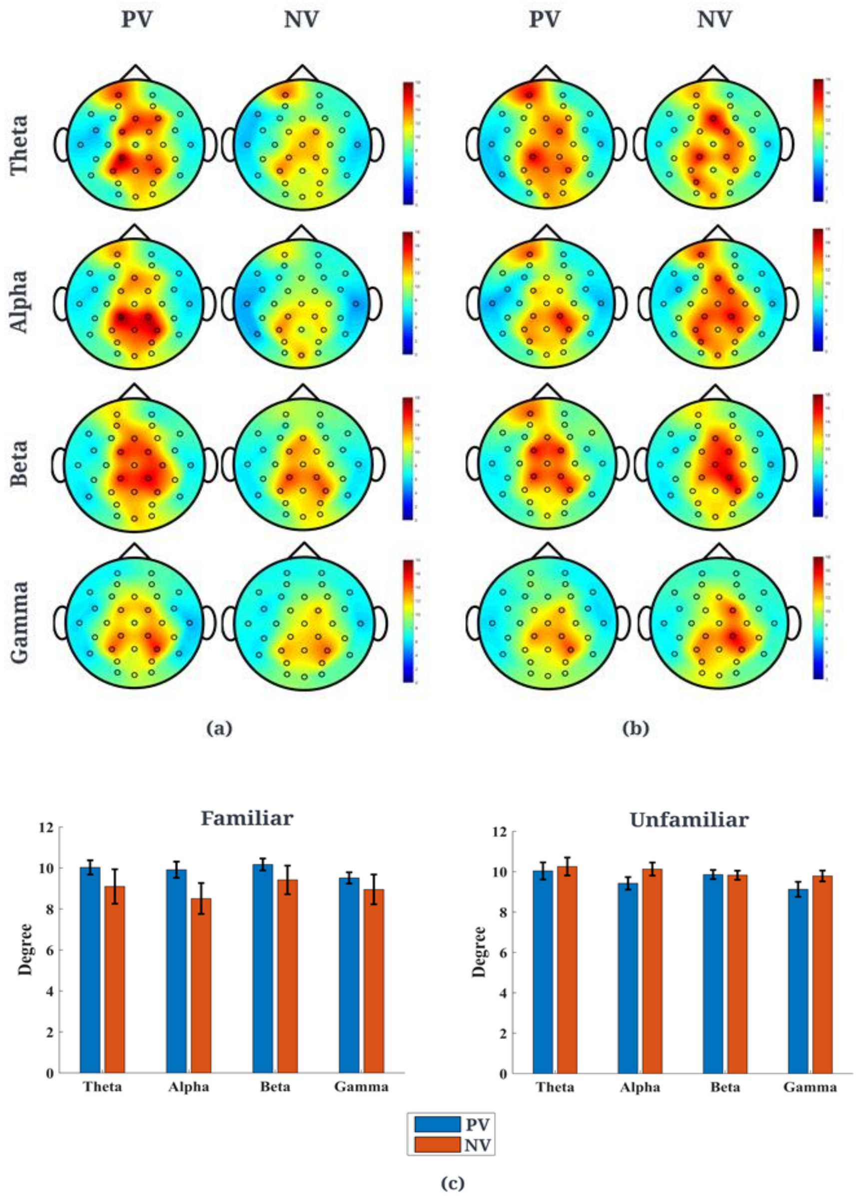

Figure 4.6: Average node degree for positive valence (PV) and negative valence (NV) under (a) familiar, (b) unfamiliar, and (c) both familiar and unfamiliar conditions.

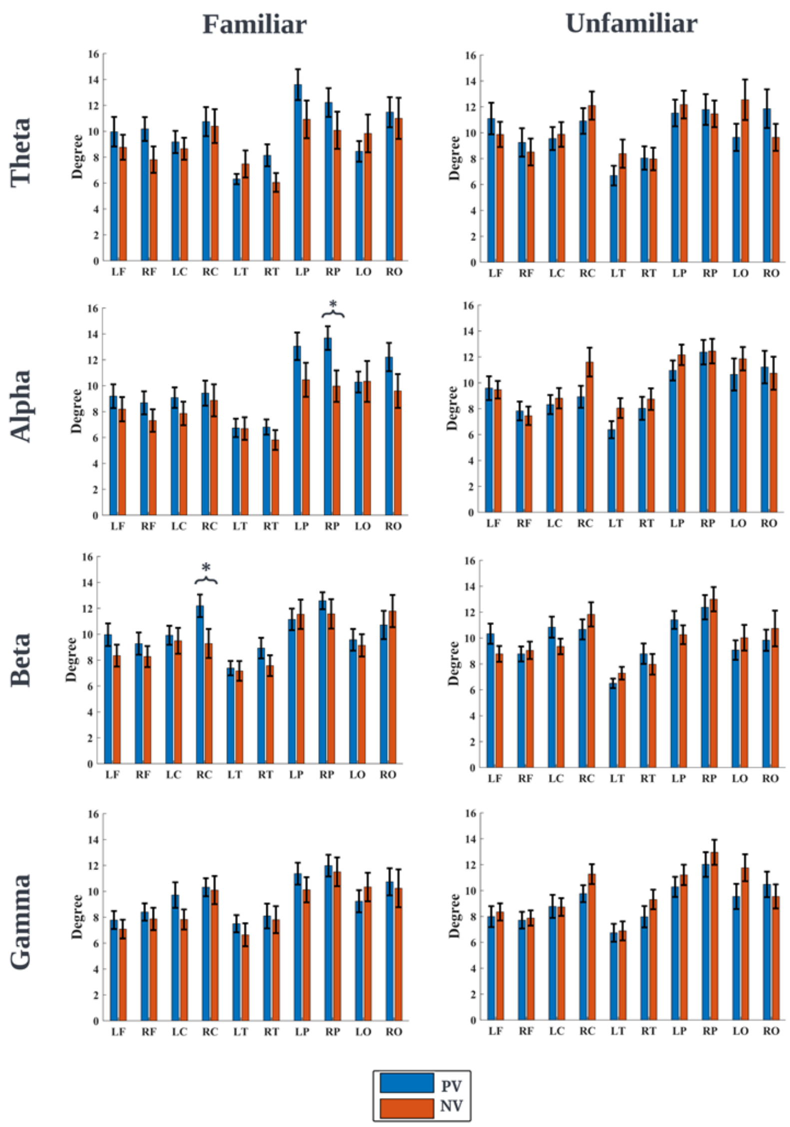

Figure 4.7: The node degree of connectivity during positive valence (PV) and negative valence (NV) under familiar and unfamiliar conditions at 10 ROIs in four frequency bands was compared. LF, RF, LC, RC, LT, RT, LP, RP, LO, and RO represent left frontal, right frontal, left central, right central, left temporal, right temporal, left parietal, right parietal, left occipital, and right occipital, respectively. The error bar represents the standard error.

Figure 4.7 depicts the results of 10 ROIs in four frequency bands, evaluating the node degree of connection for positive valence (PV) and negative valence (NV) under familiar and unfamiliar conditions. Significant differences between PV and NV under the familiar state (Figure 4.7a) were observed at RP ($\rho = 0.019$) in the alpha band and at RC ($\rho = 0.048$) in the beta band. Generally, the node degree values were relatively stronger for PV than NV during familiar states across most evaluated ROIs in the four frequency bands. Figure 4.7b shows the node degree of connectivity under the unfamiliar state. In contrast, NV was higher than PV in most ROIs, especially in the RC and LO, in the four bands. However, there was no significant difference observed in this state.

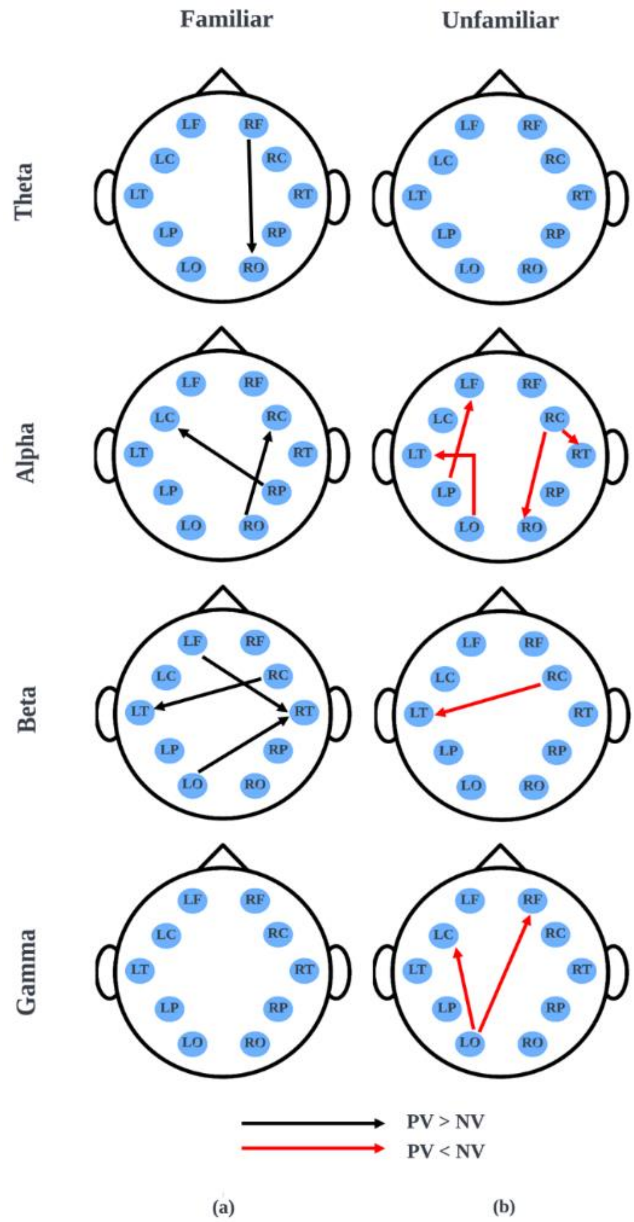

Figure 4.8: ANOVA results of the comparison of information outflow strength between positive valence (PV) and negative valence (NV) in the four frequency bands under (a) familiar and (b) unfamiliar conditions.

4.3.2 Node Strength

Figure 4.8 presents statistical comparisons of the information flow strength of PV and NV under familiar and unfamiliar conditions. In Figure 4.8, PV had a significantly higher information flow than NV at the (i) frontal to occipital (RF→RO, $\rho = 0.023$) in the theta band; (ii) occipital to central (RO→RC, $\rho = 0.031$), and parietal to central (RP→LC, $\rho = 0.047$) in the alpha band; (iii) frontal to temporal (LF→RT, $\rho = 0.046$), central to temporal (RC→LT, $\rho = 0.026$), and occipital to temporal (LO→RT, $\rho = 0.049$) in the beta band. In Figure 4.8b, we identified that NV was significantly stronger compared to PV at the (i) central to temporal (RC → RT, $\rho = 0.028$), central to occipital (RC → RO, $\rho = 0.015$), parietal to frontal (LP → LF, $\rho = 0.031$), and occipital to temporal (LO → LT, $\rho = 0.048$) in the alpha band; (ii) central to temporal (RC → LT ($\rho = 0.031$) in the beta band; (iii) occipital to frontal (LO → RF, $\rho = 0.011$) and occipital to central, (LO → LC, $\rho = 0.019$) in the gamma band.

4.3.3 Clustering Coefficient

The results of the clustering coefficient (CC) are shown in Figure 4.9. The mean of CC was increased in the theta, alpha, beta, and gamma bands over all ROIs for PV compared to NV under the familiar state. Significant differences between PV and NV were found at (1) LF ($\rho = 0.013$) in the theta band; (2) LF ($\rho = 0.040$), RC ($\rho = 0.023$), RT ($\rho = 0.021$), and RO ($\rho = 0.012$) in the beta band; (3) RF ($\rho = 0.038$) in the gamma band. Meanwhile, the mean of CC of NV was significantly higher than PV at RC ($\rho = 0.035$). Furthermore, a higher CC of NV than PV under the unfamiliar state was found over several ROIs, specifically in the regions of (1)

LO and RO in the theta band, (2) RF in the alpha band, and (3) RF in the beta band.

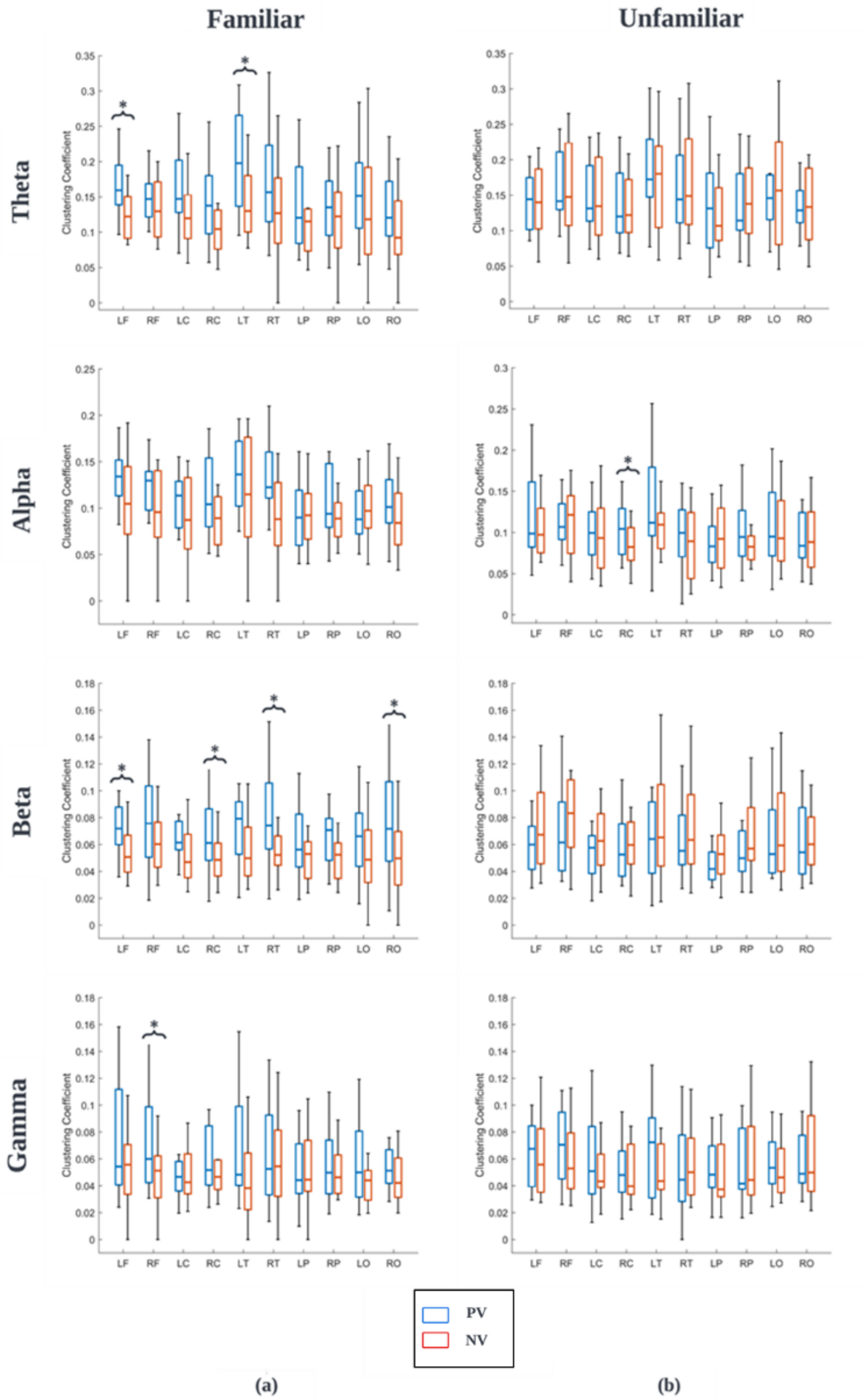

Figure 4.9: Boxplot showing the clustering coefficient for positive valence (PV) and negative valence (NV) under (a) familiar and (b) unfamiliar conditions.

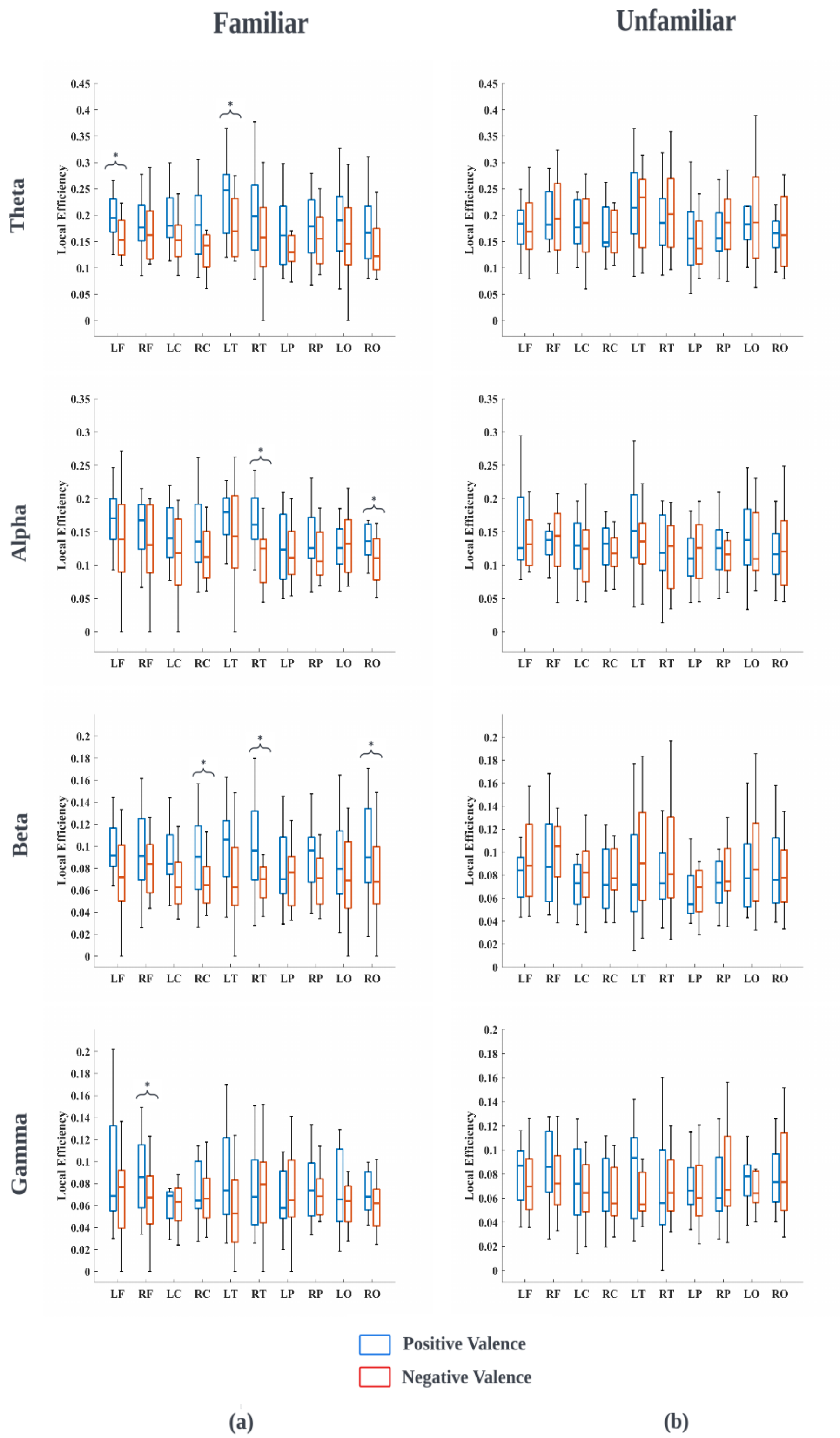

Figure 4.10: Boxplot showing the local efficiency for positive valence (PV) and negative valence (NV) under (a) familiar and (b) unfamiliar conditions.

4.3.4 Local Efficiency

Figure 4.10 show the results for local efficiency (LE). Significant differences between PV and NV under the familiar state (Figure 4.10a) were observed at (1) LF and LT in the theta band; (2) RT and RO in the alpha band; (3) RC, RT, and RO in the beta band; (4) RF in the gamma band. Generally, the LE values were relatively stronger for PV than NV during the familiar state across all evaluated ROIs in the four frequency bands. Figure 4.10b shows the local efficiency under the unfamiliar state. In contrast, NV was higher than PV in most of the ROIs, especially in the theta and beta bands. There was no significant difference observed in the unfamiliar state.

4.3.5 Hemispheric Analysis

Fig. 11 presents statistical comparisons of the information flow of PV and NV under familiar and unfamiliar conditions in hemispheric analysis. Information flows were calculated in four cases, as follows: (1) The right hemisphere to the right hemisphere (RH2RH); (2) the right hemisphere to the left hemisphere (RH2LH); (3) the left hemisphere to the left hemisphere (LH2LH); (4) the left hemisphere to the right hemisphere (LH2RH). Fig. 11a demonstrates hemispheric analysis under familiar state, in which information flows in the RH2RH and RH2LH were stronger for PV than NV in the theta and alpha bands. Specifically, significant flows were found for PV compared to NV in RH2RH in the alpha band ($\rho = 0.048$). In the beta band, the flows of PV were stronger than NV in the RH2RH, LH2LH, and LH2RH.

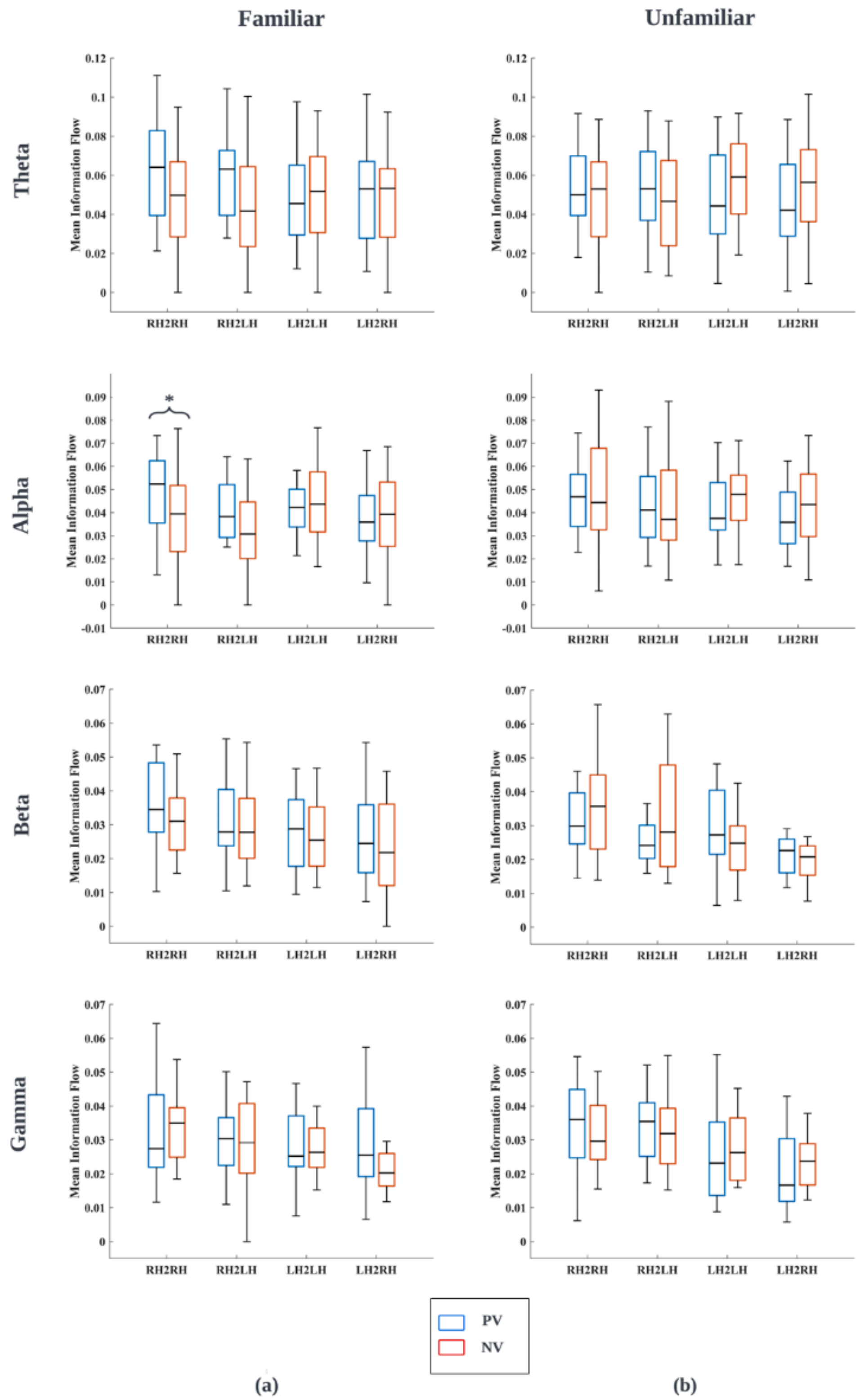

Figure 4.11: Boxplot showing the intra- and inter-hemispheric analysis for positive valence (PV) and negative valence (NV) under (a) familiar and (b) unfamiliar conditions. RH2H, RH2LH, LH2LH, and LH2RH indicate right hemisphere to right hemisphere, right hemisphere to left hemisphere, left hemisphere to left hemisphere, and left hemisphere to right hemisphere, respectively.

Meanwhile, in the gamma band, information flows for PV were higher than NV in the RH2RH and LH2RH. Fig. 11b shows hemispheric analysis under unfamiliar state, in which no significant difference was observed for all cases.

4.4 Discussion

In our study, we found slight differences in network characteristics in terms of the degree of node connectivity between positive valence (PV) and negative valence (PV) for both familiar and unfamiliar conditions. However, there were significant differences in the degree of specific ROIs in the alpha and beta bands. Moreover, the one-way ANOVA results indicated significant difference of strength between PV and NV for both familiar and unfamiliar conditions in the alpha and beta band. In line with our results, recent studies on emotion classification have found that the highest classification accuracy occurred in the high-frequency band (15–32 Hz) [169].

According to the earliest theory of brain asymmetry, the right hemisphere is involved in emotion processing. This hypothesis has been supported by a large number of studies [170]–[172]. For example, Sackeim *et al.* [170] discovered that facial expressions were more intense on the left side of the face, implying that the right hemisphere was more involved in producing emotional displays. Adolphs *et al.* [171] discovered that patients with damage to the right hemisphere had greater difficulty identifying facial expressions than patients with damage to the left hemisphere. In line with previous results, as referred to in and Figure 4.7, we found a higher degree of node connectivity for PV than NV, with a high degree of PV over the right parietal in the alpha band and over the right central in the beta band.

Furthermore, under familiar conditions, a comparison of information flow between PV and NV showed consistent results with the degree above: PV showed higher significant information flow compared to NV and stronger significant HA than LA during familiar stimuli. Our results imply that, with familiar stimuli, PV stimulates greater brain connectivity than NV. This suggests that parts of the brain are more structured and linked globally for PV compared to NV when presented with familiar stimuli.

Task performance is positively related to an increase in clustering coefficients during the augmentation period [80]. Improved cognitive performance in multiple cognitive areas is linked to increased clustering coefficients in the delta, theta, and gamma bands [173]. Greater EEG activity in the gamma band is associated with stronger cognitive performance in the frontal lobe in healthy subjects [174]. The efficient integration of information relies on parallel processing, which is facilitated by high local efficiency [41]. In our study, we found a significantly clustered brain network for PV during the familiar state in the theta, beta, and gamma bands. Moreover, significantly higher local efficiency for PV than NV was observed in the four frequency bands. This could be because a high level of familiarity evokes positive emotions and motivational effects that enhance cognitive information processing [174].

It has been discovered that familiarity can intuitively elicit visual short-term memory consolidation [175]. According to a review by Sestieri *et al.* [176], the posterior parietal cortex (PPC) has generally been connected with attention, sensory judgment, somatic alterations, and episodic memory retrieval. Furthermore, the right posterior parietal cortex has been found to be a key factor in the formation of long-term memories [177]. A memory-related brain network, the parietal memory network (PMN), has recently been dissociated from the default mode network's posterior segment (DMN) [178]. Previous studies have reported that activity in the PMN reflects stimulus familiarity during memory encoding and retrieval and across task conditions [178]–[180]. In accordance with previous findings, our study found that the right parietal is more active during positive valence (PV) than negative valence (NV), particularly under familiar conditions, in the alpha band.

Both familiar and unfamiliar stimuli cause lateralized cortical power stimulation. However, the recent literature reveals conflicting results. There is evidence that familiar stimuli enhance activation of the EEG of the left hemisphere [181] [182], while novel stimuli increase activation of the EEG of the right hemisphere [183], [184]. On the contrary, new research indicates that the right hemisphere is more active when recognizing familiar faces and sounds than when recognizing unfamiliar appearances and voices [185]. According to an EEG study by Kreiman *et al.* [186], familiar speech is processed in the right hemisphere, whereas unfamiliar speech is processed in the left. According to another finding, the same areas in the right hemisphere of the brain are activated in response to both familiar and novel emotional inputs [187]. As a result, we conclude that there is no evidence of a consistent lateralization of familiarity perception in terms of functional connectivity and emotion

Chapter 5 Conclusions and Future Research

5.1 Conclusion

The objective of this dissertation was to examine alterations in the familiarity effect on human attention and emotion that employed a directed functional connectivity approach, i.e., DTF, during watching music videos. Two studies were performed to achieve this objective.

The first study (chapter 3) investigated whether watching familiar and unfamiliar emotional music videos can elicit different attention across subjects. The work proposed the use of information flows of alpha/theta ratio from frontal to central and from central to frontal to categorize different attention indexes across subjects via hierarchical clustering into two well-known datasets, i.e., the DEAP and AMIGOS datasets. This study demonstrated that subjects were clustered into two groups based on their attention index, i.e., low index (LI) and high index (HI). Our study reported that with an increase in attention index, connection strengths from the frontal area to other regions (central, parietal, and occipital) were strengthened in the DEAP dataset. These regions include the central, parietal, and occipital regions. In the AMIGOS dataset, there was difference in the information flows that occurred between the central and parietal lobes during competition across attention index groups under familiar and unfamiliar conditions. Our results also confirmed that visual stimuli induced emotional attention that involved inflow over the occipital region.

The second study (chapter 4) reported the first evaluation of the influence of different levels of familiarity on emotional valence using directed functional connectivity and graph theory analysis. Our study demonstrated that familiar stimuli induce positive valence (PV), indicated by a greater connection (node degree) compared to negative valence (NV). Moreover, under familiar stimuli, PV had a higher clustering coefficient and local efficiency, indicating enhanced information processing in the brain. We believe that EEG observations of how familiarity affects emotion and thought processes can be used as a starting point in learning and other fields.

5.2 Methodological considerations and limitation

Although dataset applied in this study has been widely used in several published works, and this study has reports new findings regarding the impact familiar and unfamiliar stimuli on attention and emotional valence, some limitations should be considered. First, subjective annotations were collected between stimuli for both the DEAP and AMIGOS datasets, in which this matter has potential to increase cognitive load during emotion reporting. Second, since familiarity was not the primary objective for both datasets and the experimenters determined the set of stimuli, then, each subject had a different number of stimuli with a certain level of familiarity. Third, number of channels applied with a low-density setup (32 channels in the DEAP dataset and 16 channels in the AMIGOS dataset). Consequently, the accurate result will decrease.

This dissertation implements hierarchical clustering techniques to cluster directed functional connectivity features across subjects (in chapter 3). Clustering is a kind of unsupervised learning that comprises grouping data. We constructed the hierarchical tree through an agglomerative procedure (bottom-up strategy) [102]. In the agglomerative approach, individual features are treated as clusters, which then iteratively combine them into bigger clusters based on their similarities [102]. Agglomerative clustering has the advantage of providing comprehensive hierarchical levels inductively and being relatively simple to implement [188], and the result can be provided in the form of a two-dimensional diagram, namely a dendrogram [189], [190]. However, when dealing with large datasets, this technique does not perform well.

The application of directional measures, i.e., Directed Transfer Function (DTF), was applied in this dissertation [33]. DTF, which is based on Granger causality principles and multivariate autoregressive modeling (MVAR), can simultaneously estimate causal influences between multiple cortical sources of an EEG signal. The MVAR method has the advantage of accounting for the entire multivariate set of signals; thus, the analysis does not have to be done separately for each pair of signals (pair-wise). This way, we avoid problems that may occur if the set of signals has similar sources, which may cause inaccurate results. The DTF approach is relatively insensitive to the problem of volume conduction since electromagnetic fields travel practically instantly in brain tissue with no apparent phase variations between electrodes [154]. Using sensor space analysis, it is possible to identify the source of underlying structures with greater precision while avoiding the known issues associated with connection computations over the source-space signals [191]. Therefore, it was suggested that DTF only be used in sensor space and not in source space.

After connectivity matrices were constructed using DTF, a threshold approach was performed which aimed to eliminate poor connections from functional connectivity data. To our knowledge, currently, there is no consensus on the proper threshold for the functional connectivity matrix. In this dissertation, we applied a liberal threshold based on data distribution introduced by Cohen [98], i.e., one standard deviation above the median connectivity value. It was reported that overall topographical distributions and condition differences were minimally affected by this approach [98]. In our study (chapter 3 and chapter 4), the threshold was set to one standard deviation above the median of each subject's DTF connectivity matrix, thus producing a subject-specific data-based thresholding approach, in which connectivity values below the thresholds were defined as spurious interactions and discarded.

5.3 Future directions

In this dissertation, brain activity was recorded using 32 EEG channels in the DEAP dataset and 14 channels in the AMIGOS dataset. This provides EEG signals with high temporal resolution. However, data analysis with a high-density setup is required to obtain a more accurate result and corroborate our findings. Also, combining EEG with functional magnetic resonance imaging (fMRI) or near-infrared spectroscopy (NIRS) may help find out how functional connections are set up at high temporal and spatial resolutions.

In this study, we adopted two public dataset in which the rating sessions were conducted after each trial. This has the effect of raising cognitive load as a result of the reporting of emotions. To avoid this issue, experiment design will be improved with a separate EEG recording session and annotation session. Moreover, in the adopted DEAP dataset, the range of familiarity ratings is on a scale ranging from 1 to 5. In the future, a wide range of rating scales (1–10) will be used to make works more diverse and unique.

References

[1] H. T. Reis, M. R. Maniaci, P. A. Caprariello, P. W. Eastwick, and E. J. Finkel, "In live interaction, does familiarity promote attraction or contempt?," *Journal of Personality and Social Psychology*, vol. 101, no. 3, pp. 575–578, 2011.

[2] R. Sheridan, K. M. Tanaka, and N. Hogg, "Foreign Language, Local Culture: How Familiar Contexts Impact Learning and Engagement," *The Electronic Journal for English as a Second Language*, vol. 23, no. 1, pp. 1–27, 2019.

[3] D. Saplacan and J. Herstad, "Fear , Feedback , Familiarity … How are These Connected ?," in *ACHI 2018: The Eleventh International Conference on Advances in Computer-Human Interactions Fear*, 2018, pp. 171–179.

[4] F. A. C. Azevedo *et al.*, "Equal numbers of neuronal and nonneuronal cells make the human brain an isometrically scaled-up primate brain," *Journal of Comparative Neurology*, vol. 513, no. 5, pp. 532–541, 2009.

[5] B. Pakkenberg *et al.*, "Aging and the human neocortex," *Experimental Gerontology*, vol. 38, no. 1–2, pp. 95–99, 2003.

[6] N. R. Carlson, *Foundations of Physiological Psychology*, 6th ed. Boston, Mass. London: Allyn and Bacon, 2005.

[7] A. Siegel and H. N. Sapru, *Essential Neuroscience*, Second. Toronto, Philadelphia: Lippincott Williams & Wilkins, 2011.

[8] S. Siuly, Y. Li, and Y. Zhang, *EEG Signal Analysis and Classification Techniques and Applications*, First. Springer, 2016.

[9] Siuly, *ANALYSIS AND CLASSIFICATION OF EEG SIGNALS*. 2012.

[10] L. Kelly, *Essentials of Human Physiology for Pharmacy*, Second., vol. 148. CRC Press LLC, 2004.

[11] G. Hall, *The Human Central Nervous System*. 2017.

[12] M. Chappell and S. Payne, *The Central Nervous System*, vol. 24. 2020.

[13] R. Jung and W. Berger, “Fiftieth Anniversary of Hans Berger’s Publication of the Electroencephalogram,” *Archives of Psychiatry and Neurological Sciences*, vol. 227, no. 4, pp. 279–300, 1979.

[14] P. Olejniczak, “Neurophysiologic basis of EEG,” *Journal of Clinical Neurophysiology*, vol. 23, no. 3, pp. 186–189, 2006.

[15] E. Niedermeyer and F. Lopes da Silva, *Electroencephalography: basic principles, clinical applications, and related fields*, 6th ed. Lippincott Williams & Wilkins, 2005.

[16] G. Pfurtscheller and F. H. Lopes da Silva, “Event-related EEG/MEG synchronization and desynchronization: basic principles,” *Clinical Neurophysiology*, vol. 110, pp. 1842–1857, 1999.

[17] F. Terms, “The Ten Twenty Electrode System: International Federation of Societies for Electroencephalography and Clinical Neurophysiology,” *American Journal of EEG Technology*, vol. 1, no. 1, pp. 13–19, 1961.

[18] N. Boutros, S. Galderisi, O. Pogarell, and S. Riggio, *Standard EEG in Clinical Psychiatry*. 2011.

[19] C. D. Binnie and P. F. Prior, “Electroencephalography,” *Journal of Neurology, Neurosurgery, and Psychiatry*, vol. 57, pp. 1308–1319, 1994.

[20] R. Elul, "The Genesis of the Eeg," *International Review of Neurobiology*, vol. 15, no. C, pp. 227–272, 1972.

[21] V. JIRSA and A. MCINTOSH, "Handbook of brain activity," *Zhurnal Eksperimental'noi i Teoreticheskoi Fiziki*, 2007.

[22] K. J. Friston, "Models of brain function in neuroimaging," *Annual Review of Psychology*, vol. 56, pp. 57–87, 2005.

[23] B. Horwitz, "The elusive concept of brain connectivity," *NeuroImage*, vol. 19, no. 2, pp. 466–470, 2003.

[24] H. Johansen-Berg and M. F. S. Rushworth, "Using diffusion imaging to study human connectional anatomy," *Annual Review of Neuroscience*, vol. 32, pp. 75–94, 2009.

[25] L. Lee, L. M. Harrison, and A. Mechelli, "The Functional Brain Connectivity Workshop: Report and commentary," *Network: Computation in Neural Systems*, vol. 14, no. 2, pp. 1–15, 2003.

[26] V. Sakkalis, "Review of advanced techniques for the estimation of brain connectivity measured with EEG/MEG," *Computers in Biology and Medicine*, vol. 41, no. 12, pp. 1110–1117, 2011.

[27] E. Pereda, R. Q. Quiroga, and J. Bhattacharya, "Nonlinear multivariate analysis of neurophysiological signals," *Progress in Neurobiology*, vol. 77, no. 1–2, pp. 1–37, 2005.

[28] X. Wu, X. Wen, J. Li, and L. Yao, "A new dynamic Bayesian network approach for determining effective connectivity from fMRI data," *Neural Computing and Applications*, vol. 24, no. 1, pp. 91–97, 2014.

[29] T. Westin, B. Hotel, and L. Angeles, “Computational Methods for Analyzing Functional and Effective Brain Network Connectivity Using fMRI,” in *iInternational Conference on Applied Human Factors and Ergonomics*, 2018, pp. 101–112.

[30] R. E. Greenblatt, M. E. Pflieger, and A. E. Ossadtchi, “Connectivity measures applied to human brain electrophysiological data,” *Journal of Neuroscience Methods*, vol. 207, no. 1, pp. 1–16, 2012.

[31] B. Gourévitch, R. Le Bouquin-Jeannès, and G. Faucon, “Linear and nonlinear causality between signals: Methods, examples and neurophysiological applications,” *Biological Cybernetics*, vol. 95, no. 4, pp. 349–369, 2006.

[32] C. W. J. Granger, “Investigating Causal Relations by Econometric Models and Cross-spectral Methods,” *Journal of International Econometric Society*, vol. 37, no. 3, pp. 424–438, 2013.

[33] M. J. Kaminski and K. J. Blinowska, “A new method of the description of the information flow in the brain structures,” *Biological Cybernetics*, vol. 65, no. 3, pp. 203–210, 1991.

[34] M. Kamiński, M. Ding, W. A. Truccolo, and S. L. Bressler, “Evaluating causal relations in neural systems: Granger causality, directed transfer function and statistical assessment of significance,” *Biological Cybernetics*, vol. 85, no. 2, pp. 145–157, 2001.

[35] L. A. Baccalá and K. Sameshima, “Partial directed coherence: A new concept in neural structure determination,” *Biological Cybernetics*, vol. 84,

no. 6, pp. 463–474, 2001.

[36] O. Sporns, G. Tononi, and R. Kötter, "The human connectome: A structural description of the human brain," *PLoS Computational Biology*, vol. 1, no. 4, pp. 0245–0251, 2005.

[37] D. C. Van Essen *et al.*, "The Human Connectome Project: A data acquisition perspective," *NeuroImage*, vol. 62, no. 4, pp. 2222–2231, 2012.

[38] O. Sporns, "The human connectome: Origins and challenges," *NeuroImage*, vol. 80, pp. 53–61, 2013.

[39] Y. He and A. Evans, "Graph theoretical modeling of brain connectivity," *Current Opinion in Neurology*, vol. 23, no. 4, pp. 341–350, 2010.

[40] O. Sporns, *Networks of the Brain*. 2010.

[41] E. Bullmore and O. Sporns, "Complex brain networks: Graph theoretical analysis of structural and functional systems," *Nature Reviews Neuroscience*, vol. 10, no. 3, pp. 186–198, 2009.

[42] E. T. Bullmore and D. S. Bassett, "Brain graphs: Graphical models of the human brain connectome," *Annual Review of Clinical Psychology*, vol. 7, pp. 113–140, 2011.

[43] C. J. Stam, "Modern network science of neurological disorders," *Nature Reviews Neuroscience*, vol. 15, no. 10, pp. 683–695, 2014.

[44] J. T. Duda, P. A. Cook, and J. C. Gee, "Reproducibility of graph metrics of human brain structural networks," *Frontiers in Neuroinformatics*, vol. 8, no. MAY, pp. 1–11, 2014.

[45] T. H. E. C. Matrix, "Connectivity Matrices and Brain Graphs," in

Fundamentals of Brain Network Analysis, 2016, pp. 89–113.

[46] M. L. Stanley, M. N. Moussa, B. M. Paolini, R. G. Lyday, J. H. Burdette, and P. J. Laurienti, "Defining nodes in complex brain networks," *Frontiers in Computational Neuroscience*, vol. 7, no. NOV, pp. 1–14, 2013.

[47] M. Rubinov and O. Sporns, "Complex network measures of brain connectivity: Uses and interpretations," *NeuroImage*, vol. 52, no. 3, pp. 1059–1069, 2010.

[48] P. Hagmann *et al.*, "Mapping human whole-brain structural networks with diffusion MRI," *PLoS ONE*, vol. 2, no. 7, 2007.

[49] M. T. Chai *et al.*, "Exploring EEG Effective Connectivity Network in Estimating Influence of Color on Emotion and Memory," *Frontiers in Neuroinformatics*, vol. 13, no. October, pp. 1–21, 2019.

[50] P. Hagmann *et al.*, "Mapping the structural core of human cerebral cortex," *PLoS Biology*, vol. 6, no. 7, pp. 1479–1493, 2008.

[51] C. R. Buchanan *et al.*, "The effect of network thresholding and weighting on structural brain networks in the UK Biobank," *NeuroImage*, vol. 211, 2020.

[52] M. A. de Reus and M. P. van den Heuvel, "Estimating false positives and negatives in brain networks," *NeuroImage*, vol. 70, pp. 402–409, 2013.

[53] L. Heathrow and T. Roman, "Node Degree and Strength," in *Fundamentals of Brain Network Analysis*, 2016, pp. 115–136.

[54] D. J. Watts and S. H. Strogatz, "Collective dynamics of 'small-world' networks," *Nature*, vol. 393, no. June, pp. 440–442, 1998.

[55] D. J. Watts and S. H. Strogatz, "Collectivedynamics of 'small-world'

networks," *Nature*, vol. 393, no. June, pp. 440–442, 1998.

[56] A. Bartels and S. Zeki, "Functional Brain Mapping during Free Viewing of Natural Scenes," *Human Brain Mapping*, vol. 21, no. 2, pp. 75–85, 2004.

[57] D. R. Andersen, K. V. Fite, N. Petrovich, and J. Hirsch, "Cortical activation while watching video montage: An fMRI study," *Media Psychology*, vol. 8, no. 1, pp. 7–24, 2006.

[58] S. D'Mello, A. Graesser, B. Schuller, and J.-C. Martin, "EEG Correlates of Different Emotional States Elicited during Watching Music Videos," in *Affective computing and intelligent interaction: 4th international conference, ACII*, 2011, pp. 457–466.

[59] J. Moon, Y. Kwon, J. Park, and W. C. Yoon, "Detecting user attention to video segments using interval EEG features," *Expert Systems with Applications*, vol. 115, pp. 578–592, 2019.

[60] J. Mercado, I. Espinosa-Curiel, L. Escobedo, and M. Tentori, "Developing and evaluating a BCI video game for neurofeedback training: the case of autism," *Multimedia Tools and Applications*, vol. 78, no. 10, pp. 13675–13712, 2019.

[61] A. Mintz, "Foreign Policy Decision Making in Familiar and Unfamiliar Settings: An experimental study of high-ranking military officers," *Journal of Conflict Resolution*, vol. 48, no. 1, pp. 91–104, 2004.

[62] J. Ang, A. de Jong, and M. van der Poel, "Does familiarity with business segments affect CEOs' divestment decisions?," *Journal of Corporate Finance*, vol. 29, pp. 58–74, 2014.

[63] A. M. Kareem and C. J. Barnard, “The importance of kinship and familiarity in social interactions between mice,” *Animal Behaviour*, vol. 30, no. 2, pp. 594–601, 1982.

[64] G. Van de Walle, P. Turner, and E. Davenport, “A Study of Familiarity,” in *Proceedings of the 3th Interntionnal Conference on Human-Computer Interaction-INTERACT*, 2003, pp. 463–470.

[65] Y. Kumagai, R. Matsui, and T. Tanaka, “Music familiarity affects EEG entrainment when little attention is paid,” *Frontiers in Human Neuroscience*, vol. 12, no. November, pp. 1–11, 2018.

[66] N. Thammasan, K. Moriyama, K. Fukui, and M. Numao, “Familiarity effects in EEG-based emotion recognition,” *Brain Informatics*, vol. 4, no. 1, pp. 39–50, 2017.

[67] E. Barenholtz, L. Mavica, and D. J. Lewkowicz, “Language familiarity modulates relative attention to the eyes and mouth of a talker,” *Cognition*, vol. 147, pp. 100–105, 2016.

[68] M. C. Jackson and J. E. Raymond, “The role of attention and familiarity in face identification,” vol. 68, no. 4, pp. 543–557, 2006.

[69] G. Patsis, H. Sahli, W. Verhelst, and O. De Troyer, “Evaluation of attention levels in a tetris game using a brain computer interface,” *Lecture Notes in Computer Science*, vol. 7899. Springer, Berlin Heidelberg, pp. 127–138, 2013.

[70] C. G. Lim *et al.*, “A Brain-Computer Interface Based Attention Training Program for Treating Attention Deficit Hyperactivity Disorder,” *PLoS ONE*,

vol. 7, no. 10, 2012.

[71] M. D. Rosenberg *et al.*, "A neuromarker of sustained attention from whole-brain functional connectivity," *Nature Neuroscience*, vol. 19, no. 1, pp. 165–171, 2015.

[72] F. E. Dupuy, A. R. Clarke, R. J. Barry, R. McCarthy, and M. Selikowitz, "Girls with attention-deficit/hyperactivity disorder: EEG differences between DSM-IV types," *Clinical EEG and Neuroscience*, vol. 42, no. 1, pp. 1–5, 2011.

[73] R. J. Barry, A. R. Clarke, and S. J. Johnstone, "A review of electrophysiology in attention-deficit/hyperactivity disorder: I. Qualitative and quantitative electroencephalography," *European Journal of Cardio-Thoracic Surgery*, vol. 23, no. 114, pp. 171–183, 2003.

[74] B. E. Juel, L. Romundstad, F. Kolstad, J. F. Storm, and P. G. Larsson, "Distinguishing anesthetized from awake state in patients: A new approach using one second segments of raw EEG," *Frontiers in Human Neuroscience*, vol. 12, no. 40, pp. 1–14, 2018.

[75] S. Afshari and M. Jalili, "Directed Functional Networks in Alzheimer's Disease: Disruption of Global and Local Connectivity Measures," *IEEE Journal of Biomedical and Health Informatics*, vol. 21, no. 4, pp. 949–955, 2017.

[76] M. S. Tahaei, M. Jalili, and M. G. Knyazeva, "Synchronizability of EEG-based functional networks in early alzheimer's disease," *IEEE Transactions on Neural Systems and Rehabilitation Engineering*, vol. 20, no. 5, pp. 636–

641, 2012.

[77] J. Buckelmüller, H. P. Landolt, H. H. Stassen, and P. Achermann, "Trait-like individual differences in the human sleep electroencephalogram," *Neuroscience*, vol. 138, no. 1, pp. 351–356, 2006.

[78] V. A. Maksimenko *et al.*, "Human personality reflects spatio-temporal and time-frequency EEG structure," *PLoS ONE*, vol. 13, no. 9, 2018.

[79] A. Y. Shestyuk, K. Kasinathan, V. Karapoondinott, R. T. Knight, and R. Gurumoorthy, "Individual EEG measures of attention, memory, and motivation predict population level TV viewership and Twitter engagement," *PLoS ONE*, vol. 14, no. 3, pp. 1–27, 2019.

[80] F. Al-shargie, U. Tariq, O. Hassanin, H. Mir, and F. Babiloni, "Brain Connectivity Analysis Under Semantic Vigilance and Enhanced Mental States," *Brain Sciences*, vol. 9, no. 12, pp. 363–392, 2019.

[81] S. Koelstra, M. Soleymani, S. Member, and J. Lee, "DEAP : A Database for Emotion Analysis Using Physiological Signals," *IEEE Transactions on Affective Computing*, vol. 3, no. 1, pp. 18–31, 2012.

[82] J. A. Miranda-Correa, M. K. Abadi, N. Sebe, and I. Patras, "AMIGOS: A Dataset for Affect, Personality and Mood Research on Individuals and Groups," *IEEE Transactions on Affective Computing*, vol. 12, no. 2, pp. 479–493, 2021.

[83] D. S. Naser and G. Saha, "Influence of music liking on EEG based emotion recognition," *Biomedical Signal Processing and Control*, vol. 64, no. October 2020, 2021.

[84] E. T. Pereira, H. M. Gomes, L. R. Veloso, and M. R. A. Mota, “Empirical Evidence Relating EEG Signal Duration to Emotion Classification Performance,” *IEEE Transactions on Affective Computing*, vol. 12, no. 1, pp. 154–164, 2021.

[85] M. Khateeb, S. M. Anwar, and M. Alnowami, “Multi-Domain Feature Fusion for Emotion Classification Using DEAP Dataset,” *IEEE Access*, vol. 9. pp. 12134–12142, 2021.

[86] R. Sharma, R. B. Pachori, and P. Sircar, “Automated emotion recognition based on higher order statistics and deep learning algorithm,” *Biomedical Signal Processing and Control*, vol. 58, p. 101867, 2020.

[87] Z. Lan, O. Sourina, L. Wang, R. Scherer, and G. R. Muller-Putz, “Domain Adaptation Techniques for EEG-Based Emotion Recognition: A Comparative Study on Two Public Datasets,” *IEEE Transactions on Cognitive and Developmental Systems*, vol. 11, no. 1, pp. 85–94, 2019.

[88] W. L. Zheng, J. Y. Zhu, and B. L. Lu, “Identifying stable patterns over time for emotion recognition from eeg,” *IEEE Transactions on Affective Computing*, vol. 10, no. 3, pp. 417–429, 2019.

[89] R. Alazrai, R. Homoud, H. Alwanni, and M. I. Daoud, “EEG-based emotion recognition using quadratic time-frequency distribution,” *Sensors (Switzerland)*, vol. 18, no. 8, pp. 1–32, 2018.

[90] R. W. Homan, J. Herman, and P. Purdy, “Cerebral location of international 10-20 system electrode placement,” *Electroencephalography and Clinical Neurophysiology*, vol. 66, no. 4, pp. 376–382, 1987.

[91] L. A. Martínez-Tejada, Y. Maruyama, N. Yoshimura, and Y. Koike, "Analysis of Personality and EEG Features in Emotion Recognition Using Machine Learning Techniques to Classify Arousal and Valence Labels," *Machine Learning and Knowledge Extraction*, vol. 2, no. 2, pp. 99–124, 2020.

[92] V. Padhmashree and A. Bhattacharyya, "Human emotion recognition based on time–frequency analysis of multivariate EEG signal," *Knowledge-Based Systems*, vol. 238. 2022.

[93] G. Yin, S. Sun, D. Yu, D. Li, and K. Zhang, "A Multimodal Framework for Large-Scale Emotion Recognition by Fusing Music and Electrodermal Activity Signals," *ACM Transactions on Multimedia Computing, Communications and Applications*, vol. 18, no. 3, 2022.

[94] A. Topic and M. Russo, "Emotion recognition based on EEG feature maps through deep learning network," *Engineering Science and Technology, an International Journal*, vol. 24, no. 6. pp. 1442–1454, 2021.

[95] Y. Zhao, X. Cao, J. Lin, D. Yu, and X. Cao, "Multimodal Affective States Recognition Based on Multiscale CNNs and Biologically Inspired Decision Fusion Model," *IEEE Transactions on Affective Computing*, vol. 14, no. 8, 2021.

[96] J. A. Miranda-Correa, M. K. Abadi, N. Sebe, and I. Patras, "AMIGOS: A Dataset for Affect, Personality and Mood Research on Individuals and Groups," *IEEE Transactions on Affective Computing*, vol. 12, no. 2. pp. 479–493, 2021.

[97] A. L. He B, Dai Y, “eConnectome: A MATLAB Toolbox for Mapping and Imaging of Brain Functional Connectivity,” *NeurosciMethods*, vol. 195, no. 2, pp. 261–269, 2011.

[98] M. X. Cohen, “Error-related medial frontal theta activity predicts cingulate-related structural connectivity,” *NeuroImage*, vol. 55, no. 3, pp. 1373–1383, 2011.

[99] R. Gordon, J. Ciorciari, and T. van Laer, “Using EEG to examine the role of attention, working memory, emotion, and imagination in narrative transportation,” *European Journal of Marketing*, vol. 52, no. 1–2, pp. 92–117, 2018.

[100] S. B. Kotsiantis and P. E. Pintelas, “Recent Advances in Clustering : A Brief Survey,” *WSEAS Trans. Information Science and Applications*, vol. 1, no. 1, pp. 73–81, 2004.

[101] M. P. Milali, M. T. Sikulu-Lord, S. S. Kiware, F. E. Dowell, R. J. Povinelli, and G. F. Corliss, “Do NIR spectra collected from laboratory-reared mosquitoes differ from those collected from wild mosquitoes?,” *PLoS ONE*, vol. 13, no. 5, pp. 1–16, 2018.

[102] S. C. Johnson, “Hierarchical clustering schemes,” *Psychometrika*, vol. 32, no. 3, pp. 241–254, 1967.

[103] J. C. Dunn, “Well-Separated Clusters and Optimal Fuzzy Partitions,” *Journal of Cybernetics*, vol. 4, no. 1, pp. 95–104, 1974.

[104] F. Kovács, C. Legány, and A. Babos, “Cluster Validity Measurement Techniques,” in *Proceedings of the 6th International Symp. of Hungarian*

Researchers on Computational Intelligence (CINTI), 2005, pp. 18–19.

[105] N. V. Lutsyuk, E. V. Éismont, and V. B. Pavlenko, “Correlation of the characteristics of EEG potentials with the indices of attention in 12-to 13-year-old children,” *Neurophysiology*, vol. 38, no. 3, pp. 209–216, 2006.

[106] S. Palva and J. M. Palva, “Functional roles of alpha-band phase synchronization in local and large-scale cortical networks,” *Frontiers in Psychology*, vol. 2, no. 204, pp. 1–15, 2011.

[107] E. L. Maclin *et al.*, “Learning to multitask: Effects of video game practice on electrophysiological indices of attention and resource allocation,” *Psychophysiology*, vol. 48, no. 9, pp. 1173–1183, 2011.

[108] M. E. Smith and A. Gevins, “Attention and brain activity while watching television: Components of viewer engagement,” *Media Psychology*, vol. 6, no. 3, pp. 285–305, 2004.

[109] L. S. Globa and V. V. Kyrylkov, “Action video game modifies visual selective attention,” *Nature*, vol. 423, pp. 463–464, 2003.

[110] S. Sadaghiani, R. Scheeringa, K. Lehongre, B. Morillon, A. L. Giraud, and A. Kleinschmidt, “Intrinsic connectivity networks, alpha oscillations, and tonic alertness: A simultaneous electroencephalography/functional magnetic resonance imaging study,” *Journal of Neuroscience*, vol. 30, no. 30, pp. 10243–10250, 2010.

[111] S. K. Loo and S. Makeig, “Clinical Utility of EEG in Attention-Deficit/Hyperactivity Disorder: A Research Update,” *Neurotherapeutics*, vol. 9, no. 3, pp. 569–587, 2012.

[112] C. A. Mann, J. F. Lubar, A. W. Zimmerman, C. A. Miller, and R. A. Muenchen, "Quantitative analysis of EEG in boys with attention-deficit-hyperactivity disorder: Controlled study with clinical implications," *Pediatric Neurology*, vol. 8, no. 1, pp. 30–36, 1992.

[113] A. R. Clarke, R. J. Barry, R. McCarthy, and M. Selikowitz, "Electroencephalogram differences in two subtypes of Attention-Deficit/Hyperactivity Disorder," *Psychophysiology*, vol. 38, no. 2, pp. 212–221, 2001.

[114] G. Bush, P. J. Whalen, B. R. Rosen, M. A. Jenike, S. C. Mcinerney, and S. L. Rauch, "The Counting Stroop : An Interference Task Specialized for Functional Neuroimaging — Validation Study With Functional MRI," *Human Brain Mapping*, vol. 6, no. 4, pp. 270–282, 1998.

[115] H. Yamasaki, K. S. Labar, and G. Mccarthy, "Dissociable prefrontal brain systems for attention and emotion," in *Proceedings of the National Academy of Sciences of the United States of America*, 2002, vol. 99, no. 17, pp. 11447–11451.

[116] N. U. F. Dosenbach, D. A. Fair, A. L. Cohen, B. L. Schlaggar, and S. E. Petersen, "A dual-networks architecture of top-down control," *Trends in Cognitive Sciences*, vol. 12, no. 3, pp. 99–105, 2008.

[117] M. T. Banich, K. L. Mackiewicz, B. E. Depue, A. Whitmer, A. Miller, and W. Heller, "Cognitive Control Mechanisms, Emotion & Memory: A neural perspective with implications for psychopathology," *Neurosci Biobehavioral Reviews*, vol. 33, no. 5, pp. 613–630, 2009.

[118] A. A. Valldares, C. M. Gomez, and C. I. Barriga-Paulino, “Attention-deficit_hyperactivity disorder in children and adolescents_ An event-related potential study of working memory _ Enhanced Reader.pdf,” *European Journal of Neuroscience*, vol. 52, pp. 4356–4369, 2020.

[119] S. G. Horovitz, P. Skudlarski, and J. C. Gore, “Correlations and dissociations between BOLD signal and P300 amplitude in an auditory oddball task: A parametric approach to combining fMRI and ERP,” *Magnetic Resonance Imaging*, vol. 20, no. 4, pp. 319–325, 2002.

[120] V. Ferrari, M. Codispoti, R. Cardinale, and M. M. Bradley, “Directed and motivated attention during processing of natural scenes,” *Journal of Cognitive Neuroscience*, vol. 20, no. 10, pp. 1753–1761, 2008.

[121]J. Cacioppo, L. G. Tassinary, and G. G. Berntson, “Emotion and Motivation,” in *The Handbook of Psychophysiology*, Third., M. M. Bradley and P. J. Lang, Eds. New York: Cambridge University Press, pp. 581–607.

[122] A. Kok, “On the utility of P3 amplitude as a measure of processing capacity,” *Psychophysiology*, vol. 38, pp. 557–577, 2001.

[123] M. Codispoti, V. Ferrari, and M. M. Bradley, “Repetition and event-related potentials: Distinguishing early and late processes in affective picture perception,” *Journal of Cognitive Neuroscience*, vol. 19, no. 4, pp. 577–586, 2007.

[124] A. I. Wilterson, S. A. Nastase, B. J. Bio, A. Guterstam, and M. S. A. Graziano, “Attention, awareness, and the right temporoparietal junction,” *Proceedings of the National Academy of Sciences of the United States of America*, vol.

118, no. 25, 2021.

[125] C. Bledowski, D. Prvulovic, R. Goebel, F. E. Zanella, and D. E. J. Linden, "Attentional systems in target and distractor processing: A combined ERP and fMRI study," *NeuroImage*, vol. 22, no. 2, pp. 530–540, 2004.

[126] S. C. Krall *et al.*, "The role of the right temporoparietal junction in attention and social interaction as revealed by ALE meta-analysis," *Brain Structure and Function*, vol. 220, no. 2, pp. 587–604, 2015.

[127] M. I. Posner and C. D. Gilbert, "Attention and primary visual cortex," in *Proceedings of the National Academy of Sciences of the United States of America*, 1999, vol. 96, no. 6, pp. 2585–2587.

[128] S. P. Pantazatos, T. K. Yanagihara, X. Zhang, T. Meitzler, and J. Hirsch, "Frontal–Occipital Connectivity During Visual Search," *Brain Connectivity*, vol. 2, no. 3, pp. 164–175, 2012.

[129] K. Pierce, F. Haist, F. Sedaghat, and E. Courchesne, "The brain response to personally familiar faces in autism: Findings of fusiform activity and beyond," *Brain*, vol. 127, no. 12, pp. 2703–2716, 2004.

[130] C. Calmels, M. Foutren, and C. J. Stam, "Beta functional connectivity modulation during the maintenance of motion information in working memory: Importance of the familiarity of the visual context," *Neuroscience*, vol. 212, pp. 49–58, 2012.

[131] C. L. Leveroni, M. Seidenberg, A. R. Mayer, L. A. Mead, J. R. Binder, and S. M. Rao, "Neural systems underlying the recognition of familiar and newly learned faces," *Journal of Neuroscience*, vol. 20, no. 2, pp. 878–886, 2000.

[132] E. Halgren, A. M. Dale, M. I. Sereno, R. B. H. Tootell, K. Marinkovic, and B. R. Rosen, "Location of human face-selective cortex with respect to retinotopic areas," *Human Brain Mapping*, vol. 7, no. 1. pp. 29–37, 1999.

[133] M. Schurz, M. Kronbichler, J. Crone, F. Richlan, J. Klackl, and H. Wimmer, "Top-down and bottom-up influences on the left ventral occipito-temporal cortex during visual word recognition: An analysis of effective connectivity," *Human Brain Mapping*, vol. 35, no. 4, pp. 1668–1680, 2014.

[134] J. J. Gross, "The emerging field of emotion regulation: An integrative review," *Review of General Psychology*, vol. 2, no. 3, pp. 271–299, 1998.

[135] P. C. Petrantonakis and L. J. Hadjileontiadis, "A novel emotion elicitation index using frontal brain asymmetry for enhanced EEG-based emotion recognition," *IEEE Transactions on Information Technology in Biomedicine*, vol. 15, no. 5, pp. 737–746, 2011.

[136] D. T. Hettich, E. Bolinger, T. Matuz, N. Birbaumer, W. Rosenstiel, and M. Spüler, "EEG responses to auditory stimuli for automatic affect recognition," *Frontiers in Neuroscience*, vol. 10, no. JUN, pp. 1–10, 2016.

[137] Y. P. Lin *et al.*, "EEG-based emotion recognition in music listening," *IEEE Transactions on Biomedical Engineering*, vol. 57, no. 7, pp. 1798–1806, 2010.

[138] X. Hu *et al.*, "EEG correlates of ten positive emotions," *Frontiers in Human Neuroscience*, vol. 11, no. 26, 2017.

[139] T. Garcia-Marques, M. Prada, and D. M. Mackie, "Familiarity increases subjective positive affect even in non-affective and non-evaluative contexts,"

Motivation and Emotion, vol. 40, no. 4, pp. 638–645, 2016.

[140] E. Harmon-Jones and J. J. B. Allen, “The Role of Affect in the Mere Exposure Effect: Evidence from Psychophysiological and Individual Differences Approaches,” *Personality and Social Psychology Bulletin*, vol. 27, no. 7, pp. 889–898, 2001.

[141] P. Guerra, C. Vico, R. Campagnoli, A. Sánchez, L. Anllo-Vento, and J. Vila, “Affective processing of loved familiar faces: Integrating central and peripheral electrophysiological measures,” *International Journal of Psychophysiology*, vol. 85, no. 1, pp. 79–87, 2012.

[142] H. Sharon *et al.*, “Emotional Processing of Personally Familiar Faces in the Vegetative State,” *PLoS ONE*, vol. 8, no. 9, 2013.

[143] C. S. Pereira, J. Teixeira, P. Figueiredo, J. Xavier, S. L. Castro, and E. Brattico, “Music and Emotions in the Brain: Familiarity Matters,” *PLoS ONE*, vol. 6, no. 11, 2011.

[144] C. E. Schwartz *et al.*, “Differential amygdalar response to novel versus newly familiar neutral faces: A functional MRI probe developed for studying inhibited temperament,” *Biological Psychiatry*, vol. 53, no. 10, pp. 854–862, 2003.

[145] H. Kosaka *et al.*, “Neural substrates participating in acquisition of facial familiarity: An fMRI study,” *NeuroImage*, vol. 20, no. 3, pp. 1734–1742, 2003.

[146] N. S. Suhaimi, J. Mountstephens, and J. Teo, “EEG-Based Emotion Recognition: A State-of-the-Art Review of Current Trends and

Opportunities," *Computational Intelligence and Neuroscience*, vol. 2020, pp. 8 875 426(1)–8 875 426(19), 2020.

[147] M. M. Bradley and P. J. Lang, "Measuring emotion: The self-assessment manikin and the semantic differential," *Journal of Behavior Therapy and Experimental Psychiatry*, vol. 25, no. 1, pp. 49–59, 1994.

[148] J. D. Morris, "OBSERVATIONS: SAM: The Self-Assessment Manikin - An Efficient Cross-Cultural Measurement of Emotional Response," *Journal of Advertising Research*, vol. 35, no. 6, pp. 63–68, 1995.

[149] D. Nie, X. W. Wang, L. C. Shi, and B. L. Lu, "EEG-based emotion recognition during watching movies," in *2011 5th International IEEE/EMBS Conference on Neural Engineering, NER 2011*, 2011, pp. 667–670.

[150] Y. Mizuno-Matsumoto, Y. Inoguchi, S. Kobayashi, S. M. A. Carpels, and A. Muramatsu, "How do the parasympathetic nervous system and EEG respond to emotional memory recall?," *IEEJ Transactions on Electrical and Electronic Engineering*, vol. 14, no. 7, pp. 1082–1090, 2019.

[151] Y. Mizuno-Matsumoto, Y. Inoguchi, S. M. A. Carpels, A. Muramatsu, and Y. Yamamoto, "Cerebral cortex and autonomic nervous system responses during emotional memory processing," *PLoS ONE*, vol. 15, no. 3, pp. 1–15, 2020.

[152] J. M. van Peer, D. Grandjean, and K. R. Scherer, "Sequential unfolding of appraisals: EEG evidence for the interaction of novelty and pleasantness," *Emotion*, vol. 14, no. 1, pp. 51–63, 2014.

[153] S. Mishra and U. S. Tiwary, "The degree of context un/familiarity impacts

the emotional feeling and preaware cardiac-brain activity: a study with emotionally salient naturalistic paradigm using DENS Dataset," pp. 1–15, 2021.

[154] M. Kaminski and K. J. Blinowska, "Directed Transfer Function is not influenced by volume conduction-inexpedient pre-processing should be avoided," *Frontiers in Computational Neuroscience*, vol. 8, no. JUN, pp. 1–3, 2014.

[155] K. J. Blinowska *et al.*, "Functional and effective brain connectivity for discrimination between Alzheimer's patients and healthy individuals: A study on resting state EEG rhythms," *Clinical Neurophysiology*, vol. 128, no. 4, pp. 667–680, 2017.

[156] B. E. Juel, L. Romundstad, J. F. Storm, and P. G. Larsson, "Validation of a new approach for distinguishing anesthetized from awake state in patients using directed transfer function applied to raw EEG," *Journal of Clinical Monitoring and Computing*, no. 0123456789, 2020.

[157] J. Ying, D. Zhou, K. Lin, and X. Gao, "Network analysis of functional brain connectivity driven by gamma-band auditory steady-state response in auditory hallucinations," *Journal of Medical and Biological Engineering*, vol. 35, no. 1, pp. 45–51, 2015.

[158] M. A. Ferdek, C. M. van Rijn, and M. Wyczesany, "Depressive rumination and the emotional control circuit: An EEG localization and effective connectivity study," *Cognitive, Affective and Behavioral Neuroscience*, vol. 16, no. 6, pp. 1099–1113, 2016.

[159] E. B. Assi, D. K. Nguyen, S. Rihana, and M. Sawan, “A functional-genetic scheme for seizure forecasting in canine epilepsy,” *IEEE Transactions on Biomedical Engineering*, vol. 65, no. 6, pp. 1339–1348, 2018.

[160] D. Huang *et al.*, “Combining partial directed coherence and graph theory to analyse effective brain networks of different mental tasks,” *Frontiers in Human Neuroscience*, vol. 10, no. MAY2016, pp. 1–11, 2016.

[161] P. Ghosh, A. Mazumder, S. Bhattacharyya, D. N. Tibarewala, and M. Hayashibe, “Functional connectivity analysis of motor imagery EEG signal for brain-computer interfacing application,” *International IEEE/EMBS Conference on Neural Engineering, NER*, vol. 2015-July, no. July, pp. 210–213, 2015.

[162] E. Olejarczyk, A. Jozwik, V. Valiulis, K. Dapsys, G. Gerulskis, and A. Germanavicius, “Statistical Analysis of Graph-Theoretic Indices to Study EEG-TMS Connectivity in Patients With Depression,” *Frontiers in Neuroinformatics*, vol. 15, no. April, pp. 1–9, 2021.

[163] T. S. Ligeza, I. Nowak, M. Maciejczyk, Z. Szygula, and M. Wyczesany, “Acute aerobic exercise enhances cortical connectivity between structures involved in shaping mood and improves self-reported mood: An EEG effective-connectivity study in young male adults,” *International Journal of Psychophysiology*, vol. 162, no. January, pp. 22–33, 2021.

[164] C. J. Stam, B. F. Jones, G. Nolte, M. Breakspear, and P. Scheltens, “Small-world networks and functional connectivity in Alzheimer’s disease,” *Cerebral Cortex*, vol. 17, no. 1, pp. 92–99, 2007.

[165] K. W. Thee, H. Nisar, and C. S. Soh, “Graph Theoretical Analysis of Functional Brain Networks in Healthy Subjects: Visual Oddball Paradigm,” *IEEE Access*, vol. 6, pp. 64708–64727, 2018.

[166] B. Prakash, G. K. Baboo, and V. Baths, “A novel approach to learning models on eeg data using graph theory features—a comparative study,” *Big Data and Cognitive Computing*, vol. 5, no. 3, 2021.

[167] C. Lithari, M. A. Klados, and P. D. Bamidis, “Graph analysis on functional connectivity networks during an emotional paradigm,” in *IFMBE Proceedings*, 2010, vol. 29, pp. 115–118.

[168] H. Iddas and K. Iramina, “Directed EEG Functional Connectivity Features to Reveal Different Attention Indexes Using Hierarchical Clustering,” *IEEE Access*, vol. 9, pp. 59328–59335, 2021.

[169] J. Kortelainen, E. Väyrynen, and T. Seppänen, “High-frequency electroencephalographic activity in left temporal area is associated with pleasant emotion induced by video clips,” *Computational Intelligence and Neuroscience*, vol. 2015, 2015.

[170] H. A. Sackeim, R. C. Gur, and M. C. Saucy, “Emotions Are Expressed More Intensely on the Left Side of the Face,” *Science*, vol. 201, pp. 434–436, 1978.

[171] R. Adolphs, “Neural systems for recognizing emotion,” *Current Opinion in Neurobiology*, vol. 12, no. 2, pp. 169–177, 2002.

[172] J. C. Borod *et al.*, “Right hemisphere emotional perception: Evidence across multiple channels,” *Neuropsychology*, vol. 12, no. 3, pp. 446–458, 1998.

[173] L. Douw *et al.*, “Cognition is related to resting-state small-world network

topology: An magnetoencephalographic study," *Neuroscience*, vol. 175, pp. 169–177, 2011.

[174] S. Pauligk, S. A. Kotz, and P. Kanske, "Differential Impact of Emotion on Semantic Processing of Abstract and Concrete Words: ERP and fMRI Evidence," *Scientific Reports*, vol. 9, no. 1. 2019.

[175] W. Xie and W. Zhang, "Familiarity Speeds Up Visual Short-term Memory Consolidation: Electrophysiological Evidence from Contralateral Delay Activities," *Cognitive Neuroscience*, vol. 30, no. 1, pp. 1–13, 2017.

[176] C. Sestieri, G. L. Shulman, and M. Corbetta, "The contribution of the human posterior parietal cortex to episodic memory," *Nature Reviews Neuroscience*, vol. 18, no. 3, pp. 183–192, 2017.

[177] I. Alekseichuk, Z. Turi, S. Veit, and W. Paulus, "Model-driven neuromodulation of the right posterior region promotes encoding of long-term memories," *Brain Stimulation*, vol. 13, no. 2, pp. 474–483, 2020.

[178] A. W. Gilmore, S. M. Nelson, and K. B. McDermott, "A parietal memory network revealed by multiple MRI methods," *Trends in Cognitive Sciences*, vol. 19, no. 9, pp. 534–543, 2015.

[179] S. M. Nelson, K. M. Arnold, A. W. Gilmore, and K. B. Mcdermott, "Neural signatures of test-potentiated learning in parietal cortex," *Journal of Neuroscience*, vol. 33, no. 29, pp. 11754–11762, 2013.

[180] K. B. McDermott, A. W. Gilmore, S. M. Nelson, J. M. Watson, and J. G. Ojemann, "The parietal memory network activates similarly for true and associative false recognition elicited via the DRM procedure," *Cortex*, vol.

87, pp. 96–107, 2017.

[181] J. Plailly, B. Tillmann, and J. P. Royet, “The feeling of familiarity of music and odors: The same neural signature?,” *Cerebral Cortex,* vol. 17, no. 11, pp. 2650–2658, 2007.

[182] “neural systems.pdf.” .

[183] P. Rämä and S. M. Courtney, “Functional topography of working memory for face or voice identity,” *NeuroImage,* vol. 24, no. 1, pp. 224–234, 2005.

[184] S. Lattner, M. E. Meyer, and A. D. Friederici, “Voice perception: Sex, pitch, and the right hemisphere,” *Human Brain Mapping*, vol. 24, no. 1, pp. 11–20, 2005.

[185] G. Gainotti, “Laterality effects in normal subjects’ recognition of familiar faces, voices and names. Perceptual and representational components,” *Neuropsychologia*, vol. 51, no. 7. pp. 1151–1160, 2013.

[186] J. Kreiman and D. Sidtis, *Foundations of voice studies: An interdisciplinary approach to voice production and perception*. John Wiley & Sons, 2011.

[187] K. V. Kriegstein and A. L. Giraud, “Distinct functional substrates along the right superior temporal sulcus for the processing of voices,” *NeuroImage*, vol. 22, no. 2, pp. 948–955, 2004.

[188] I. Davidson and S. S. Ravi, “Agglomerative hierarchical clustering with constraints: Theoretical and empirical results,” *Lecture Notes in Computer Science (including subseries Lecture Notes in Artificial Intelligence and Lecture Notes in Bioinformatics),* vol. 3721 LNAI, no. December, pp. 59–70, 2005.

[189] B. Basaran and F. Günes, “Data clustering: A Review,” *Intelligent multidimensional data clustering and analysis*, vol. 31, no. 3, pp. 28–72, 2016.

[190] T. Hastie, R. Tibshirani, and J. Friedman, “The Elements of Statistical Learning,” Second., S. S. in Statistics, Ed. New York, 2001.

[191] K. Mahjoory, V. V. Nikulin, L. Botrel, K. Linkenkaer-Hansen, M. M. Fato, and S. Haufe, “Consistency of EEG source localization and connectivity estimates,” *NeuroImage*, vol. 152, no. February, pp. 590–601, 2017.